PHASE TRANSITIONS IN DISORDERED SYSTEMS

by

FAWAZ Y. HRAHSHEH

A DISSERTATION

Presented to the Faculty of the Graduate School of the

MISSOURI UNIVERSITY OF SCIENCE AND TECHNOLOGY

In Partial Fulfillment of the Requirements for the Degree

DOCTOR OF PHILOSOPHY

in

PHYSICS

2013

Approved by

Dr. Thomas Vojta, Advisor
Dr. Paul Parris
Dr. Alexey Yamilov
Dr. Julia Medvedeva
Dr. Ilya Vekhter

This work is licensed under the Creative Commons Attribution-NonCommercial-ShareAlike 3.0 Unported License. To view a copy of this license, visit http://creativecommons.org/licenses/by-nc-sa/3.0/ or send a letter to Creative Commons, 444 Castro Street, Suite 900, Mountain View, California, 94041, USA.

Published journal articles retain their original copyrights.

Copyright 2013

FAWAZ Y. HRAHSHEH

All Rights Reserved

PUBLICATION DISSERTATION OPTION

This dissertation contains two parts, a general introduction (Section 1) and preprints of six research papers (Papers I-VI) that have already been published. The introductory chapter is written in normal dissertation style. Paper I is published in Phys. Rev. B, vol. 84, p. 184202, 2011. Paper II is published in Phys. Rev. B, vol. 83, p. 224402, 2011. Paper III is published in EPL (Europhysics Letters), vol. 97, p. 20007, 2012. Paper IV is published in Phys. Rev. Lett., vol. 108, p. 185701, 2012. Paper V is published in Phys. Rev. B, vol. 86, p. 214204, 2012. Paper VI is published in Phys. Rev. Lett., vol. 109, p. 265303, 2012. All articles in Paper I-II and IV-VI are written in the style (REVTEX4) of the American Physical Society. Article in Paper III is written in the style (EPL2) of the journal Europhysics Letters.

ABSTRACT

Disorder can have a wide variety of consequences for the physics of phase transitions. Some transitions remain unchanged in the presence of disorder while others are completely destroyed. In this thesis we study the effects of disorder on several classical and quantum phase transitions in condensed matter systems. After a brief introduction, we study the ferromagnetic phase transition in a randomly layered Heisenberg magnet using large-scale Monte-Carlo simulations. Our results provide numerical evidence for the exotic infinite-randomness scenario.

We study classical and quantum smeared phase transitions in substitutional alloys $A_{1-x}B_x$. Our results show that the disorder completely destroys the phase transition with a pronounced tail of the ordered phase developing for all compositions $x < 1$. In addition, we find that short-ranged disorder correlations can have a dramatic effect on the transition. Moreover, we show an experimental realization of the composition-tuned ferromagnetic-to-paramagnetic quantum phase transition in $Sr_{1-x}Ca_xRuO_3$.

We investigate the effects of disorder on first-order quantum phase transitions on the example of the N-color quantum Ashkin-Teller model. By means of a strong-disorder renormalization group, we demonstrate that disorder rounds the first-order transition to a continuous one for both weak and strong coupling between the colors.

Finally, we investigate the superfluid-insulator quantum phase transition of one-dimensional bosons with off-diagonal disorder by means of large-scale Monte-Carlo simulations. Beyond a critical disorder strength, we find nonuniversal, disorder-dependent critical behavior.

Dedicated to the memory of my late mother Maryam

and my late father Yousef.

ACKNOWLEDGMENTS

First and foremost, I would like to document my immense gratitude to my dissertation advisor, Professor Thomas Vojta, for being my teacher and guide throughout my educational program at Missouri University of Science and Technology. Prof. Vojta went beyond normal means in helping me and answering my numerous questions with stamping the answers by cheerful smiles.

I would like to thank my advisor, Prof. Gerald Wilemski for being my teacher, my philosopher, and my friend during my PhD study. Prof. Wilemski has a unique way of thinking which always receive my admiration.

I would like to thank Dr. Abdalla Obeidat for his constant guidance, encouragement, comments and care. Dr. Obeidat was my master thesis advisor and he put me on the first step toward my PhD study when he introduced me to Prof. Wilemski.

I am particularly indebted to my great friend Eng. Tewfik Al Reheme. Thank you Tewfik for moral support and encourage.

I would like to thank all my teachers and committee members for creating a supportive environment. This includes Dr. P. Parris, Dr. A. Yamilov, Dr. J. Medvedeva, Dr. B. Hale, and Dr. I. Vekhter from LSU. Also, I would like to thank all my teachers since I was in the elementary school for their contributions in my education.

I am heartily thankful to my brothers and sisters: Awad, Abdulrazzaq, Mowafaq, Faeq, Fedha, Hilalah, Eidah, Zainah, Yumna for their moral encourage and support. My thanks also dedicated to all my friends in Jordan and USA.

Finally, a great thank you to my wife, um Yusuf for patience, care and support.

TABLE OF CONTENTS

Page

LIST OF ILLUSTRATIONS

PAPER IV

PAPER V

PAPER VI

1. INTRODUCTION

1.1 PHASE TRANSITIONS AND QUANTUM PHASE TRANSITIONS

Phase transitions are one of the most active condensed matter research areas, undergoing intensive investigations by both theorists and experimentalists. The main question is how the macroscopic properties of many-particle systems change under the variation of a control parameter such as temperature, pressure, magnetic field or disorder. The phase transitions occur when the system reaches a point of non-analyticity in the free energy F. Based on the continuity or discontinuity of the free energy derivatives, the phase transition can be classified as a first-order or a second-order transition. First-order phase transitions, at which a first derivative is discontinuous, are distinguished by latent heat and phase coexistence on the phase boundary. Second-order phase transitions are also known as continuous phase transitions because the first derivatives of the free energy, such as entropy and magnetization, are continuous at the transition point while the second derivatives, such as magnetic susceptibility and specific heat, show a divergence in the control parameter space. Non-analytic properties of systems near a second-order phase transition are known as *critical phenomena* while the point of transition in the phase diagram is called the *critical point*. At absolute zero temperature, the phase transition can be driven by a non-thermal control parameter such as pressure, magnetic field, and disorder. This type of phase transition is called quantum phase transition because it occurs due to quantum fluctuations [1, 2, 3, 4, 5].

1.1.1. Order Parameter and Landau Theory. In 1937, Landau [6, 7, 8, 9] developed a theory of phase transitions by introducing the general concept of an *order parameter*, a macroscopic thermodynamic quantity, which is zero in a disordered phase

and develops a finite value in an ordered phase. The magnetization m is an order parameter in the case of a ferromagnetic phase transition.

Landau theory is a thermodynamic approach. It starts from the free energy in terms of the order parameter $F_L(m)$. Landau suggested that the free energy is an analytic function of the order parameter and that the critical phenomena can be explained by expanding the free energy $F_L(m)$ in a power series of a spatially uniform order parameter m (m is small at the vicinity of a critical point)

$$F_L(m) = F_0 - hm + rm^2 + vm^3 + um^4 + \mathcal{O}(m^5). \tag{1.1}$$

Here r, v, u are m-independent system parameters and h is an external field conjugate to the order parameter. If the system is invariant under the symmetry transformation $m \to -m$, the coefficients of the odd powers of m vanish. The physical state is obtained by minimizing $F_L(m)$ with respect to m. In the absence of an external magnetic field h, the minimum free energy for $r < 0$ is always located at $m \neq 0$ (ordered phase) and at $m = 0$ for $r > 0$ (disordered phase). At $r = 0$, the transition from $m = 0$ to $m \neq 0$ occurs discontinuously for $v \neq 0$ (first-order phase transition) and continuously for $v = 0$ (second-order phase transition). Thus, r is measuring the distance from the critical point in the control parameter space, $r \propto (T - T_c)$ for a thermal transition. In the case of a second-order phase transition, the order parameter vanishes as $m = \pm\sqrt{-r/2u}$ when $r \to -0$. Landau theory thus predicts the order parameter singularity $m \sim |r|^\beta$ with $\beta = 1/2$ for all critical points. This is an example of the so-called super-universality of Landau theory.

The deficiency of Landau theory is that it assumes that there are no fluctuations in the order parameter about its average value. It turns out that the validity of this assumption depends on the system's dimensionality d and on the number of the order parameter components n since the order parameter fluctuations decreases with increasing d and n. This leads to the introduction of the *upper critical dimension* d_c^+

and the *lower critical dimension* d_c^-. Above d_c^+, fluctuations can be neglected and Landau theory provides the correct description of critical behavior. On the other hand, below d_c^-, the fluctuations are sufficiently strong to prevent any ordered phase, and thus there is no phase transition. If $d_c^- < d < d_c^+$, the phase transition exists but with a critical behavior different from Landau theory predictions. For the thermal ferromagnetic transition, for example, $d_c^+ = 4$ for any symmetry and $d_c^- = 2$ or 1, respectively, for Heisenberg and Ising symmetries.

The failure of Landau theory below d_c^+ can be overcome by generalizing the Landau order parameter m to a coarse-grained position-dependent field $\phi(x)$. It is not a microscopic variable but represents the average of the order parameter over some small region of space. The Landau free energy (1.1) can now be generalized to the Landau-Ginzburg-Wilson free energy functional

$$F_{LGW} = \int d^d x \left[|\nabla \phi(x)|^2 + r\phi^2(x) + u\phi^4(x) - h\phi(x) \right]. \tag{1.2}$$

Here, the term $|\nabla \phi(x)|^2$ punishes rapid spatial variations of the order parameter. The partition function can be found by integrating over all possible fluctuations in $\phi(x)$, which leads to the functional integral,

$$Z_{LGW} = \int D[\phi] e^{-F_{LGW}}. \tag{1.3}$$

1.1.2. The Scaling Hypothesis and Universality. In general, observables exhibit power-law behavior in the vicinity of the critical point (similar to the order parameter in the Landau theory), characterized by critical exponents.

Consider, for example, the fluctuations of the order parameter. They are characterized by its correlation function

$$G(x) = \langle \phi(x)\phi(0) \rangle \tag{1.4}$$

which is generically short-ranged in the bulk disordered phase and decays exponentially with separation x as

$$G(x) \sim e^{-|x|/\xi}. \tag{1.5}$$

Here ξ is the typical length scale of correlations (correlation length). When the critical point is approached, $r \to +0$, the correlations become longer and longer ranged; ξ diverges at the transition point,

$$\xi \sim |r|^{-\nu} \tag{1.6}$$

where ν is the correlation length critical exponent. The diverging correlation length suggests that it is the only length scale affecting thermodynamic observables at criticality.

The crucial idea of scaling theory is that thermodynamics properties are invariant under a rescaling of all length by positive length scale factor b if the external parameters are adjusted such that the correlation length retains its old value. This leads to a homogeneity relation for the singular part of the free energy density $f = -(T/V)\ln Z$,

$$f_s(r,h) = b^{-d} f_s(rb^{1/\nu}, hb^{y_h}) \tag{1.7}$$

where y_h is another critical exponent [10]. As the scale factor b is arbitrary, we can set it, for example, equal to $r^{-\nu}$. Inserting this into the free energy density, we obtain

$$f_s(r,h) = r^{d\nu}\psi_s\left(\frac{h}{r^{\nu y_h}}\right) \tag{1.8}$$

where ψ_s is a scaling function that depends on the combination $hr^{-\nu y_h}$ only. Analogous homogeneity relations can be derived for other thermodynamic quantities by taking the appropriate derivatives of $f_s(r,h)$:

$$m(r,h) = r^{\beta} M_s\left(\frac{h}{r^{\nu y_h}}\right),\ \chi(r,h) = r^{-\gamma}\chi_s\left(\frac{h}{r^{\nu y_h}}\right),\ C(r,h) = r^{-\alpha} C_s\left(\frac{h}{r^{\nu y_h}}\right) \tag{1.9}$$

where m, χ and C are the order parameter, susceptibility, and specific heat, respectively. Here β, γ, and α denote the order parameter, susceptibility, and specific heat critical exponents. For example, the zero field magnetization m can be found by differentiating the free energy with respect to h giving

$$m\big|_{h=0} = -\left(\frac{\partial f_s}{\partial h}\right)_T = r^{d\nu-\nu y_h} M_s(0) \propto r^{\beta}. \tag{1.10}$$

Therefore, by comparison, $\beta = d\nu - \nu y_h$. Similarly, at the critical point ($r = 0$), $m \sim h^{1/\delta} \sim h^{(d-y_h)/y_h}$. Because the free energy (1.8) contains only two independent critical exponents, the other critical exponents are related by the so-called scaling relations

$$\delta - 1 = \frac{\gamma}{\beta} \qquad \text{Widom's Identity} \tag{1.11}$$

$$2\beta + \gamma + \alpha = 2 \qquad \text{Rushbrooke's Identity.} \tag{1.12}$$

Finally, consider the scaling of the correlation function $G(x, r, h)$,

$$G(x, r, h) = b^{-2\beta/\nu} G_s(xb^{-1}, rb^{1/\nu}, hb^{y_h}) \sim x^{-(d-2+\eta)}, \tag{1.13}$$

for $x \lesssim \xi$. As the susceptibility is given by the following integral

$$\chi \sim \int_1^{\xi} d^d x G(x), \tag{1.14}$$

this leads to

$$\gamma = \nu(2 - \eta) \qquad \text{Fisher's identity.} \tag{1.15}$$

Now, if one uses the correlation length to scale the free energy ($b = \xi$), one obtains $f_s \sim \xi^{-d} \sim r^{2-\alpha}$ with

$$2 - \alpha = d\nu \qquad \text{Josephson's Identity.} \tag{1.16}$$

All these scaling relations hold below d_c^+ where the critical behavior is dominated by fluctuations. In dimensions higher than the upper critical dimension d_c^+, the critical behavior is governed by the conventional mean field theory (MFT) where all the critical exponents assume dimension independent values. Therefore, the Josephson relation (also known as the *hyperscaling relation*) which depends on the dimensionality d is valid only below the upper critical dimension, $d < d_c^+$.

1.1.3. Finite-Size Scaling. In general, a sharp phase transition can only emerge for infinite system size (thermodynamic limit) where the correlation length is the only relevant length scale. The effects of a finite system size on the critical behavior are very important for computational applications and also for many experiments, for instance in nano-materials. Finite-size effects are quantitatively described by the finite-size scaling theory [11, 12, 13]. This theory starts from the observation that the inverse linear system size L acts as an additional parameter similar to the reduced temperature r on the external field h which drives the system away from the critical point at $L = \infty$. For sufficiently large but finite systems, the finite-size effects are governed by the ratio L/ξ_∞ only. Thus, the classical homogeneity relation (1.7) for the free energy density [10] can by generalized to

$$f(r, h, L) = b^{-d} f_s(rb^{1/\nu}, hb^{y_h}, Lb^{-1}). \tag{1.17}$$

As b is arbitrary, one can set $b = L$ and $h = 0$ to obtain $f(r, L) = L^{-d}\Theta_f(rL^{1/\nu})$ where $\Theta_f(rL^{1/\nu})$ is a dimensionless scaling function. Let us apply this scaling form to a situation in which the finite-size system does have a sharp phase transition (for example, a layered system in which only the thickness is finite). As this transition corresponds to a singularity in Θ_f at some nonzero argument $x_c = r_c L^{1/\nu}$, its transition temperature $T_c(L)$ is shifted from the bulk value $T_{c0}(L = \infty)$ as $T_c(L) = T_{c0} + AL^{-1/\nu}$. Here, A is non-universal constant. This finite-size scaling argument is only valid below the upper critical dimension d_c^+ of the phase transition. Above d_c^+, finite-size scaling can

be generalized and the shift in the critical temperature is given by

$$T_c(L) = T_{c0} + AL^{-\phi} \tag{1.18}$$

where the shift exponent ϕ is in general different from $1/\nu$.

This finite-size scaling theory is widely used to analyze computer simulations data of phase transitions. By fitting the simulation data to finite-size scaling forms, we can get values of the critical exponents which are required to describe the critical behavior.

1.1.4. Quantum Phase Transitions. So far, we have discussed phase transitions occurring at nonzero temperatures. In 1976, Hertz [14] pioneered the investigation of a new class of phase transitions occurring at zero temperature. He started from the fact that the critical temperature T_c of a given transition depends on other parameters such as the doping and external magnetic field. In some systems, the critical temperature can be suppressed without limit, leading to $T_c = 0$. This can be seen in Figure 1.1 where the classical critical point (dotted line) decreases continuously with increasing nonthermal parameter g. At g_c where the transition temperature reaches $T = 0$, there will be no thermal fluctuations, and thus the order-disorder phase transition must be driven by nonthermal fluctuations. At this point, quantum mechanics starts playing an important role. The zero-temperature phase transition is driven by quantum fluctuations [3] which stem from Heisenberg's uncertainty principle. It is thus called a quantum phase transition.

The basic phenomenology of a second-order quantum phase transition is similar to that of a second-order classical transition. As the phase transition point, i.e., the critical point, is approached, the spatial correlations of the order parameter fluctuations become long-ranged. Close to the critical point their typical length scale, the correlation length ξ, diverges as $\xi \sim r^{-\nu}$ where ν is the correlation length critical

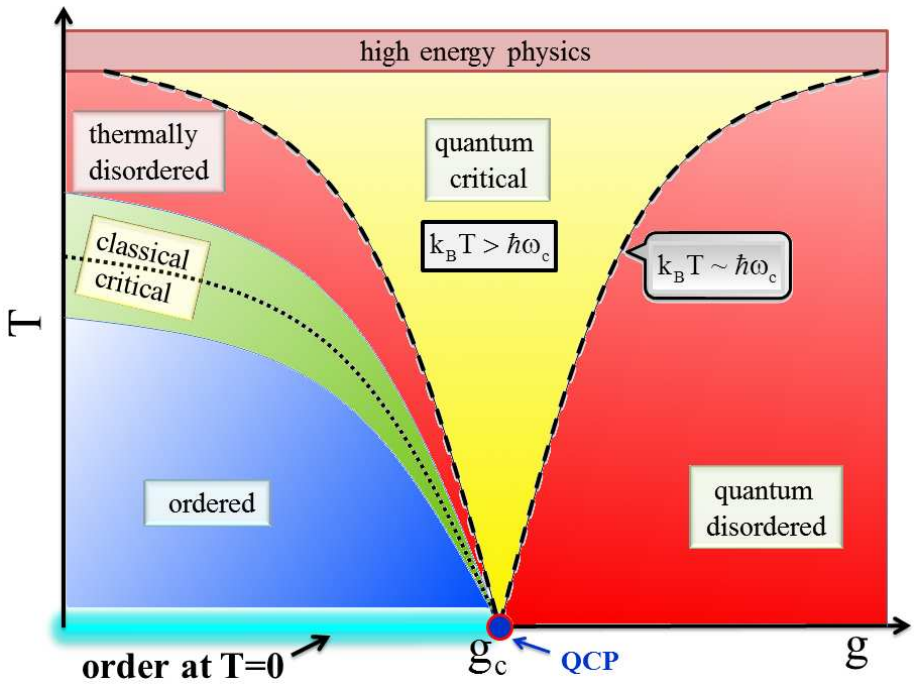

Figure 1.1: Schematic phase diagram in the vicinity of a quantum critical point (QCP). The dotted line is the finite-temperature phase boundary while the dashed lines are crossover lines separating different regions within the disordered phase.

exponent and r is some dimensionless distance from the quantum critical point. Analogously, the typical time scale for a decay of the fluctuations is the correlation time ξ_τ. As the critical point is approached the correlation time diverges as $\xi_\tau \sim \xi^z \sim r^{-z\nu}$ where z is the dynamical critical exponent. Correspondingly, the typical frequency scale ω_c goes to zero and with it the typical energy scale $\hbar\omega_c \sim r^{\nu z}$.

An argument for explaining when quantum phase transitions become important can be achieved by distinguishing fluctuations with predominantly thermal and quantum character. Because of the competition between the thermal energy $k_B T$ and the quantum energy scale $\hbar\omega_c$, quantum fluctuations are important as long as $\hbar\omega_c > k_B T$. The zero-temperature phase transition is thus completely controlled by quantum physics. Consequently, transitions at zero temperature are called quantum phase transitions. However, if the phase transition occurs at a finite temperature, it is entirely classical even if the properties of the order state are determined quantum

mechanically because $\omega_c \to 0$ at criticality. The crossover to quantum behavior occurs when $|r| > r_x \propto T_c^{1/\nu z}$, see Fig. 1.1. Here, r is the reduced distance from the quantum critical point along the quantum tuning parameter axis, $r = (g - g_c)/g_c$.

To generalize the homogeneity law (1.7) to the case of a quantum phase transition, one can consider a system characterized by a Hamiltonian $H = H_{kin} + H_{pot}$. Because the quantum Hamiltonian terms H_{kin} and H_{pot} in general do not commute, the partition function does not factorize, $Z \neq Z_{kin} Z_{pot}$. However, the canonical density operator $e^{H/k_B T}$ can be reformulated to look exactly like a time evolution operator in imaginary time τ. This can be achieved by identifying $1/k_B T = \tau = -it/\hbar$ where t denotes the real time. This introduces the so-called imaginary time direction into the system.

As we will see later in this subsection, since the extension of the system in imaginary time direction is infinite at zero-temperature ($1/k_B T = \infty$), the imaginary time acts similarly to an additional spatial dimension. Using the fact that the time and the length scales are related by the dynamic critical exponent z as $\xi_\tau \sim \xi^z$, one can adapt the homogeneity relation (1.7) to the case of a quantum phase transition. It therefore reads

$$f(r, h) = b^{-(d+z)} f(r b^{1/\nu}, h b^{y_h}). \tag{1.19}$$

Comparing the homogeneity laws in a thermal case (1.7) and a quantum case (1.19) explicitly shows that a quantum phase transition in d dimension and a classical phase transition in $d + z$ spatial dimension are equivalent.

The behavior at small but finite temperatures is determined by the crossover between the quantum critical behavior at $T = 0$ and classical critical behavior at non-zero temperatures, see Fig. 1.1. The crossover from quantum to classical behavior occurs when the correlation time ξ_τ reaches $1/(k_B T)$. The quantum-classical crossover can be observed by fixing the temperature at a small finite value and tuning

the nonthermal parameter g from the quantum-disordered regime all the way to the ordered phase.

The quantum homogeneity law (1.20) can be generalized to finite temperature by including the temperature as an explicit parameter which scales like inverse time (imaginary time). Thus, the free energy reads

$$f(r,h) = b^{-(d+z)} f(rb^{1/\nu}, hb^{y_h}, Tb^z). \tag{1.20}$$

The quantum critical point also controls the so-called quantum critical region [15]. This region is located at g_c but at relatively high temperatures where the fluctuations are thermal. In this region the system is driven away from criticality at g_c by the temperature (i.e., the temperature protects the system from being singular). Therefore the temperature scaling at the quantum critical point can be observed by carrying an experiment that lowers the temperature at fixed $g = g_c$. Because statics and dynamics are coupled, the scaling properties of static quantities in the quantum critical region are also affected by the dynamical scaling exponent z of the quantum phase transition. Thus, quantum criticality is not just an abstract concept, it can be observed experimentally.

Now, we briefly demonstrate the quantum-to-classical mapping method which connects the observables of a d-dimensional quantum system to that of a $(d+1)$-dimensional classical system. Technically, this method relies on factorizing the canonical quantum partition function Z into kinetic and potential energy parts even if they are coupled (do not commute)! This can be performed as follows: One can rewrite the partition function using the Trotter decomposition [16, 17] as

$$Z = Tre^{-H/k_BT} = \lim_{N\to\infty} Z^{(N)} \tag{1.21}$$

where $Z^{(N)}$ is the N-approximant of the partition function given by

$$Z^{(N)} = Tr\left[e^{-\tau H/N}\right]^N = Tr\left[e^{-\Delta\tau H}\right]^N. \tag{1.22}$$

where $\Delta\tau = \tau/N$. The commutator of the kinetic and potential energies is obtained by including the imaginary time increment $\Delta\tau$ in the calculations which leads to

$$[\Delta\tau H_{kin}, \Delta\tau H_{pot}] = (\Delta\tau)^2[H_{kin}, H_{pot}] \approx 0. \tag{1.23}$$

Thus, since $\Delta\tau H_{kin}$ and $\Delta\tau H_{pot}$ commute to leading order in τ, the Trotter decomposition $e^{(A+B)} = e^A e^B e^{-1/2[A,B]}$ can be applied to factorizing the N-approximant of the partition function as

$$Z^{(N)} = Tr\left[e^{-\Delta\tau H_{kin}} e^{-\Delta\tau H_{pot}}\right]^N. \tag{1.24}$$

By inserting N complete sets of eigenstates for the H_{kin} terms, the partition function can be written as

$$Z^{(N)} = \sum_{\{\alpha_{j,n}\}} \prod_{n=1}^{N} e^{-\Delta\tau H_{kin}(\alpha_j)} \left\langle \{\alpha_j\}_n \left| e^{-\Delta\tau H_{pot}(\alpha_j)} \right| \{\alpha_j\}_{n+1} \right\rangle. \tag{1.25}$$

Here, n is the index of the imaginary time. To get the classical Hamiltonian of the system, we need to evaluate the off-diagonal terms (H_{pot} terms in Eqn. 1.25). As an example, consider the transverse-field Ising model,

$$H = -\sum_{<i,j>} J_{ij} S_i^z S_j^z - \sum_i h_i S_i^x, \tag{1.26}$$

one of the famous models in the theory of quantum phase transition. After the quantum-to-classical mapping, the classical Hamiltonian of the transverse-field Ising

model is found to be

$$H_{class} = -\sum_{\langle i,j\rangle,n} \tilde{J}_i S^z_{i,n} S^z_{i+1,n} - \sum_{i,n} \tilde{J}^\tau_i S^z_{i,n} S^z_{i,n+1} \tag{1.27}$$

where $\tilde{J}_i = \beta J_{ij}/N$ and $\tilde{J}^\tau_i = \ln\sqrt{\coth(\beta h_j/N)}$ are the coupling in the space and time directions, respectively.

1.2 QUENCHED DISORDER EFFECTS

Completely pure systems rarely exist in the real world and thus many investigations focus on disordered systems. Disorder can appear in various forms including impurity atoms and crystal defects. This work focuses on time-independent disorder (quenched disorder). This means the impurities and defects are frozen-in, in contrast to so-called annealed disorder which fluctuates on short time scales. Moreover, we consider weak (random-T_c or random-mass) disorder, whose main effects are spatial variations of the coupling strength.

Random-T_c disorder does not change the bulk phases qualitatively and it only affects the phase transition point. Random-T_c disorder can be considered in a LGW theory by making the bare distance from the critical point a random function of spatial position, $r \to r_0 + \delta r(x)$. For example, a d-dimensional LGW theory in the presence of disorder reads

$$F_{LGW} = \int d^d x \left[|\nabla\phi(x)|^2 + (r_0 + \delta r(x))\phi^2(x) + u\phi^4(x) - h\phi(x)\right]. \tag{1.28}$$

Adding weak, random-T_c, quenched disorder to a clean system that exhibits a phase transition raises the following questions:

(a) Will the transition remain sharp (associated with a true singularity in free energy F), or it will be smeared out?

(b) Will the order of the transition (first-order vs. continuous) change?

(c) If the transition remains sharp and continuous, does the disorder change the critical behavior quantitatively (different universality class with new exponents) or qualitatively (exotic non-power law scaling)?

(d) Does the disorder only affect the transition itself or also the behavior in its vicinity?

1.2.1. Harris Criterion. Harris [18] derived a criterion for the stability of a clean critical point against weak, random-T_c, disorder. He divided the system into blocks of volume $V = \xi^d$ [13]. Each block i behaves independently so that it has its own effective local critical temperature T_{ci} found by averaging $r + \delta r(x)$ over the volume of block i, see Fig. 1.2. Harris observed that a sharp phase transition can only occur if the standard deviation Δr of these local critical temperatures from block to block is smaller than the global distance from the critical point r. For short-range correlated disorder, the standard deviation of Δr can be found using the central limit theorem yielding $\Delta r \sim \xi^{-d/2}$. By considering the definition of $\xi \sim r^{-\nu}$ we have $\Delta r \sim r^{d\nu/2}$. Thus, a clean critical point is perturbatively stable for $r \to 0$, if the clean critical exponents fulfill the inequality $r^{d\nu/2} < r$ or $d\nu > 2$.

The behavior of the disorder strength with increasing the length scale, i.e, under coarse graining, can be used to classify critical points with quenched disorder [19, 20, 21] as:

(i) The Harris criterion is fulfilled. In this, case the relative disorder $\Delta r/r$ decreases under coarse graining, and the system becomes asymptotically homogeneous at large scales. Consequently, the critical behavior of the dirty system is *identical* to that of the clean system. An example of this class is the three dimensional Heisenberg model which has $\nu = 0.698$ [22] for both clean and dirty cases.

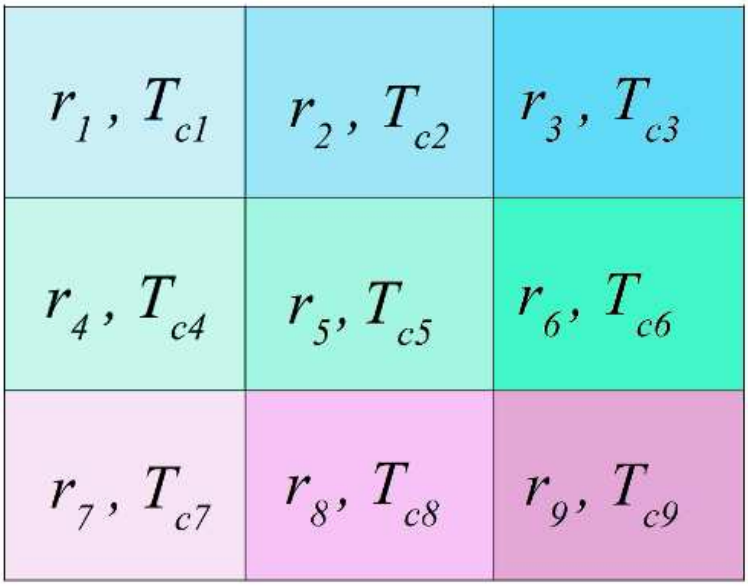

Figure 1.2: Schematic depiction of a random-T_c model shows the fragmentation of the system by disorder into independent blocks with different local critical temperature.

(ii) The relative disorder strength increases to a finite value, i.e., the system stays inhomogeneous at large length scales. In this case, quenched disorder generally makes *quantitative* changes to the critical behavior of the clean system. The phase transition stays sharp and features power-law scaling but with new critical exponents, i.e., the system is in a new universal class. The three-dimensional Ising model is an example of this class with $\nu = 0.627$ in the clean case [23] and a different value $\nu = 0.684$ in the disordered one [24]. Note that the new value of $\nu = 0.684$ satisfies the inequality $d\nu \geq 2$.

(iii) The relative disorder strength increases without limit under coarse graining. In this class, quenched disorder makes *qualitative* changes to the critical behavior of the clean system, i.e., the scaling is qualitatively modified to be exponential instead of power-law. This class was first found in the McCoy-Wu model [25, 26] (two-dimensional Ising model with disorder perfectly correlated in one dimension) or in the one-dimensional random quantum Ising model.

The critical point of class (iii) is known as an infinite-randomness critical point [19, 27, 28]. Its macroscopic observables have extremely broad probability distributions whose widths diverge with system size. Consequently, the averages of the observables are dominated by rare events, e.g., spatial regions with atypical disorder configurations. This type of critical point was fully understood only when Fisher [28] solved the random transverse-field Ising chain using the Ma-Dasgupta-Hu real space renormalization group [29, 30].

1.2.2. Rare Regions and Griffiths Effects. In the last subsection, it was mentioned that if the critical point belongs to Harris class (iii), it will be dominated by rare events. In this subsection, we explain the physics of these rare events in more detail, using a diluted classical ferromagnet as an example. The random dilution reduces the clean system's critical temperature T_{c0} to T_c. In a sufficiently large system, one can find arbitrarily large regions that are devoid of impurities and are known as *rare regions* (RR), see Fig. 1.3. For temperatures between the clean and disordered critical temperatures, these regions show local magnetic order even though the bulk system is globally in the paramagnetic phase (disordered phase). Griffiths [31] found that these rare regions lead to a singularity in the free energy, the Griffiths singularity, in the entire temperature range $T_c < T < T_{c0}$ which is now known as the Griffiths region or Griffiths phase [32]. Analogous singularities also exists on the ordered side of T_c. The probability of finding a rare region depends on its volume V_{RR} as $P(V_{RR}) \sim \exp(-pV_{RR})$ where p depends on the impurity concentration. In addition, the dynamics of rare regions are very slow because flipping them requires a coherent change of the order parameter over a large volume V_{RR}. In classical systems with short-ranged disorder, the Griffiths singularity in the free energy is only an essential one [33, 34, 35, 36] implying very weak thermodynamic Griffiths effects. The rare regions effects can be qualitatively increased by long-range correlated disorder. In particular, if the disorder is perfectly correlated in some spatial direction, the rare regions are extended objects in space which generally enhances their effects.

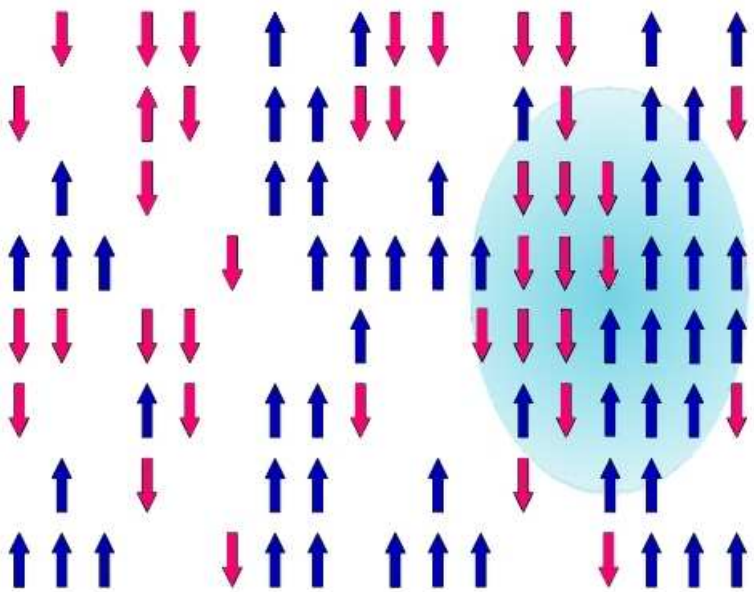

Figure 1.3: Sketch of a diluted magnet. The shaded region is devoid of impurities and therefore acts as a piece of the clean bulk system.

The significance of rare regions in a given system can be characterized based on the competition between their probability $P(V_{RR})$ and their contributions to the thermodynamic observables. We know how their probability exponentially depends on their volume, $P(V_{RR}) \sim \exp\left(-pL_{RR}^{d}\right)$, so we need to know how the thermodynamic quantities depend on L_{RR}. For this purpose, let us consider a rare region that is locally in the ordered phase. Its bare distance from criticality in the LGW theory is $r < 0$. Three different scenarios emerge depending on the effective dimensionality d_{RR} of the rare regions [21, 37]:

(i) For $d_{RR} < d_c^-$, the rare region can not undergo the phase transition by itself. Thus, its *renormalized* distance from criticality $\tilde{r}(L_{RR}) > 0$ decreases as a power of L_{RR} for $L_{RR} \to \infty$. Therefore, the contributions of the rare region to the thermodynamic quantities increase at most as power-laws in L_{RR} which can not overcome the exponential reduction in $p(V_{RR})$. Thus, all the rare regions effects are exponentially weak at the critical point.

(ii) For $d = d_c^-$, the rare region still can not undergo the phase transition by itself but the renormalized distance form the criticality $\tilde{r}$ decreases exponentially with V_{RR}. Its contributions to observables therefore grow exponentially with L_{RR} which can overcome the suppression in $P(V_{RR})$. The resulting effect is that the rare regions dominate the critical point leading to exotic exponential scaling (e.g., infinite-randomness critical point of McCoy-Wu model) and power-law (quantum) Griffiths singularities.

(iii) For $d_{RR} > d_c^-$, the rare region can undergo the phase transition by itself and independently from the bulk system. This case implies that the dynamics of the locally ordered rare regions completely freezes leading to a true static order parameter. Because the transition point depends on L_{RR} (see section 1.2.3), different rare regions can order at different values of the control parameter. These local phase transitions destroy the sharpness of the global second-order phase transition leading to a smeared phase transition. The ordered phase features an exponential tail. The three-dimensional Ising model with planar defect (layered Ising model) is an example of such behavior [38, 39, 40].

Indications of quantum Griffiths singularities (class ii) were recently observed in experiments on some metallic systems such as magnetic semiconductor $Fe_{1-x}Co_xS_2$ [41, 42, 43], Kondo lattice ferromagnet $CePd_{1-x}Rh_x$ [44, 45], and transition metal ferromagnet $Ni_{1-x}V_x$ [46, 47].

1.2.3. Smeared Phase Transition. In the last subsection, we have seen that disorder smears the global phase transition if the rare regions can undergo the transition independently, i.e., if their dimensionality $d_{RR} > d_c^-$. This can happen both for thermal phase transitions (see e.g., [38, 39, 40]) and for quantum phase transitions (see e.g., [48, 49, 50]).

The first route to a smeared phase transition involves extended defects. At nonzero temperatures (i.e., for thermal transitions), a rare region can only undergo

a true phase transition if it is infinitely large in at least one dimension. Thus, the smearing of the thermal phase transition requires extended defects of a dimensionality larger than d_c^- (disorder perfectly correlated in some of the directions). For example, the layered Ising model with planar defects has rare region dimensionality $d_{RR} = 2$ larger than the lower critical dimensionality of Ising symmetry $d_c^- = 1$. This model was shown to have a smeared phase transition [39, 40]. On the other hand, the same layered system but with Heisenberg spin symmetry has $d_{RR} = d_c^- = 2$. We will show in this thesis that its transition is not smeared but sharp and governed by an infinite-randomness critical point [51].

At zero-temperature quantum phase transitions, the quantum-to-classical mapping relates the d-dimensional quantum system to a (d+1)-dimensional classical system where the extra dimension represents imaginary time τ. Quenched disorder is time-independent, thus it is perfectly correlated in time direction. These strong correlations dramatically increase the effects of the rare regions because they are infinitely extended in the time direction (see Fig, 1.4) even if they are finite in space. For example the d-dimensional random quantum Ising model maps onto a $(d+1)$-dimensional classical Ising model. Point defects in the quantum model correspond to line defects in the classical one. In this case $d_{RR} = 1 \leq d_c^-$, thus the transition is still sharp. However, line defects in the quantum model lead to plane defects in classical one and thus a smeared phase transition.

The second route to a smeared phase transition involves damping of the order parameter fluctuations and works only for zero-temperature quantum phase transitions. The damping of the order parameter fluctuations in a metal is an example of this case. This damping is caused by the coupling between the magnetic modes and the gapless particle-hole excitations in the metal. Quantum phase transitions in metals are theoretically approached by the so-called Hertz-Millis theory [14, 52] which can be derived from an appropriate microscopic Hamiltonian of interacting electrons. By integrating out the fermionic degrees of freedom in the partition function in favor of

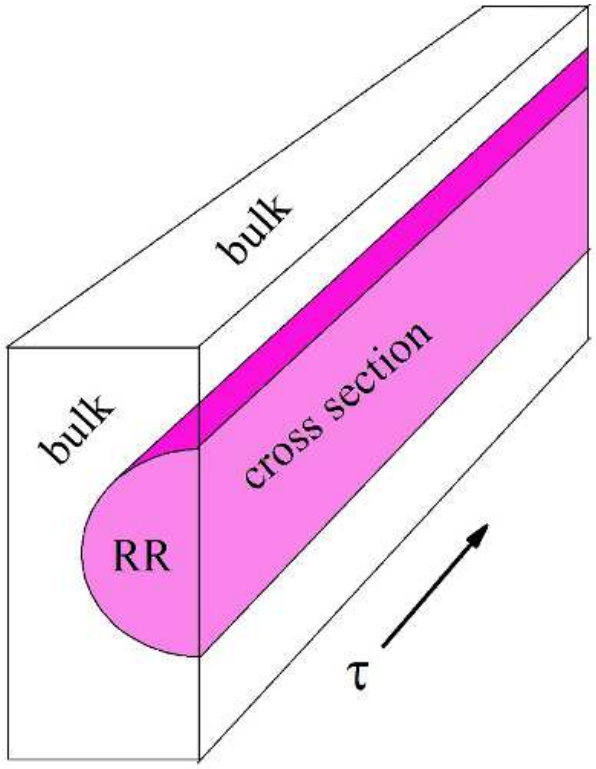

Figure 1.4: Sketch of the rare region in a quantum system. The rare region is perfectly correlated in imaginary time direction τ.

the order parameter field ϕ, one can obtain the free energy functional $S[\phi]$. Assuming that the resulting free energy functional $S[\phi]$ can be expanded in a power series in the order parameter field ϕ with spatially local coefficients yields a $(d+1)$-dimensional Landau-Ginzburg-Wilson (LGW) order parameter field theory [53, 54, 55, 56]. For definiteness, let us consider the itinerant antiferromagnetic transition at $d > 2$. The Landau-Ginzburg-Wilson free energy functional of the clean transition reads [14]

$$S = \int d^d x d^d y d\tau d\tau' \phi(\mathbf{x}, \tau) \Gamma(\mathbf{x}, \tau, \mathbf{y}, \tau') \phi(\mathbf{y}, \tau') + u \int d^d x d\tau \phi^4(\mathbf{x}, \tau) \tag{1.29}$$

where $\Gamma(\mathbf{x}, \tau, \mathbf{y}, \tau')$ is the bare interaction (bare two-point vertex) and its Fourier transform has a linear dependence on the Matsubara frequency ω_n as

$$\Gamma(\mathbf{q}, \omega_n) = r + \xi_0 \mathbf{q}^2 + \gamma(\mathbf{q}) |\omega_n|. \tag{1.30}$$

Here, r is the bare distance from criticality, ξ_0 is a microscopic length scale, and the dynamic term $\gamma(\mathbf{q})|\omega_n|$ accounts for the damping of the order parameter fluctuations due to the excitation of fermionic particle-hole pairs. This linear dependence on ω_n implies that the so-called Landau damping is Ohmic. In contrast, undamped dynamics would lead to an ω_n^2 term.

Weak, random-mass disorder can be introduced by making r a random function of position, $r \to r_0 + \delta r(x)$ [14, 57]. The rare regions in this system are large spatial regions where the local r is smaller than its average value. The significant difference between the itinerant magnets and localized spin systems is in the dynamics of the rare regions. Millis, Morr, and Schmalian [58, 59] explicitly calculated the tunneling rate of a locally ordered rare region in an itinerant Ising magnet. Their results showed that the tunneling rate vanishes for sufficiently large rare regions. This means, these rare regions completely stop tunneling, and thus they undergo a true phase transition. In other words, the low-energy behavior changes qualitatively in the presence of damping. In particular, each locally ordered cluster (Griffiths rare region) corresponds to a dissipative two-level system [60] whose dissipation strength increases with its size. This model undergoes a quantum phase transition from a fluctuating ground state (weak dissipation) to a localized ground state (strong dissipation). Thus, if rare regions are sufficiently large, they freeze and develop static order [58, 59]. The same result can be obtained from the quantum-to-classical mapping [48]. In the equivalent classical system (quasi-one-dimensional Ising model), the rare region is finite in the space directions and infinite in the time-like direction. The linear frequency dependence in the two-point vertex Γ is equivalent to a long-range interaction in imaginary time of the form $(\tau - \tau')^{-2}$. Each rare region is thus equivalent to one-dimensional Ising model with a $1/x^2$ interaction. This model is known to have a phase transition [61, 62]. Thus, true static order can develop on those rare regions which are locally in the ordered phase. As a result, the global phase transition

in the itinerant Ising magnet is smeared [48] by the same mechanism as the transition in a classical Ising model with planer defects.

Moreover, smeared phase transitions can be modified by short-range spatial disorder correlations (changes in the exponents that characterize the order parameter and the critical temperature), thus systems with uncorrelated disorder and short-range correlated disorder behave differently [63]. This stems from the fact that forming Griffiths rare-regions is easier in case of short-range correlated disorder than for uncorrelated disorder leading to an enhancement of the smeared phase transition's tail. It is in contrast to continuous phase transitions, where both uncorrelated and short-range correlated disorder lead to the same critical point. The reason is that smeared phase transitions are governed by a finite length scale (the minimum size of ordered rare region) whereas the critical behavior emerges at infinitely large length scales.

1.2.4. Rounding of First-Order Phase Transitions. All previous discussions about quenched disorder effects were based on assuming that the clean system undergoes a second-order phase transition. Thus, the obvious question is what are the effects of quenched disorder on a first-order phase transition? As first-order phase transitions are characterized by phase coexistence, we can ask, is macroscopic phase coexistence at the transition point still possible in the presence of disorder?

Imry and Ma [64] first attacked this question by extending Peierls argument * [65, 66] to the case with randomness. They noticed that disordered systems tend to lower their free energy by forming domains of the competing phases. The free energy difference due to forming a domain contains two contributions, bulk and surface terms.

Consider a clean system undergoing a first-order phase transition between phases A and B. At the transition point, the Gibbs free energy densities are identical $f_A = f_B = f_0$. In the presence of disorder, one phase is locally preferred over the

*in order to deform the ground state $\{\uparrow\}$ in the interior of a contour $\mathcal{C}$ to another ground state $\{\downarrow\}$ costs a "surface energy" $2|\mathcal{C}|$, while by symmetry, the "bulk energies" of the two ground states are the same.

other

$$f_A(x) = f_0 + \delta f(x), \qquad f_B(x) = f_0 - \delta f(x) \tag{1.31}$$

where $\delta f(x)$ is a random quantity with standard deviation ω. The domain wall between the A and B phases has a surface energy (energy per area) σ. For an Ising magnet, the surface energy between the up and down phases at low temperatures is $\sigma = 2J$. The free energy density $f_d = f_{surf} + f_{bulk}$ of a domain of size L_d is given by

$$f_d = \frac{\sigma}{L_d} - \frac{\omega}{L_d^{d/2}}. \tag{1.32}$$

The first term is the domain wall energy. The second term stems from aligning the domain with the average $\delta f(x)$; the $L_d^{d/2}$ dependence stems from the central limit theorem.

To find the minimum size L_d^{min} for a stable ordered phase, one can differentiate the free energy density, Eqn. 1.32, with respect to L_d to get

$$L_d^{min} = \left(\frac{2}{d}\frac{\sigma}{\omega}\right)^{\frac{2}{2-d}}. \tag{1.33}$$

For $d > 2$, the surface term dominates with an unphysical peak at L_d smaller than the lattice space a; and the minimum free energy can be reached only at $L_d^{min} \to \infty$, see Fig. 1.5. Thus, the formation of finite-size domains is unfavorable, and quenched disorder does not round the first-order phase transition for $d > 2$. If $d < 2$, the minimum free energy occurs for finite domains with typical linear size L_d^{min}. Consequently, disorder prevents macroscopic phase coexistence, and thus destroys the first-order phase transition. Often, this results in a continuous phase transition, but other scenarios such as intermediate phases or a complete destruction of the transition cannot be excluded. For $d = 2$, the two parts of free energy density f_d compete and a more rigorous analysis is required. Aizenman and Wehr [67] rigorously proved

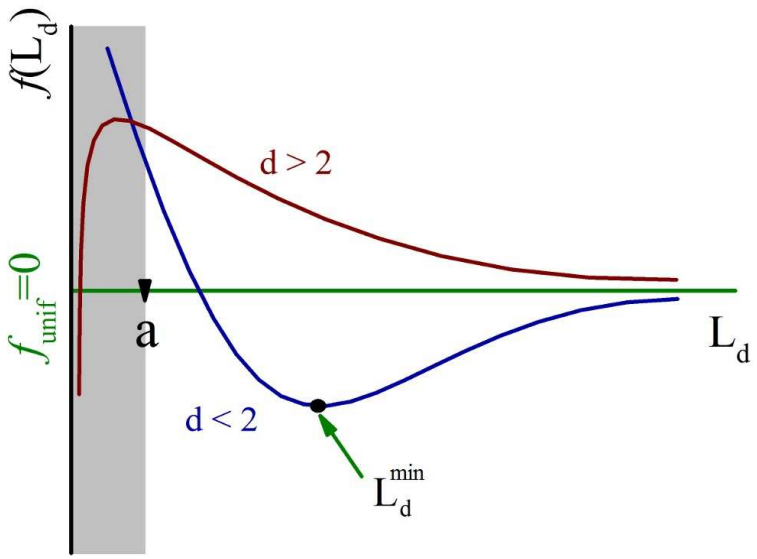

Figure 1.5: Sketch of the free energy density vs. domain linear size.

that phase coexistence cannot be found for $d \leq 2$. Greenblatt et al. [68] extended the Aizenman-Wehr theorem to quantum systems at zero temperature.

1.3 RENORMALIZATION GROUP THEORY

The renormalization group is a theoretical framework for investigating how the properties of a physical system change with changing length scale. Coarse graining to larger length scales introduces a mapping of the physical system onto itself but with changed parameters. The fixed points of this mapping correspond to self-similar systems. Critical points are examples of such fixed points, they are self-similar because the correlation length is infinite. The renormalization group (RG) technique for critical phenomena was inspired by the scaling concept of Kadanoff [69] and subsequently developed by Wilson [70] to be a powerful technique for the understanding of the phase transition problems.

The basic idea of the RG can be illustrated by Kadanoff's block-spin argument. As the critical point of a system is approached, its correlation length increases dramatically. Kadanoff argued that since spins are correlated over scales up to the

correlation length ξ, it is plausible to regard spins within regions up to size ξ to behave as a single block spin. Thus, one should be able to describe the physics close to the transition in terms of these block-spin variables. In this spirit, Kadanoff's real-space renormalization group procedure can be summarized as follows: (a) Divide the system into blocks of linear size $b \lesssim \xi$ where each block contains b^d spins (b) Replace each block of spins by a single spin using some coarse graining rule (c) Rescale all lengths by b to restore the original lattice space. After each RG step, the system's partition function has to retain its original form but in terms of the new couplings so that the transformed system has the same physical behavior as the original one. This RG procedure decreases the number of degrees of freedom and generates a flow in parameter space. Analyzing this flow gives access to the critical behavior.

1.3.1. Strong-Disorder Renormalization Group Technique. Conventional RG methods only treat the evolution of a small number of parameters in the Hamiltonian under coarse graining. Moreover, they are often implemented in momentum space. These methods are not particularly well suited to disordered systems which are not translationally invariant and contain a large number of independent parameters. In 1979, Ma, Dasgupta, and Hu [29, 30] developed an RG method for disordered systems. Because it works the better the stronger the disorder is, this method is now called the strong-disorder renormalization group (SDRG).

The basic idea of the SDRG method is to determine the largest local energy (e.g., the strongest exchange coupling in a spin system) and the ground state of its corresponding local Hamiltonian exactly. Then we perturbatively treat the interaction of this degree of freedom with the remaining system. After neglecting the excited states of our strongest coupling, a new effective Hamiltonian arises with a reduced number of degrees of freedom. This step is iterated till we reach the desired low-energy description of the system.

D. Fisher [27, 28] successfully applied the SDRG technique to the one-dimensional random transverse-field Ising model (RTFIM)

$$H = -\sum_i J_i \sigma_i^z \sigma_{i+1}^z - \sum_i h_i \sigma_i^x \tag{1.34}$$

where he exactly calculated the critical behavior. Here, the transverse field $h_i > 0$ and the nearest-neighbor interaction $J_i > 0$ at the lattice site i are independent random variables drawn from random distributions. $\{\sigma_i^\alpha\}$ are quantum spin operators represented by Pauli matrices.

At zero temperature, in the absence of a transverse field, all the spins will be aligned in the z-direction leading to a magnetic moment μ_z. If we gradually apply a transverse field at zero temperature, tunneling events between up and down will occur due to Heisenberg uncertainty principle between σ_z and σ_x. These fluctuations are known as quantum fluctuations which lead to an order-disorder quantum phase transition (QPT) when the transverse field reaches a critical value h_c [2, 3].

1.3.2. SDRG Recursions. We start the procedure by determining the maximum local energy in the system, $\Omega = \max(J_i, h_i)$. Suppose the maximum local energy is the bond at site 2, $\Omega = J_2$. The two spins that interact via Ω like to be parallel and flip coherently. The unperturbed Hamiltonian of this segment of the system $H_\Omega = -\Omega\sigma_2^z\sigma_3^z$, has two degenerate ground states $|\uparrow_2\uparrow_3\rangle$ and $|\downarrow_2\downarrow_3\rangle$ where each is separated by the energy gap $2J_2$ from two excited states $|\uparrow_2\downarrow_3\rangle$ and $|\downarrow_2\uparrow_3\rangle$. Then, the interactions of the two adjacent spins with the transverse field, $V(h) = -h_2\sigma_2^x - h_3\sigma_3^x$, are treated in second-order degenerate perturbation theory which results in an effective Hamiltonian $H_{\text{eff}} = \text{const.} - \tilde{h}\tilde{\sigma}_2^x$ with a renormalized field

$$\tilde{h} = \frac{h_2 h_3}{\Omega}. \tag{1.35}$$

This renormalized field interacts with a single effective spin $\tilde{\sigma}_2^x$ composed of the rigidly locked connected spins σ_2 and σ_3 as a spin cluster. Then, the excited states of H_Ω are

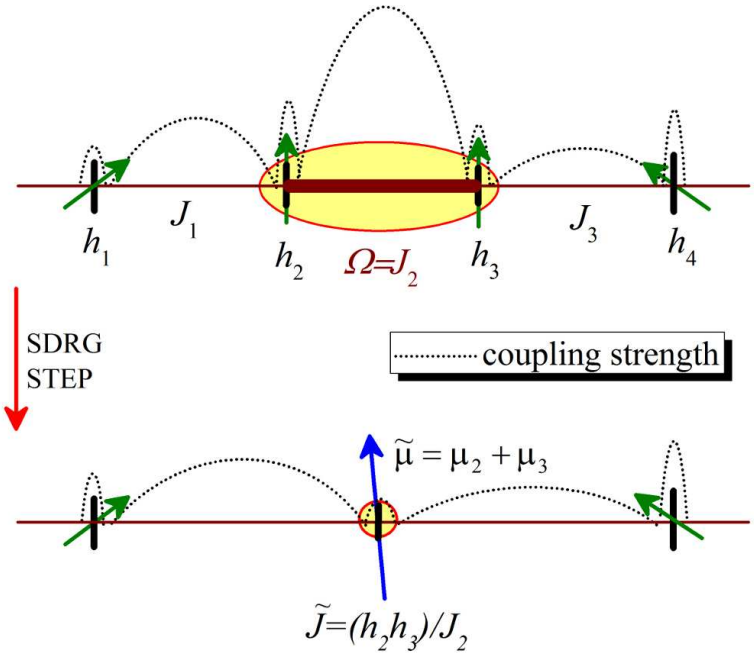

Figure 1.6: A schematic representation of a single strong disorder renormalization group step for the special case of $\Omega = J_2$. The height of the dotted line represents the coupling's (J and h) strengths.

neglected, and a new effective Hamiltonian is derived with the number of degrees of freedom reduced by one. This procedure is explained schematically in Fig. 1.6. The effective spin $\tilde{\sigma}_2$ has a renormalized magnetic moment given by

$$\tilde{\mu} = \mu_2 + \mu_3. \tag{1.36}$$

On the other hand, suppose the strongest coupling in the system is a field, say $\Omega = h_2$, therefore the local unperturbed Hamiltonian of this piece is given by $H_\Omega = -\Omega\sigma_2^x$ with ground state $|\rightarrow\rangle = \frac{1}{\sqrt{2}}|\uparrow\rangle + \frac{1}{\sqrt{2}}|\downarrow\rangle$ separated by energy gap $2h_2$ from its excited state $|\leftarrow\rangle = \frac{1}{\sqrt{2}}|\uparrow\rangle - \frac{1}{\sqrt{2}}|\downarrow\rangle$. The coupling to the nearest neighbors given by $V(J) = -J_1\sigma_1^z\sigma_2^z - J_2\sigma_2^z\sigma_3^z$ is considered as a perturbation. Because the spin at site 2 points in the x-direction, it does not contribute to the order parameter. The SDRG suggests to decimate it, leading to a direct effective interaction $\tilde{J}$ between its nearest neighbors. This procedure is explained schematically in Fig. 1.7. The

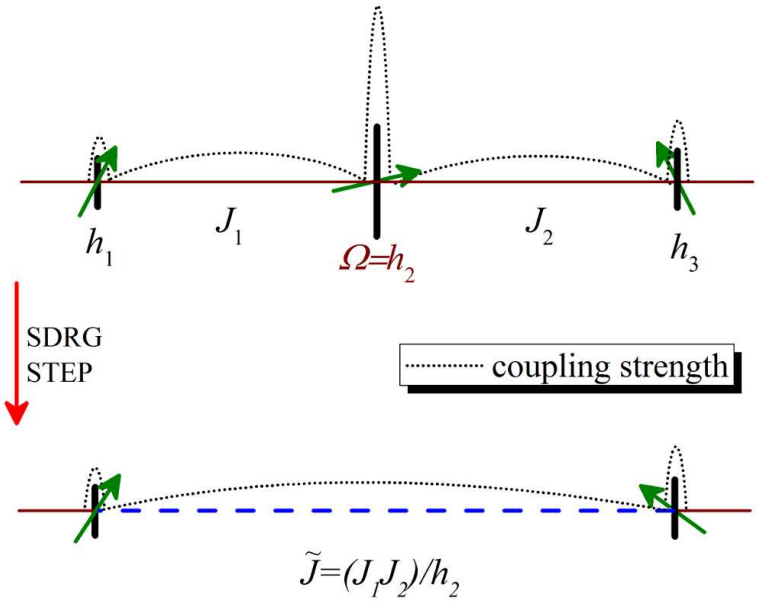

Figure 1.7: A schematic representation of a single strong disorder renormalization group step for the special case of $\Omega = h_2$. The height of the dotted line represents the couplings (J and h) strengths.

new effective coupling can be obtained from treating $V(J)$ in the second-order of perturbation theory. The result is an effective Hamiltonian $H_{\text{eff}} = \text{const.} - \tilde{J}\sigma_1^z\sigma_3^z$, and the effective coupling $\tilde{J}$ reads

$$\tilde{J} = \frac{J_1 J_3}{\Omega}. \tag{1.37}$$

Since both $\tilde{J}$ and $\tilde{h}$ are always weaker than any of the original couplings, the SDRG steps reduce the overall energy scale of the system. The quantum phase transition can be reached by iterating SDRG steps until we lower the energy level to $\Omega = T = 0$. In the paramagnetic phase, decimating sites dominates as $\Omega \to 0$. Therefore, no large cluster of spins are formed whereas in the ferromagnetic phase, gathering of sites dominates, and an infinite cluster is built at $\Omega = 0$.

1.3.3. Flow Equations. Iterating the above SDRG steps results in a renormalization of the probability distributions of the couplings (h and J) and magnetic moments μ. For the random-transverse field Ising chain, closed form solutions of the

fixed-point distributions can be found, and many physical quantities can be derived from them.

The random transverse-field Ising chain is topologically preserved and the couplings $\tilde{J}$ and $\tilde{h}$ are independent at each stage of SDRG but the probability distributions of the transverse fields, $P(h)$, and interactions, $R(J)$, evolve during the SDRG process. To describe how $P(h)$ and $R(J)$ behave as the energy scale is reduced, Fisher [28] wrote RG flow equations of these distributions. Due to the multiplicative form of the recursion relations, Fisher worked with logarithmic variables $\ln J$ and $\ln h$, and the resulting flow equations showed that the distributions get broader and broader with decreasing Ω. Therefore, the perturbative decimation approximation in the SDRG steps gradually improves with iterating the SDRG steps. In the case of an unbounded increase of the distribution's width, which is the case in RTFIM at criticality, the SDRG technique becomes asymptotically exact, and the errors made during the early stage of SDRG only affect nonuniversal coefficients but not the critical behavior. This result can be simply explained: An infinite width of the distributions means that one is very unlikely to find two neighboring couplings with high energy, thus any ratio h_i/J_i either goes to zero or to infinity.

The flow equations were solved using logarithmic variables, $\Gamma = \ln(\Omega_I/\Omega)$, $\zeta = \ln(\Omega/J)$, and $\beta = \ln(\Omega/h)$ where Ω_I is the strongest coupling initially found in the system. At the critical point $r = 0$ where $r \sim \langle \ln h \rangle - \langle \ln J \rangle$ measures the distance from criticality, the probability distributions were found analytically as

$$p(\zeta) = \frac{1}{\Gamma} e^{-\zeta/\Gamma}, \qquad R(\beta) = \frac{1}{\Gamma} e^{-\beta/\Gamma} \tag{1.38}$$

where the diverging width Γ gives the infinite-randomness critical point (IRCP) its name. Note that the couplings and the transverse fields are dual variables (RTFIM Hamiltonian is invariant under the transformations: $\sigma_i^z \sigma_{i+1}^z \to \tau_i^x$, $\sigma_i^x \to \tau_i^z \tau_{i+1}^z$, and $h_i \leftrightarrow J_i$ where $\{\tau^\alpha\}$ are the dual Pauli operators). Thus, the quantum critical point

is located at the self-duality point $r = 0$. In order to completely solve the critical behavior, the magnetic moment μ and the cluster length l have to be included in the SDRG calculations in the form of joint distributions $R(\beta, l_b : \Gamma)$ and $P(\zeta, l_s, \mu; \Gamma)$.

In addition to this fixed point at $r = 0$, there are two lines of fixed points for the ordered ($r < 0$) and the disordered ($r > 0$) Griffiths phases.

1.3.4. Summary of Key Quantities. The solution of the critical behavior is characterized by three independent critical exponents, the correlation length exponent $\nu = 2$, the tunneling exponent $\psi = 1/2$, and the exponent characterizing the moments of the clusters $\phi = (1+\sqrt{5})/2$. The correlation length exponent ν describes how the correlation length diverges when approaching the critical point via

$$\xi \sim |r|^{-\nu}. \tag{1.39}$$

On the other hand, the tunneling critical exponent ψ controls relation between length scale L and the energy scale Ω,

$$L \sim [\ln (\Omega_I/\Omega)]^{\frac{1}{\psi}}. \tag{1.40}$$

It owes its name to cluster dynamics being due to tunneling between up and down states. This activated scaling formally corresponds to dynamic critical exponent $z = \infty$ and is an indication of the qualitative change in the critical behavior due to the disorder. In other words, the flipping of spin clusters is exponentially slow with broadly distributed time scales $\ln \tau_L \sim L^{\psi}$ at the critical point. In addition, ψ describes how the density of surviving clusters n_Ω behaves with reducing the energy scale Ω. Its scaling form reads

$$n_\Omega = [\ln (\Omega_I/\Omega)]^{-d/\psi} X_n[r^{\nu\psi} \ln (\Omega_I/\Omega)] \tag{1.41}$$

where the scaling function at the critical point behaves as $X_n(0) =$ constant and thus $n_\Omega \sim [\ln(\Omega_I/\Omega)]^{-d/\psi}$. In the disordered quantum Griffiths phase, $r > 0$ and $\Omega \to 0$, the density of surviving clusters is smaller because the strongest couplings are most likely fields. Fisher found $X_n(y) \sim y^{d/\psi} e^{-\text{const.}dy}$ and thus $n_\Omega \sim r^{d\nu}\Omega^{d/z}$ where the nonuniversal dynamical exponent $z \sim r^{-\nu\psi}$ in the Griffiths phase. From the duality transformation between fields and interactions, he found $n_\Omega \sim |r|^{d\nu}\Omega^{d/z}$ in the ordered quantum Griffiths phase.

The value of the exponent ϕ was found by solving the flow equation for the probability distribution of the moments μ. Fisher found that $\phi = (1+\sqrt{5})/2$, the golden mean. The exponent ϕ characterizes the typical magnetic moment of a single cluster μ_Ω (the number of active spins) at Ω as

$$\mu_\Omega = [\ln(\Omega_I/\Omega)]^\phi X_\mu[r^{\nu\psi}\ln(\Omega_I/\Omega)]. \tag{1.42}$$

At the critical point, $\mu_\Omega \sim [\ln(\Omega_I/\Omega)]^\phi$ where the scaling function $X_\mu(0) =$ const. In the disordered quantum Griffiths phase, $\mu_\Omega \sim r^{\nu\psi(1-\psi)}\ln(\Omega_I/\Omega)$. We cannot use the duality transformation to calculate the magnetic moment in the ordered quantum Griffiths phase because it depends on the number of active spins in the surviving clusters not on the number of clusters itself. In the disordered phase, most of the surviving clusters are single spins, whereas they are effective spins in the ordered phase. Thus, the typical magnetic moment is inversely proportional to the probability density of surviving clusters yielding $\mu_\Omega \sim 1/n_\Omega \sim |r|^{-d\nu}\Omega^{-d/z}$. The scaling behavior of n_Ω and μ_Ω can be used to derive thermodynamic quantities like the entropy as $S \sim n_\Omega \ln 2$ and the magnetic susceptibility as $\chi \sim n_\Omega \mu_\Omega^2/T$.

1.4 KOSTERLITZ-THOULESS TRANSITION

All phase transitions we have considered so far were order-disorder transitions that separate a phase without long-range order from a long-range ordered and

symmetry-broken phase. In this section, we discuss a kind of phase transition that does not involve long-range order.

1.4.1. General Features of the XY Model. Classical lattice spin systems can be characterized by two parameters: the dimensionality of the underlying lattice d and the symmetry of the spin space (the number n of its components). Here, $n = 1$ for Ising models, $n = 2$ for XY models, and $n = 3$ for Heisenberg models. In this section we will focus on the case $d = 2$ and $n = 2$, i.e., on the 2D XY model which is particularly interesting. The XY spin at any lattice point can be described by a unit vector in the XY-plane as $\vec{\mathbf{S}}_i = (\cos(\theta_i), \sin(\theta_i))$. The Hamiltonian of this model can be written as

$$H_{XY} = -\sum_{<i,j>} J_{i,j}\vec{\mathbf{S}}_i \cdot \vec{\mathbf{S}}_j = -\sum_{<i,j>} J_{i,j}\cos(\theta_i - \theta_j) \tag{1.43}$$

where J_{ij} is a ferromagnetic interaction between the spins, and $(\theta_i - \theta_j)$ is the phase difference between the spins at neighboring sites i and j. Notice that the Hamiltonian is invariant under any global rotation of all spins and thus has a $O(2)$ symmetry (equivalently, we can consider the spin components as real and imaginary part of a complex variable giving $U(1)$ symmetry). Unlike the Ising model, this system has an infinite number of ground states because any uniform alignment, see Fig. 1.8, of the spins is a ground state regardless of its direction in the XY-plane. In addition to planar magnets, superfluids, and superconducting thin films are known as physical realizations of the 2D XY model. These systems have a complex order parameter ψ which represents the boson or Cooper pair "condensate wavefunction". So, the order parameter can either be viewed as a two-dimensional vector $\langle\vec{\mathbf{S}}\rangle = S(\cos(\theta), \sin(\theta))$ or a complex number $\langle\psi\rangle = |\langle\psi\rangle|e^{i\theta}$ where θ is its respective phase or direction.

Let us now consider nonuniform spin configurations. Assuming the direction of spins to be slowly varying across the lattice, see Fig. 1.9, we can expand the free energy in powers of $\vec{\nabla}\theta$. Because the minimum free energy of the system occurs at

any uniform θ, the free energy F is not expected to have a linear term of $\vec{\nabla}\theta(\vec{x})$. Thus, to leading order in $\nabla\theta(\vec{x})$, we obtain

$$F_{el} = \frac{1}{2}\int \rho_s[\vec{\nabla}(\theta)]^2 d^2x. \tag{1.44}$$

where ρ_s is known as the spin-wave stiffness or helicity modulus in magnetic systems or the superfluid density in superfluids. This quantity is a measure of the change in the energy due to the spatially varying order parameter, and it has the units of $[energy]/[length]^{d-2}$.

In order to obtain the free energy, we need to minimize the elastic free energy, Eqn. 1.44 with respect to the order parameter $\theta(\vec{x})$, this gives

$$\frac{\delta F_{el}}{\delta\theta(\vec{x})} = -\rho_s\vec{\nabla}^2\theta(\vec{x}) = 0. \tag{1.45}$$

There are two types of solutions for this equation: The first type is $\theta(x) = \vec{a}\cdot\vec{x} + b$, and the second type of solutions consists of vortices centered by defect point, see subsection (1.4.3) for more details. Assume we have a system with boundary conditions $\theta(x = 0) = 0$ and $\theta(x = L) = \theta_0$. Solving (1.45) under the boundary conditions gives $\theta(x) = \theta_0 x/L$ and the elastic free energy thus reads $F_{el} = \frac{1}{2}\rho_s\theta_0^2 L^{d-2}$.

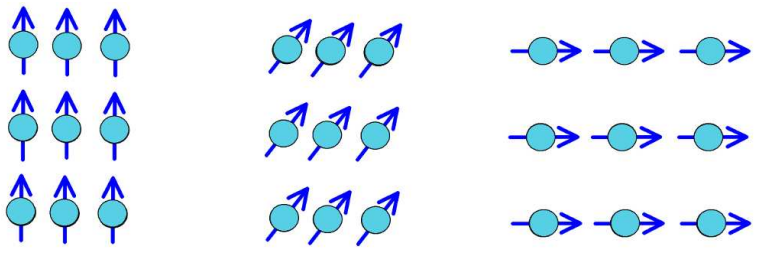

Figure 1.8: Different ground states for the XY-Hamiltonian represented by spin configurations with a spatially uniform θ.

For two-dimensional XY system, the elastic free energy becomes

$$F_{el} = \frac{1}{2}\rho_s\theta_0^2. \tag{1.46}$$

1.4.2. Kosterlitz-Thouless Transition. We now discuss the phases and transitions of the 2D XY model in detail. At sufficiently high temperatures, the system is in a conventional paramagnetic phase. At zero temperature one might expect a long-range ferromagnetic phase similar to the one in the 3D XY model. However, in 1966 Mermin and Wagner [71] showed that two-dimensional systems having an order parameter with continuous symmetry do not have any long-rage ordered phase, i.e., the expectation value of the order parameter vanishes for all non-zero temperatures. In 1973, Kosterlitz and Thouless [72] suggested that the low-temperature phase of the 2D XY model is actually quasi-long range ordered which implies that the order parameter correlation function behaves as

$$G(\mathbf{x}) \sim |\mathbf{x}|^{-\eta(T)}. \tag{1.47}$$

for large distances $|\vec{x}|$. The exponent $\eta(T)$ is not universal. This vanishing of the correlation function as $\mathbf{x} \to \infty$ implies that there is no true long-range order in agreement with the Mermin-Wagner theorem. On the other hand, the decay of the correlation function in the low-temperature phase is much slower than the exponential

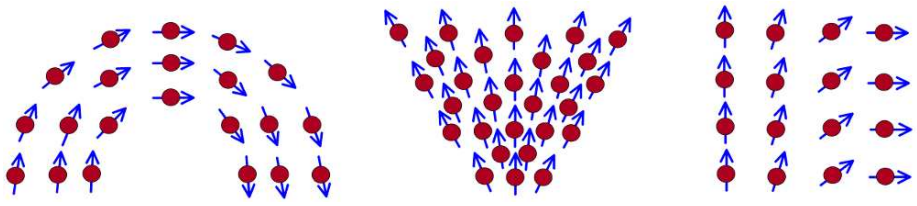

Figure 1.9: Spin configurations with a spatially non-uniform θ.

decay

$$G(\mathbf{x}) \sim e^{-\frac{|X|}{\xi(T)}} \tag{1.48}$$

in the high-temperature phase.

Although the 2D XY system has no true long-range order, the decay of the correlation function changes its behavior from power-law at low temperatures to exponential decay at higher temperatures. Therefore, there is a phase transition that happens when the correlation function changes its behavior. This transition is known as the Kosterlitz-Thouless (KT) phase transition and its transition temperature is known as T_{KT}.

1.4.3. Vortices. A critical role in the Kosterlitz-Thouless transition is played by the vortices which are singular solutions of Eqn. (1.45). A vortex can be thought of as a topological defect with vanishing order parameter in the center and a singularity in the phase $\theta(\vec{x})$ ($\nabla\theta(\vec{x}) = 1/|\vec{x}|$ is finite everywhere except at the center). The vorticity of the vortex n can be found by a line integral along a counter-clockwise contour surrounding the vortex center,

$$\oint \nabla\theta \cdot dl = 2\pi n \tag{1.49}$$

where n is an integer number and also called the winding number. If $n \geq 1$, the topological defect is called a vortex while if $n \leq -1$, it is an excitation known as an antivortex, see Fig. 1.10.

The elastic cost to create a vortex of vorticity n in a system of size L can be found by substituting $\nabla\theta(\vec{x}) = n/|\vec{x}|$ in equation (1.44) to obtain

$$E_{vortex} \sim \pi n^2 \rho_s \ln \frac{L}{a} \tag{1.50}$$

where a is the lattice constant. We notice that the energy of a vortex is quadratic in the winding number n and therefore it is energetically preferable to create vortices with $|n| = 1$. Furthermore, the energy of the vortex increases logarithmically with system size L which implies that the creation of a single vortex at low temperature is very unlikely. However, free vortices gain more importance as temperature increases. The Kosterlitz-Thouless transition happens when free vortices become thermodynamically favorable. To estimate T_{KT}, Kosterlitz and Thouless considered an energy-entropy argument by pointing out that the energy and the entropy depend on the system size in the same manner. Since there are $(L/a)^2$ available positions for the vortices, the entropy can be found as $S = 2k_B \ln(L/a)$. Thus, the free energy cost to introduce a single vortex with $n = \pm 1$ is

$$F_{vortex} \sim [\pi n^2 \rho_s - 2k_B T] \ln \frac{L}{a}. \tag{1.51}$$

Therefore, in the thermodynamic limit $L \to \infty$, free vortices can not be created spontaneously for temperatures $T < \pi\rho_s/(2k_B)$ since in this limit $F_{vortex} \to \infty$. However, at $T > \pi\rho_s/(2k_B)$ the system decreases its free energy by creating free

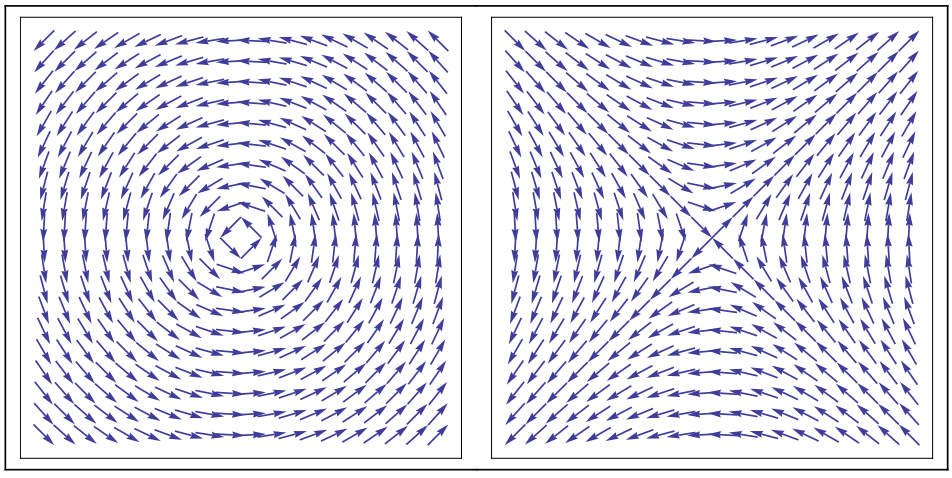

Figure 1.10: (left) Spin vortex with vorticity greater than 0. (right) Spin antivortex with vorticity smaller than 0.

vortices because $F_{vortex} \to -\infty$ as $L \to \infty$. This temperature at which the Helmholtz free energy changes its sign is equal to the transition point T_{KT}.

On the other hand, the free energy change due to forming a vortex-antivortex pair can be found to be

$$E_{pair} \sim 2\pi\rho_s \ln \frac{a}{d} \tag{1.52}$$

where $d > a$ is the distance between the vortex centers. This energy remains finite in the thermodynamic limit. Therefore, for low temperatures thermal excitations are generated in the form of bound vortex-antivortex pairs interacting via a logarithmic potential. At the Kosterlitz-Thouless transition, these pairs break down and free vortices proliferate by a mechanism known as vortex-antivortex unbinding, see Fig. 1.11.

1.4.4. Properties of the Kosterlitz-Thouless Transition. Here, we discuss some properties of the KT transition in a 2D clean XY model. The effect of the thermally activated vortex pairs is described by the temperature dependent spin wave stiffness ρ_s. One of the main features of the KT transition in an isotropic XY model is the universal jump in the spin-wave stiffness at T_{KT} where the spin-wave stiffness jumps discontinuously to zero. The spin wave stiffness describes how much free

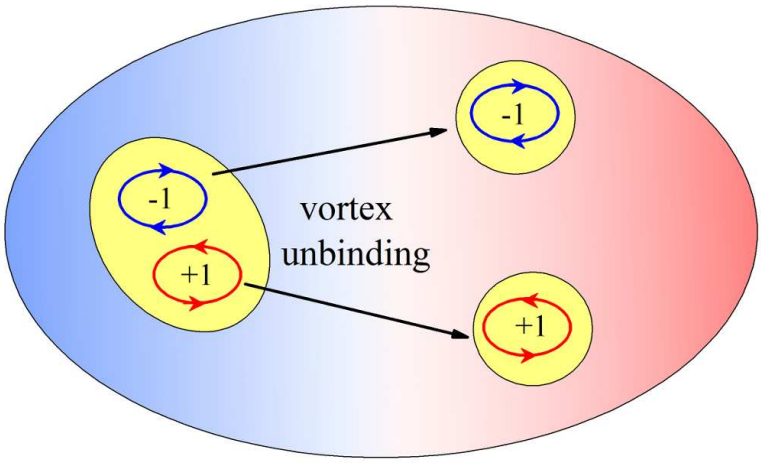

Figure 1.11: Vortex unbinding drives the Kosterlitz-Thouless phase transition at T_{KT}.

energy it costs to apply a twist to the boundary conditions to the spins. From equation (1.51), we see that this spin-wave stiffness has a universal value $\rho_s = 2k_B T_{KT}/\pi$ at the transition point. Thus, macroscopic twists of the spin direction cost energy only if $T < T_{KT}$.

In the high temperature phase but close to the transition, the correlation length diverges rapidly as [72]

$$\xi(T) = Ae^{B|T-T_{KT}|^{-1/2}}. \tag{1.53}$$

Here, A and B are non-universal constants. In addition, the order parameter susceptibility can be analogously found as [72]

$$\chi(T) \propto \xi^{2-\eta} \propto e^{D|T-T_{KT}|^{-1/2}}. \tag{1.54}$$

Here, η is the correlation function critical exponent and $D = (2-\eta)B$. The correlation function critical exponent has the same universal value as in the two-dimensional Ising model [73], $\eta = 1/4$. However, the conventional critical exponents ν and γ can not be defined since ξ and χ diverge faster than any power of $T - T_c$.

If we consider an anisotropic 2D XY model, the behavior of the spin wave stiffnesses in the x-direction is different from that in the y-direction. Thus, we need another parameter to study the universality of the KT transitions in anisotropic 2D XY models. It turns out that even though the individual stiffnesses are not universal, their product is universal. Moreover, because the 2D XY model is equivalent to the quantum-to-classical mapping of a one-dimensional bosonic system [74], the Luttinger parameter $g = \pi\sqrt{\rho_s \kappa}$ turned out to be a suited choice to study the anisotropic 2D XY model. Here, κ is the compressibility. In particular, under this quantum-to-classical mapping, the compressibility κ maps onto the spin-wave stiffness ρ_τ in the time-like direction of the classical XY model. Thus, the Luttinger parameter in a classical

anisotropic 2D XY model reads

$$g = (\pi/T)\sqrt{\rho_s \rho_\tau}. \tag{1.55}$$

It is found to have a universal value of 2 at T_{KT}.

PAPER

I. INFINITE-RANDOMNESS CRITICALITY IN A RANDOMLY LAYERED HEISENBERG MAGNET

Fawaz Hrahsheh, Hatem Barghathi, and Thomas Vojta

[1] *Department of Physics, Missouri University of Science & Technology, Rolla, MO 65409*

ABSTRACT*

We study the ferromagnetic phase transition in a randomly layered Heisenberg magnet using large-scale Monte-Carlo simulations. Our results provide numerical evidence for the infinite-randomness scenario recently predicted within a strong-disorder renormalization group approach. Specifically, we investigate the finite-size scaling behavior of the magnetic susceptibility which is characterized by a non-universal power-law divergence in the Griffiths phase. We also study the perpendicular and parallel spin-wave stiffnesses in the Griffiths phase. In agreement with the theoretical predictions, the parallel stiffness is nonzero for all temperatures $T < T_c$. In contrast, the perpendicular stiffness remains zero in part of the ordered phase, giving rise to anomalous elasticity. In addition, we calculate the in-plane correlation length which

*Published in Physical Review B **84** 184202 (2011).

diverges already inside the disordered phase at a temperature significantly higher than T_c. The time autocorrelation function within model A dynamics displays an ultraslow logarithmic decay at criticality and a nonuniversal power-law in the Griffiths phase.

1. INTRODUCTION

When weak quenched disorder is added to a system undergoing a *classical* continuous phase transition, generically the critical behavior will either remain unchanged or it will be replaced by another critical point with different exponent values. Which scenario is realized depends on whether or not the clean critical point fulfills the Harris criterion.[18] In contrast, zero-temperature quantum phase transitions generically display much stronger disorder phenomena including power-law quantum Griffiths singularities, [75, 76, 77] infinite-randomness critical points featuring exponential instead of power-law scaling, [27, 28] and smeared phase transitions.[48, 49] A recent review of these phenomena can be found in Ref. [21], while Ref. [20] focuses on metalic systems and also discusses experiments.

The reason for the disorder effects being stronger at quantum phase transitions than at classical transitions is that quenched disorder is perfectly correlated in the *imaginary time* direction. Imaginary time behaves as an additional dimension at a quantum phase transition and becomes infinitely extended at zero temperature. Therefore, the impurities and defects are effectively "infinitely large" in this extra dimension, which makes them much harder to average out than the usual finite-size defects and so increases their influence.

For this reason, one should also expect strong unconventional disorder phenomena at classical thermal phase transitions in systems in which the disorder is perfectly correlated in one or more *space* dimensions. Indeed, such behavior has been observed in the McCoy-Wu model, a disordered classical two-dimensional Ising model having perfect disorder correlations in one of the two dimensions. In a series of papers, McCoy and Wu [25, 26, 78, 79] showed that this model exhibits an unusual phase transition featuring a smooth specific heat while the susceptibility is infinite over an entire temperature range. Fisher [27, 28] achieved an essentially complete

understanding of this phase transition with the help of a strong-disorder renormalization group approach (using the equivalence between the McCoy-Wu model and the random transverse-field Ising chain). He determined that the critical point is of exotic infinite-randomness type and is accompanied by power-law Griffiths singularities. In a classical Ising model with perfect disorder correlations in *two* dimensions, the disorder effects are even stronger than in the McCoy-Wu model: the sharp critical point is destroyed, and the transition is smeared over a range of temperatures.[40, 80]

Recently, another classical system with perfect disorder correlations in two dimensions was investigated by means of a strong-disorder renormalization group.[81] This theory predicts that the randomly layered Heisenberg magnet features a sharp critical point (in contrast to the Ising case discussed above). However, it is of exotic infinite-randomness type. Somewhat surprisingly, it is in the same universality class as the quantum critical point of the random transverse-field Ising chain.

In this paper, we present the results of Monte-Carlo simulations of the randomly layered Heisenberg model. They provide numerical evidence in support of the above renormalization group predictions. Our paper is organized as follows. In Sec. 2., we define our model and discuss its phase diagram. We also briefly summarize the predictions of the strong disorder renormalization group theory.[81] In Sec. 3., we describe our Monte-Carlo simulations, we present the results and compare them to the theory. We conclude in Sec. 4..

2. MODEL AND RENORMALIZATION GROUP PREDICTIONS

We consider a ferromagnet consisting of a random sequence of layers made up of two different ferromagnetic materials, see sketch in Fig. 2.1.

Its Hamiltonian, a classical Heisenberg model on a three-dimensional lattice of perpendicular size $L_\perp$ (in z direction) and in-plane size $L_\parallel$ (in the x and y directions) is given by

$$H = -\sum_{\mathbf{r}} J_z^{\parallel} \left(\mathbf{S}_{\mathbf{r}} \cdot \mathbf{S}_{\mathbf{r}+\hat{\mathbf{x}}} + \mathbf{S}_{\mathbf{r}} \cdot \mathbf{S}_{\mathbf{r}+\hat{\mathbf{y}}} \right) - \sum_{\mathbf{r}} J_z^{\perp} \, \mathbf{S}_{\mathbf{r}} \cdot \mathbf{S}_{\mathbf{r}+\hat{\mathbf{z}}}. \tag{1.1}$$

Here, $\mathbf{S}_{\mathbf{r}}$ is a three-component unit vector on lattice site $\mathbf{r}$, and $\hat{\mathbf{x}}$, $\hat{\mathbf{y}}$, and $\hat{\mathbf{z}}$ are the unit vectors in the coordinate directions. The interactions within the layers, $J_z^{\parallel}$, and between the layers, $J_z^{\perp}$, are both positive and independent random functions of the perpendicular coordinate z.

In the following, we take all $J_z^{\perp}$ to be identical, $J_z^{\perp} \equiv J^{\perp}$, while the $J_z^{\parallel}$ are drawn from a binary probability distribution

$$P(J^{\parallel}) = (1-p)\, \delta(J^{\parallel} - J_u) + p\, \delta(J^{\parallel} - J_l) \tag{1.2}$$

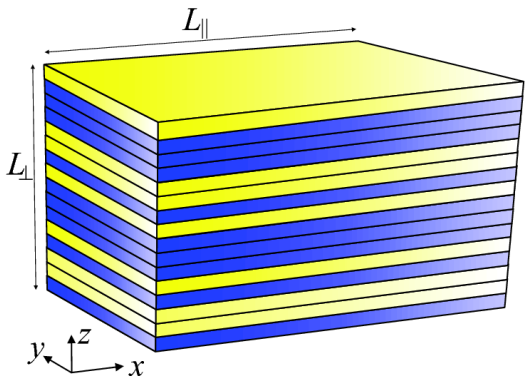

Figure 2.1: (Color online) Schematic of the layered Heisenberg magnet: It consistes of a random sequence of layers of two different ferromagnetic materials.[81]

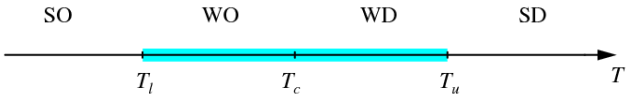

Figure 2.2: (Color online) Schematic phase diagram of the randomly layered Heisenberg magnet (1.1). SD and SO denote the conventional strongly disordered and strongly ordered phases, respectively. WD and WO are the weakly disordered and ordered Griffiths phases. T_c is the critical temperature while T_u and T_l mark the boundaries of the Griffiths phase .

with $J_u > J_l$. Here, p is the concentration of the "weak" layers while $1-p$ is the concentration of the "strong" layers.

The qualitative behavior of the model (1.1) is easily explained (see Fig. 2.2). At sufficiently high temperatures, the model is in a conventional paramagnetic (strongly disordered) phase. Below a temperature T_u (the transition temperature of a hypothetical system having $J_z^{\parallel} \equiv J_u$ for all z) but above the actual critical temperature T_c, rare thick slabs of strong layers develop local order while the bulk system is still nonmagnetic. This is the *paramagnetic* (weakly disordered) Griffiths phase (or Griffiths region). In the *ferromagnetic* (weakly ordered) Griffiths phase, located between T_c and a temperature T_l (the transition temperature of a hypothetical system having $J_z^{\parallel} \equiv J_l$ for all z), bulk magnetism coexists with rare nonmagnetic slabs. Finally, below T_l, all slabs are locally ferromagnetic and the system is in a conventional ferromagnetic (strongly ordered) phase.

In Ref. [81], the behavior in both Griffiths phases and at criticality has been derived within a strong-disorder renormalization group calculation. Here, we simply motivate and summarize the results. The probability of finding a slab of L_{RR} consecutive strong layers is given by simple combinatorics; it reads $w(L_{RR}) \sim (1-p)^{L_{RR}} = e^{-\tilde{p}L_{RR}}$ with $\tilde{p} = -\ln(1-p)$. Each such slab is equivalent to a two-dimensional Heisenberg model with an effective interaction $L_{RR}J_u$. Because the two-dimensional Heisenberg model is exactly at its lower critical dimension, the renormalized distance from criticality, ϵ, of such a slab decreases exponentially with its thickness,

$\epsilon(L_{RR}) \sim e^{-bL_{RR}}$.[21, 37] Combining the two exponentials gives a power law spectrum of locally ordered slabs,

$$\rho(\epsilon) \sim \epsilon^{\tilde{p}/a-1} = \epsilon^{1/z-1} \tag{1.3}$$

where the second equality defines the conventionally used dynamical exponent, z. It increases with decreasing temperature throughout the Griffiths phase and diverges as $z \sim 1/|T - T_c|$ at the actual critical point.

Many important observables follow from appropriate integrals of the density of states (1.3). The susceptibility can be estimated by $\chi \sim \int d\epsilon\, \rho(\epsilon)/\epsilon$. In an infinite system, the lower bound of the integral is 0; therefore, the susceptibility diverges in the entire temperature region where $z > 1$. A finite system size $L_\parallel$ in the in-plane directions introduces a nonzero lower bound $\epsilon_{\min} \sim L_\parallel^{-2}$. Thus, for $z > 1$, the susceptibility in the weakly disordered Griffiths phase diverges as

$$\chi(L_\parallel) \sim L_\parallel^{2-2/z} \tag{1.4}$$

and in the weakly ordered Griffiths phase, it diverges as

$$\chi(L_\parallel) \sim L_\parallel^{2+2/z}. \tag{1.5}$$

The strong-disorder renormalization group [81] confirms these simple estimates and gives $\chi \sim L_\parallel^2 [\ln (L_\parallel/a)]^{2\phi-1/\psi}$ at criticality where $\phi = (1+\sqrt{5})/2$ and $\psi = 1/2$ are critical exponents of the infinite randomness critical point.

The spin-wave stiffness ρ_s is defined by the work needed to twist the spins of two opposite boundaries by a relative angle θ. Specifically, in the limit of small θ and large system size, the free-energy density f depends on θ as

$$f(\theta) - f(0) = \frac{1}{2}\rho_s \left(\frac{\theta}{L}\right)^2. \tag{1.6}$$

Because the randomly layered Heisenberg model is anisotropic, we need to distinguish the parallel spin-wave stiffness $\rho_s^{\parallel}$ from the perpendicular spin-wave stiffness $\rho_s^{\perp}$. To calculate the parallel spin-wave stiffness, we apply boundary conditions at $x = 0$ and $x = L_{\parallel}$ and set $L = L_{\parallel}$ in Eq. (1.6) whereas the boundary conditions are applied at $z = 0$ and $z = L_{\perp}$ to calculate the perpendicular spin-wave stiffness with $L = L_{\perp}$ in Eq. (1.6).

Let us first discuss the parallel stiffness. In this case, the free energy difference $f(\theta)-f(0)$ is simply the sum over all layers participating in the long-range order (each having the same twisted boundary conditions). Thus, $\rho_s^{\parallel}$ is nonzero everywhere in the ordered phase. The strong-disorder renormalization group approach [81] predicts

$$\rho_s^{\parallel} \sim m \sim |T - T_c|^{\beta} \qquad\qquad (T < T_c) \tag{1.7}$$

where $\beta = (3 - \sqrt{5})/2$ is the order parameter exponent of the infinite randomness critical point.

If the twist θ is applied between the bottom ($z = 0$) and the top ($z = L_{\perp}$) layers, the local twists between consecutive layers will vary from layer to layer. Minimizing $f(\theta) - f(0)$ leads to $\rho_s^{\perp} \sim \langle 1/J_{eff}^{\perp} \rangle^{-1}$ where $J_{eff}^{\perp}$ are the effective couplings between the rare regions. Within the strong-disorder renormalization group approach, the distribution of the $J_{eff}^{\perp}$ follows a power law $p(J_{eff}^{\perp}) \sim (J_{eff}^{\perp})^{1/z-1}$. Thus, $\rho_s^{\perp} = 0$ in part of the ordered Griffiths phase. It only becomes nonzero once z falls below 1 at a temperature $T_s < T_c$. Between T_c and T_s, the system displays anomalous elasticity. Here, the free energy due to the twist scales with $f(\theta) - f(0) \sim L_{\perp}^{-1-z}$. Thus, the perpendicular stiffness formally vanishes as $\rho_s^{\perp} \sim L_{\perp}^{1-z}$ with increasing $L_{\perp}$.

To study the dynamical critical behavior, a phenomenological dynamics is added to the randomly layered Heisenberg model. The simplest case is a purely relaxational dynamics corresponding to model A in the classification of Hohenberg and Halperin.[82]

The dynamic behavior can be characterized by the average time autocorrelation function

$$C(t) = \frac{1}{L_\perp L_\parallel^2} \int d^3r \langle \mathbf{S_r}(t) \mathbf{S_r}(0) \rangle, \tag{1.8}$$

where $\mathbf{S_r}(t)$ is the value of the spin at position $\mathbf{r}$ and time t.

The behavior of $C(t)$ in the weakly disordered Griffiths phase can be easily estimated. The correlation time of a single locally ordered slab is proportional to $1/\epsilon$.[81] Summing over all slabs using the density of states (1.3) then gives

$$C(t) \sim \int d\epsilon \rho(\epsilon) e^{-\epsilon t} \sim t^{-1/z}. \tag{1.9}$$

The strong disorder renormalization group calculation [81] confirms this estimate. Moreover, at criticality, when $z \to \infty$, it gives an even slower logarithmic behavior

$$C(t) \sim [\ln(t/t_0)]^{\phi - 1/\psi}. \tag{1.10}$$

where t_0 is a microscopic length scale.

3. MONTE-CARLO SIMULATIONS

3.1. OVERVIEW. In this section we report results of Monte-Carlo simulations of the randomly layered Heisenberg magnet. Because the phase transition in this system is dominated by the rare regions, sufficiently large system sizes are required in order to get reliable results. We have simulated system sizes ranging from $L_\perp = 90$ to 800 and $L_\parallel = 10$ to 400. We have chosen $J_u = 1$ and $J_l = 0.25$ in Eq. (1.2). All the simulations have been performed for disorder concentrations $p = 0.8$. With these parameter choices, the Griffiths region ranges from $T_l \approx 0.63$ to $T_u \approx 1.443$. For optimal performance, we have used large numbers of disorder realizations, ranging from 100 to 7200, depending on the system size. While studying the thermodynamics, we have used the efficient Wolff cluster algorithm [83] to eliminate critical slowing down. We have equilibrated every run by 100 Monte-Carlo sweeps, and we have used another 100 sweeps for measurements. To investigate the critical dynamics, we have equilibrated the system using the Wolff algorithm but then propagated the system in time by means of the Metropolis algorithm [84] which implements model A dynamics.

3.2. THERMODYNAMICS . To test the finite-size behavior (1.4, 1.5) of the susceptibility, one needs to consider samples having sizes $L_\perp \gg L_\parallel$ such that $L_\perp$ is effectively infinite. We have used system sizes $L_\perp = 800$ and $L_\parallel = 10$ to 90. Figure 3.1 shows the susceptibility χ as a function of $L_\parallel$ for several temperatures in the Griffiths region between $T_l = 0.63$ and $T_u \approx 1.443$. In agreement with the theoretical predictions (1.4) and (1.5), χ follows a nonuniversal power law in $L_\parallel$ with a temperature-dependent exponent. Simulations for many more temperature values, in the range $T \approx 0.76 - 1.2$, yield analogous results.

The values of the exponent z extracted from fits to (1.4, 1.5) are shown in Fig. 3.2 for the *paramagnetic* and *ferromagnetic* sides of the Griffiths region. z can be fitted to the predicted power law $z \sim 1/|T - T_c|$, as discussed after (1.3), giving the estimate $T_c \approx 0.933$.

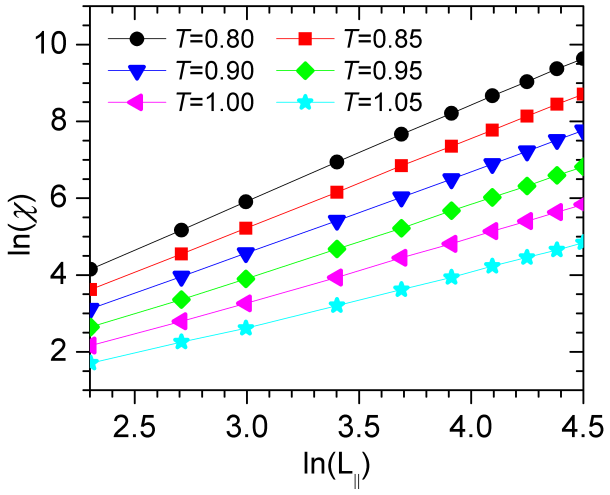

Figure 3.1: (Color online) Susceptibility χ as a function of in-plane system size $L_\parallel$ for several temperatures in the Griffiths region. The perpendicular size is $L_\perp = 800$; the data are averages over 300 disorder configurations. The solid lines are fits to the power laws (1.4, 1.5).

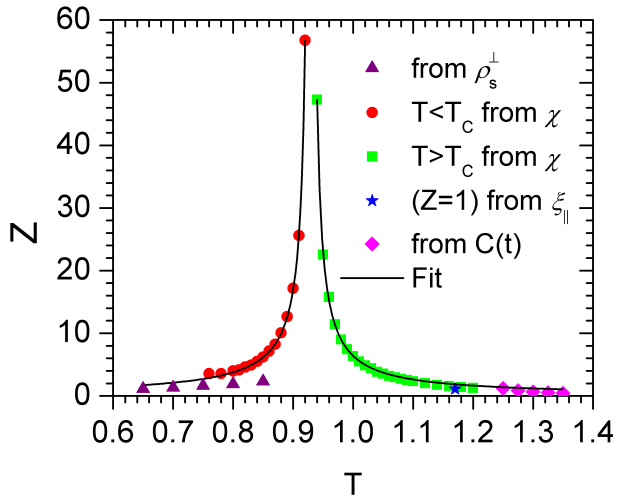

Figure 3.2: (Color online) Griffiths dynamical exponent z vs temperature. The data are extracted from the perpendicular stiffness data in Fig. 3.4b, the susceptibility data in Fig. 3.1, the parallel correlation length data in Fig. 3.3 and the autocorrelation function data in Fig. 3.5. The solid lines are a power-law fit of z (extracted from Fig. 3.1) to (1.4) and (1.5).

For a deeper understanding of the thermodynamic critical phenomena of the layered Heisenberg model, we have also studied the behavior of the in-plane correlation lengths in Griffiths phase. Figure 3.3 shows the scaled correlation length $\xi_\parallel/L_\parallel$ as a function of temperature for different values of $L_\parallel$. Surprisingly, the curves cross at

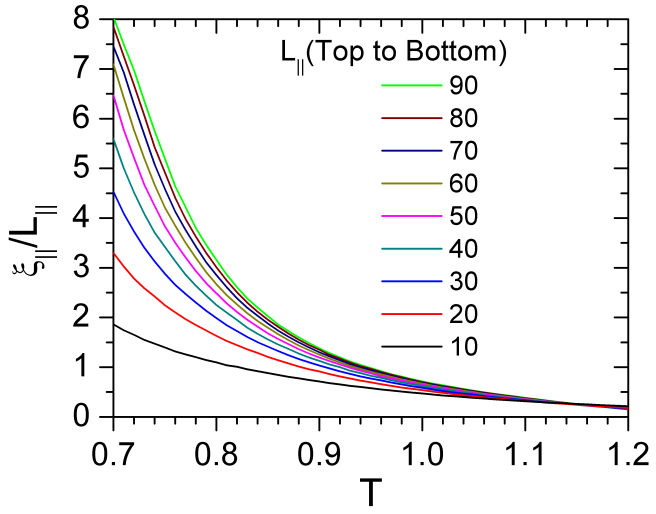

Figure 3.3: (Color online) Scaled in-plane correlation length $\xi_\parallel/L_\parallel$ as a function of temperature T for several in-plane system sizes $L_\parallel$ in the Griffiths region. The perpendicular size is $L_\perp = 800$; the data are averaged over 300 disorder configurations.

a temperature, $T \approx 1.17$, significantly higher than $T_c \approx 0.93$. This implies that the average in-plane correlation length diverges in part of the *disordered* phase.

To understand this behavior, we estimate the rare region contribution to the averaged in-plane correlation length. It can be calculated by integrating over the density of states (1.3) as

$$\xi_\parallel^2 \sim \int_0^{\epsilon_0} d\epsilon \rho(\epsilon) \xi_\parallel^2(\epsilon) \sim \int_0^{\epsilon_0} d\epsilon \epsilon^{1/z-1} \frac{1}{\epsilon} \tag{1.11}$$

where $\xi_\parallel^2(\epsilon) \sim 1/\epsilon$ is the dependence of the in-plane correlation length of a single region [81, 85] on the renormalized distance ϵ from criticality. Note that we average $\xi_\parallel^2$ instead of $\xi_\parallel$ because that is what numerically happens in the *second moment method* which defines $\xi_\parallel^2$ via

$$\xi_\parallel^2 = \frac{\sum_{\mathbf{r}} C(\mathbf{r}) \mathbf{r}^2}{\sum_{\mathbf{r}} C(\mathbf{r})} \tag{1.12}$$

with $C(\mathbf{r})$ being the spatial correlation function. The integral in (1.11) diverges for $z > 1$ and converges for $z < 1$. The in-plane correlation length therefore diverges

already in the disordered Griffiths phase at the temperature at which the Griffiths dynamical exponent is $z = 1$. From Fig. 3.3 we estimate this temperature to be $T \approx 1.17$. As can be seen in Fig. 3.2, this value is in good agreement with the result extracted from the finite size behavior of χ.

We now turn to the spin-wave stiffness. Calculating the stiffness by actually carrying out simulations with twisted boundary conditions is not very efficient. However, the stiffness can be rewritten in terms of expectation values calculated in a conventional run with periodic boundary conditions. The resulting formula which is a generalization of that used by Caffarel *et al* [86] reads

$$\begin{aligned}\rho_s^{\perp} = &\left\langle \sum_{\langle \mathbf{r},\mathbf{r}'\rangle} J_{\mathbf{r},\mathbf{r}'} \left[\mathbf{S}_{\mathbf{r}} \cdot \mathbf{S}_{\mathbf{r}'} - (\mathbf{S}_{\mathbf{r}} \cdot \hat{\mathbf{a}})(\mathbf{S}_{\mathbf{r}'} \cdot \hat{\mathbf{a}})\right] (z - z')^2 \right\rangle \\ &- \frac{1}{T} \left\langle \left(\sum_{\langle \mathbf{r},\mathbf{r}'\rangle} J_{\mathbf{r},\mathbf{r}'} \left[(\mathbf{S}_{\mathbf{r}} \times \mathbf{S}_{\mathbf{r}'}) \cdot \hat{\mathbf{a}}\right] (z - z') \right)^2 \right\rangle .\end{aligned} \tag{1.13}$$

Here, $\hat{\mathbf{a}}$ can be any unit vector perpendicular to the total magnetization $\mathbf{m}$. For $\rho_s^{\parallel}$, $(z - z')$ has to be replaced by $(x - x')$. This formula is derived in appendix A.

Figure 3.4a shows the results for the perpendicular and parallel stiffnesses of our randomly layered Heisenberg model. We have used a system of size $L_{\perp} = 100$ and $L_{\parallel} = 400$. The figure shows that the two stiffness indeed behave very differently. The parallel stiffness $\rho_s^{\parallel}$ vanishes at $T \approx 0.9 - 0.95$ in good agreement with our earlier estimate of $T_c \approx 0.93$. In contrast, the perpendicular stiffness vanishes at a much lower temperature $T \approx 0.7$. Thus, in the range between $T \approx 0.7$ and T_c, the system displays anomalous elasticity, as predicted. (Note: The slight rounding of both $\rho_s^{\parallel}$ and $\rho_s^{\perp}$ can be attributed to finite-size effects.)

The results of the perpendicular spin-wave stiffness $\rho_s^{\perp}$ are analyzed in more detail in Fig. 3.4b for perpendicular sizes $L_{\perp} = 15 - 40$. We have used a parallel size $L_{\parallel} = 400$ and a temperature range $T = 0.65 - 0.85$ where the data are averaged over 1000 disorder configurations. The plot shows a non-universal power-law dependence

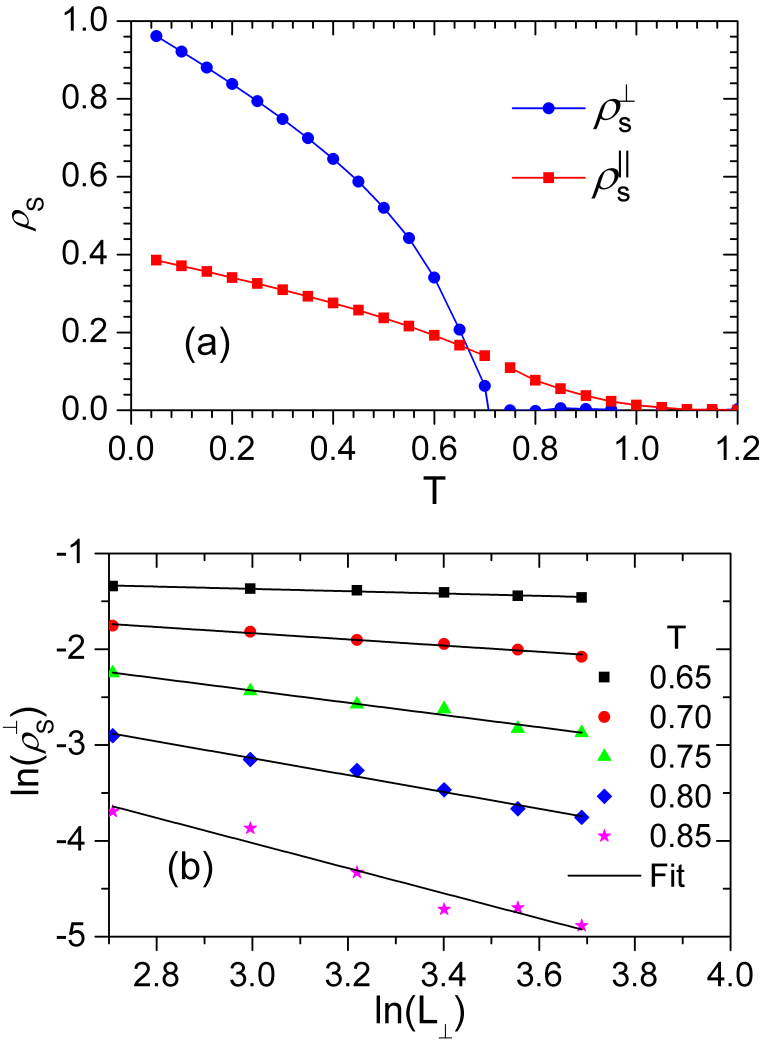

Figure 3.4: (Color online) a: Perpendicular and parallel spin-wave stiffnesses ($\rho_s^\perp$ and $\rho_s^\parallel$, respectively) as functions of temperature T for system with sizes $L_\perp = 100$ and $L_\parallel = 400$. The data are averaged over 100 disorder configurations. b: Perpendicular spin-wave stiffness as a function of $L_\perp$ for temperatures in the weakly ordered Griffiths phase and $L_\parallel = 400$. The data are averaged over 1000 disorder configurations. The solid lines are fits to (1.14).

of $\rho_s^\perp$ on $L_\perp$ which agrees with the prediction

$$\rho_s^\perp \sim L_\perp^{1-z}. \tag{1.14}$$

The dynamical exponents z extracted from fits of $\rho_s^\perp$ to (1.14) are also shown in Fig. 3.2. While they roughly agree with the values extracted from χ, the agreement is not very good. We believe this is due to the rather small $L_\perp$ values used.

3.3. CRITICAL DYNAMICS. To investigate the behavior of the autocorrelation function $C(t)$ in the weakly disordered Griffiths phase, we have used system sizes $L_\perp = 400$ and $L_\parallel = 100$ and temperatures from $T = 1.25$ to 1.35. From figure 3.5, one can see that the long-time behavior of $C(t)$ in the Griffiths phase follows a non-universal power law which is in agreement with the prediction (1.9). Fits of the data to (1.9) can be used to obtain yet another estimate of the dynamical exponent z. The resulting values are shown in Fig. 3.2, they are in good agreement with those extracted from χ.

Figure 3.6 shows the behavior of $C(t)$ near criticality plotted such that the expected logarithmic time-dependence (1.10) gives a straight line. We have used

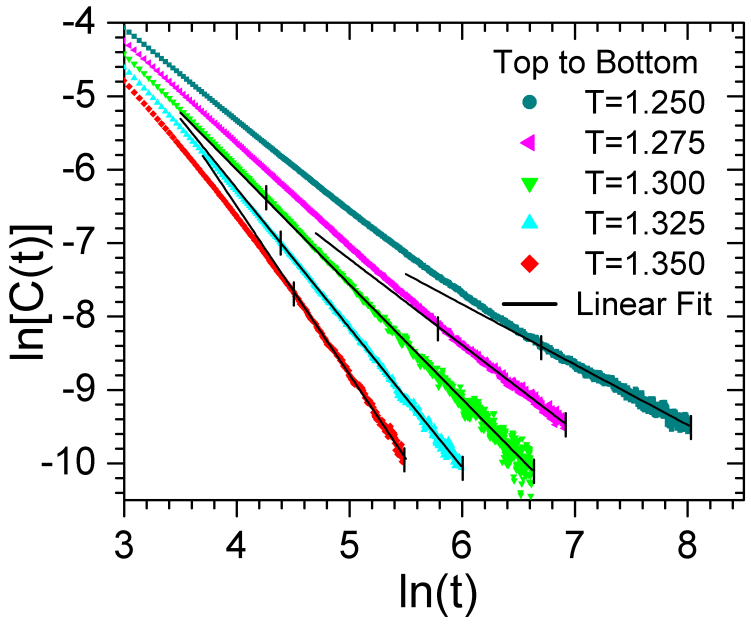

Figure 3.5: (Color online) Time autocorrelation function $C(t)$ for temperatures from $T = 1.25$ to 1.35 (within the Griffiths phase). The system sizes are $L_\perp = 400$ and $L_\parallel = 100$. The data are averaged over $1720 - 7200$ disorder configurations. The solid lines are fits to the power-law prediction (1.9) (with the fit range marked).

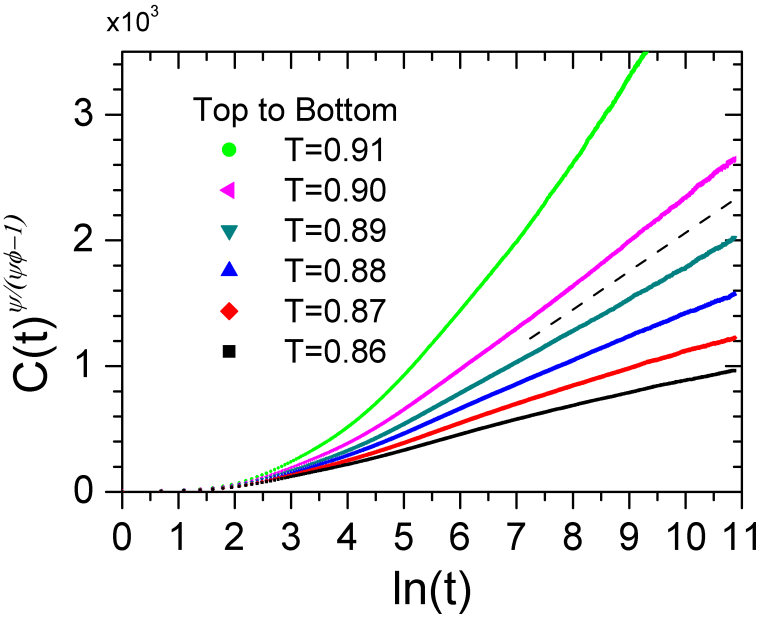

Figure 3.6: (Color online) Time autocorrelation function $C(t)$ for temperatures from $T = 0.86$ to 0.91 (near criticality). The system sizes are $L_\perp = 400$ and $L_\parallel = 230$. The data are averaged over 70 to 80 disorder configurations. The dashed line shows the logarithmic behavior (1.10) at the estimated critical temperature $T_c = 0.895$.

system sizes $L_\perp = 400$ and $L_\parallel = 230$ and temperatures from $T = 0.86$ to 0.91. We find that $C(t)$ indeed follows the prediction at an estimated $T_c \approx 0.895$. This estimate agrees reasonably well with that stemming from the finite-size behavior of χ. We attribute the remaining difference to the finite-size effects and (in case of $C(t)$) finite-time effects.

4. CONCLUSIONS

To summarize, we have reported the results of large-scale Monte-Carlo simulations of the thermodynamics and dynamic behavior of a randomly layered Heisenberg model. Our results provide strong numerical evidence in support of the infinite-randomness scenario predicted within the strong-disorder renormalization group approach [81]. Morever, our data are compatible with the prediction that the randomly layered Heisenberg model is in the same universality class as the one-dimensional random transverse-field Ising model.

We would have liked to determine the complete set of critical exponents of the infinite-randomness critical point directly from the numerical data. To this end we have attempted to perform an anisotropic finite-size scaling analysis as in Refs. [87] or [88]. However, within the accessible range of system sizes of up to about 10^7 sites, the corrections to the leading scaling behavior were so strong that we could not complete the analysis. This task thus remains for the future.

An important question left unanswered by the strong-disorder renormalization group approach[81] is whether or not weakly or moderately disordered systems actually flow to the infinite-randomness critical point. The clean Heisenberg critical point is unstable against weak layered disorder because it violates the generalized Harris criterion $d_r\nu > 2$ where $d_r = 1$ is the number of random dimensions. Thus, weak layered randomness initially increases under renormalization. Our numerical parameter choices, $p = 0.8$ and $J_u/J_l = 4$ correspond to moderate disorder as the distribution is not particularly broad *on a logarithmic scale*. The fact that we do confirm infinte-randomness behavior for these parameters suggests that the infinite-randomness critical point may control the transition for any nonzero disorder strength. A numerical verification of this conjecture by simulating very weakly disordered systems would require even larger system sizes and is thus beyond our present computational capabilities.

Experimental verifications of infinite-randomness critical behavior and the accompanying power-law Griffiths singularities have been hard to come by, in particular in higher-dimensional systems. Only very recently, promising measurements have been reported [45, 46] of the quantum phase transitions in $CePd_{1-x}Rh_x$ and $Ni_{1-x}V_x$. The randomly layered Heisenberg magnet considered here provides an alternative realization of an infinite-randomness critical point. It may be more easily realizable in experiment because the critical point is classical, and samples can be produced by depositing random layers of two different ferromagnetic materials.

Magnetic multilayers with systematic variation of the critical temperature from layer to layer have already been produced,[89] and our results would apply to random versions of these structures.

A. SPIN-WAVE STIFFNESS IN TERMS OF SPIN CORRELATION FUNCTIONS

Twisted boundary conditions, i.e., forcing the spins on one surface of the sample of size L to make an angle of θ with those on the opposite surface, lead to a change in the free energy density f. It can be parametrized by

$$f(\theta) - f(0) = \frac{1}{2}\rho_s \left(\frac{\theta}{L}\right)^2 . \tag{A.1}$$

which defines the spin-wave stiffness ρ_s.

For definiteness, assume we apply a twist of θ around the perpendicular axis between the top and bottom surfaces of the sample. We parametrize the Heisenberg spin as

$$\mathbf{S}_\mathbf{r} = \begin{pmatrix} \sin(\vartheta_\mathbf{r})\cos(\phi_\mathbf{r}) \\ \sin(\vartheta_\mathbf{r})\sin(\phi_\mathbf{r}) \\ \cos(\vartheta_\mathbf{r}) \end{pmatrix} . \tag{A.2}$$

The boundary conditions then read $\phi_\mathbf{r} = 0$ at the bottom ($z = 0$) surface and $\phi_\mathbf{r} = \theta$ at the top ($z = L_\perp$) surface. To eliminate the twisted boundary condition, we now perform the variable transformation

$$\psi_\mathbf{r} = \phi_\mathbf{r} - \theta \frac{z_\mathbf{r}}{L_\perp} \tag{A.3}$$

which gives new boundary conditions of $\psi_\mathbf{r} = 0$ at both $z_\mathbf{r} = 0$ and $z_\mathbf{r} = L_\perp$.

Substituting the variable transformation in the Heisenberg Hamiltonian (1.1), we obtain

$$H = -\sum_{\langle \mathbf{r},\mathbf{r}'\rangle} J_{\mathbf{r},\mathbf{r}'} \Big\{ \sin(\vartheta_{\mathbf{r}}) \ \sin(\vartheta_{\mathbf{r}'}) \\ \cos\left(\psi_{\mathbf{r}} - \psi_{\mathbf{r}'} + \frac{\theta}{L_\perp}(z-z')\right) + \cos(\vartheta_{\mathbf{r}}) \ \cos(\vartheta_{\mathbf{r}'}) \Big\} \tag{A.4}$$

where the twist is "distributed" over the volume. Thus, the twist angle θ now appears as a parameter of the Hamiltonian. We can use standard methods to reformulate the second derivative of the free energy F as

$$\frac{\partial^2 F}{\partial \theta^2} = \frac{1}{T}\left\langle \frac{\partial H}{\partial \theta}\right\rangle^2 + \left\langle \frac{\partial^2 H}{\partial \theta^2}\right\rangle - \frac{1}{T}\left\langle \left(\frac{\partial H}{\partial \theta}\right)^2\right\rangle \tag{A.5}$$

where the first term on the right hand side vanishes due to symmetry. Evaluating the derivatives of H for the Hamiltonian (A.4) gives the spin-wave stiffness $\rho_s = L^2(\partial^2 f/\partial\theta^2)\big|_{\theta=0}$ as

$$\rho_s^\perp = \left\langle \sum_{\langle \mathbf{r},\mathbf{r}'\rangle} J_{\mathbf{r},\mathbf{r}'} \left[\mathbf{S}_{\mathbf{r}}\cdot\mathbf{S}_{\mathbf{r}'} - (\mathbf{S}_{\mathbf{r}}\cdot\hat{\mathbf{k}})(\mathbf{S}_{\mathbf{r}'}\cdot\hat{\mathbf{k}})\right](z-z')^2 \right\rangle \\ -\frac{1}{T}\left\langle \left(\sum_{\langle \mathbf{r},\mathbf{r}'\rangle} J_{\mathbf{r},\mathbf{r}'} \left[(\mathbf{S}_{\mathbf{r}}\times\mathbf{S}_{\mathbf{r}'})\cdot\hat{\mathbf{k}}\right](z-z') \right)^2 \right\rangle . \tag{A.6}$$

Here, $\hat{\mathbf{k}}$ is the unit vector in the z-direction. The same equation was derived in Ref. [86] for the XY case. Equation A.6 needs to be evaluated with fixed boundary conditions at the top and bottom layeres. Applying this formula to simulations with periodic boundary conditions leads to incorrect results in the Heisenberg case (even though it works in XY case). The reason is that Eq. (A.6) is sensitive to twist in the XY plane only.

In the Heisenberg case this can be fixed by aligning the imaginary twist axis with a direction $\hat{\mathbf{a}}$ perpendicular to the total magnetization in each Monte-Carlo measurement. We use $\hat{\mathbf{a}} = (\mathbf{m}\times\hat{\mathbf{k}})/|\mathbf{m}\times\hat{\mathbf{k}}|$. The resulting formula for the spin-wave

stiffness can be used efficiently by Monte-Carlo simulations with periodic boundary conditions. It reads

$$\begin{aligned}\rho_s^{\perp} = &\left\langle \sum_{\langle \mathbf{r},\mathbf{r}'\rangle} J_{\mathbf{r},\mathbf{r}'} \left[\mathbf{S}_{\mathbf{r}} \cdot \mathbf{S}_{\mathbf{r}'} - (\mathbf{S}_{\mathbf{r}} \cdot \hat{\mathbf{a}})(\mathbf{S}_{\mathbf{r}'} \cdot \hat{\mathbf{a}})\right] (z - z')^2 \right\rangle \\ &-\frac{1}{T} \left\langle \left(\sum_{\langle \mathbf{r},\mathbf{r}'\rangle} J_{\mathbf{r},\mathbf{r}'} \left[(\mathbf{S}_{\mathbf{r}} \times \mathbf{S}_{\mathbf{r}'}) \cdot \hat{\mathbf{a}}\right] (z - z') \right)^2 \right\rangle .\end{aligned} \tag{A.7}$$

We have tested that this equation reproduces the results obtained directly from Eq. (A.1).

5. ACKNOWLEDGEMENTS

We acknowledge helpful discussions with S. Bharadwaj, P. Mohan, and R. Narayanan. This work was supported in part by the NSF under grant No. DMR-0906566.

II. COMPOSITION-TUNED SMEARED PHASE TRANSITIONS

Fawaz Hrahsheh, David Nozadze, and Thomas Vojta

[1]*Department of Physics, Missouri University of Science & Technology, Rolla, MO 65409*

ABSTRACT*

Phase transitions in random systems are smeared if individual spatial regions can order independently of the bulk system. In this paper, we study such smeared phase transitions (both classical and quantum) in substitutional alloys $A_{1-x}B_x$ that can be tuned from an ordered phase at composition $x = 0$ to a disordered phase at $x = 1$. We show that the ordered phase develops a pronounced tail that extends over all compositions $x < 1$. Using optimal fluctuation theory, we derive the composition dependence of the order parameter and other quantities in the tail of the smeared phase transition. We also compare our results to computer simulations of a toy model, and we discuss experiments.

*Published in Physical Review B **83** 224402 (2011).

1. INTRODUCTION

When a phase transition occurs in a randomly disordered system, one of the most basic questions to ask is whether the transition is still sharp, i.e., associated with a singularity in the free energy. Naively, one might expect that random disorder rounds or smears any critical point because different spatial regions undergo the transition at different values of the control parameter. This expectation turns out to be mistaken, as classical (thermal) continuous phase transitions generically remain sharp in the presence of weak randomness. The reason is that a finite-size region cannot undergo a true phase transition at any nonzero temperature because its partition function must be analytic. Thus, true static long-range order can only be established via a collective phenomenon in the entire system

Recent work has established, however, that some phase transitions are indeed smeared by random disorder. This can happen at zero-temperature quantum phase transitions when the order parameter fluctuations are overdamped because they are coupled to an (infinite) heat bath.[90, 91] As the damping hampers the dynamics, sufficiently large but finite-size regions can undergo the phase transition independently from the bulk system. Once several such regions have developed static order, their local order parameters can be aligned by an *infinitesimally small* mutual interaction. Thus, global order develops gradually, and the global phase transition is smeared. Classical thermal phase transitions can also be smeared provided the disorder is perfectly correlated in at least two dimensions. In these cases, individual "slabs" of finite thickness undergo the phase transition independently of the bulk system.[92, 93]

The existing theoretical work on smeared phase transitions focuses on situations in which a sample with some fixed degree of randomness is tuned through the transition by changing the temperature (for classical transitions) or the appropriate quantum control parameter such as pressure or magnetic field (for quantum phase transitions). However, many experiments are performed on substitutional alloys such

as $CePd_{1-x}Rh_x$ or $Sr_{1-x}Ca_xRuO_3$. These materials can be tuned from an ordered phase (ferromagnetic for the two examples) at composition $x = 0$ to a disordered phase at $x = 1$ while keeping the temperature and other external parameters fixed, i.e., they undergo a phase transition as a function of composition. The composition parameter x actually plays a dual role in these transitions. On the one hand, x is the control parameter of the phase transition. On the other hand, changing x also changes the degree of randomness. If such a composition-tuned phase transition is smeared, its behavior can therefore be expected to be different than that of smeared transitions occurring at fixed randomness.

In this paper, we investigate the properties of composition-tuned smeared phase transitions in substitutional alloys of the type $A_{1-x}B_x$. We show that the ordered phase extends over the entire composition range $x < 1$, and we derive the behavior of the system in the tail of the smeared transition. Our paper is organized as follows. In Sec. 2., we consider a smeared quantum phase transition in an itinerant magnet. We use optimal fluctuation theory to derive the composition dependence of the order parameter, the phase boundary, and other quantities. In Section 3. we briefly discuss how the theory is modified for smeared classical transitions in systems with correlated disorder. Section 4. is devoted to computer simulations of a toy model that illustrate and confirm our theory. We conclude in Sec. 5. by comparing composition-tuned smeared transitions with those occurring at fixed randomness. We also discuss experiments.

2. SMEARED QUANTUM PHASE TRANSITION

2.1. MODEL AND PHASE DIAGRAM. In this section we investigate the ferromagnetic or antiferromagnetic quantum phase transition of itinerant electrons with Ising order parameter symmetry. In the absence of quenched randomness, the Landau-Ginzburg-Wilson free energy functional of this transition in d space dimensions reads [94, 95]

$$S = \int dydz\ \psi(y)\Gamma(y,z)\psi(z) + u\int dy\ \psi^4(y)\,. \tag{2.1}$$

Here, ψ is a scalar order parameter field, $y \equiv (\mathbf{y},\tau)$ comprises imaginary time τ and d-dimensional spatial position $\mathbf{y}$, $\int dy \equiv \int d\mathbf{y}\int_0^{1/T} \mathrm{d}\tau$, and u is the standard quartic coefficient. $\Gamma(y,z)$ denotes the bare inverse propagator (two-point vertex) whose Fourier transform reads

$$\Gamma(\mathbf{q},\omega_n) = r + \xi_0^2\mathbf{q}^2 + \gamma_0(\mathbf{q})\,|\omega_n|\ . \tag{2.2}$$

Here, r is the distance from criticality,[†] ξ_0 is a microscopic length scale, and ω_n is a Matsubara frequency. The dynamical part of $\Gamma(\mathbf{q},\omega_n)$ is proportional to $|\omega_n|$. This overdamped dynamics reflects the Ohmic dissipation caused by the coupling between the order parameter fluctuations and the gapless fermionic excitations in an itinerant system. The damping coefficient $\gamma_0(\mathbf{q})$ is $\mathbf{q}$-independent for an antiferromagnetic transition but proportional to $1/|\mathbf{q}|$ or $1/|\mathbf{q}|^2$ for ballistic and diffusive ferromagnets, respectively.

We now consider two materials A and B. Substance A is in the magnetic phase, implying a negative distance from criticality, $r_A < 0$, while substance B is nonmagnetic with $r_B > 0$. By randomly substituting B-atoms for the A-atoms to

[†]Strictly, one needs to distinguish the bare distance from criticality that appears in (2.2) from the renormalized one that measures the distance from the true critical point. We suppress this difference because it is unimportant for our purposes.

form a binary alloy $A_{1-x}B_x$, we can drive the system through a composition-driven magnetic quantum phase transition.

A crucial role in this transition is played by rare A-rich spatial regions. They can be locally in the magnetic phase even if the bulk system is nonmagnetic. In the presence of Ohmic dissipation, the low-energy physics of each such region is equivalent to that of a dissipative two-level system which is known to undergo, with increasing dissipation strength, a phase transition from a fluctuating to a localized phase.[60] Therefore, the quantum dynamics of sufficiently large rare regions completely freezes,[96] and they behave as classical superspins. At zero temperature, these classical superspins can be aligned by an *infinitesimally small* residual interaction which is always present as they are coupled via the fluctuations of the paramagnetic bulk system. The order parameter is thus spatially very inhomogeneous, but its average is nonzero for any $x < 1$ implying that the global quantum phase transition is smeared by the disorder inherent in the random positions of the A and B atoms.[90, 97, 98]

At small but nonzero temperatures, the static magnetic order on the rare regions is destroyed, and a finite interaction of the order of the temperature is necessary to align them. This restores a sharp phase transition at some transition temperature $T_c(x)$ which rapidly decreases with increasing x but reaches zero only at $x = 1$. If the temperature is raised above T_c, the locally ordered rare regions act as independent classical moments, leading to super-paramagnetic behavior. A sketch of the resulting phase diagram is shown in Fig. 2.1.

2.2. OPTIMAL FLUCTUATION THEORY. In this section, we use optimal fluctuation theory [99, 100, 101] to derive the properties of the tail of the smeared quantum phase transition. This is the composition range where a few rare regions have developed static magnetic order but their density is so small that they are very weakly coupled.

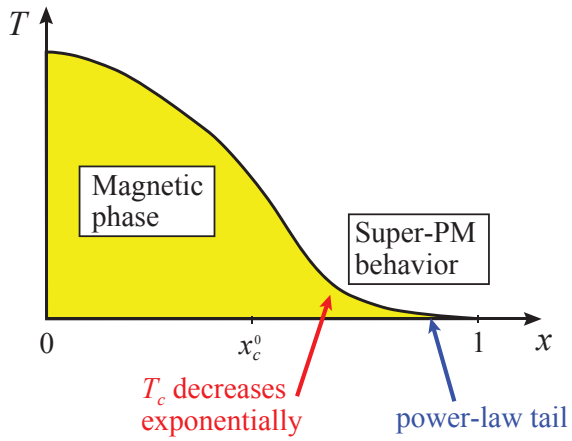

Figure 2.1: (Color online) Schematic temperature-composition phase diagram of a binary alloy $A_{1-x}B_x$ displaying a smeared quantum phase transition. In the tail of the magnetic phase, which stretches all the way to $x = 1$, the rare regions are aligned. Above T_c, they act as independent classical moments, resulting in super-paramagnetic (PM) behavior. x_c^0 marks the critical composition in average potential approximation defined in (2.3).

A crude estimate of the transition point in the binary alloy $A_{1-x}B_x$ can be obtained by simply averaging the distance from criticality, $r_{\rm av} = (1-x)r_A + xr_B$. The transition point corresponds to $r_{\rm av} = 0$. This gives the critical composition in "average potential approximation,"

$$x_c^0 = -r_A/(r_B - r_A)\ . \tag{2.3}$$

Let us now consider a single A-rich rare region of linear size L_{RR} embedded in a nonmagnetic bulk sample. If the concentration $x_{\rm loc}$ of B atoms in this region is below some critical concentration $x_c(L_{RR})$, the region will develop local magnetic order. The value of the critical concentration follows straightforwardly from finite-size scaling,[102, 103]

$$x_c(L_{RR}) = x_c^0 - DL_{RR}^{-\phi}\ , \tag{2.4}$$

where ϕ is the finite-size shift exponent and D is a constant. Within mean-field theory (which should be qualitatively correct in our case because the clean transition

is above its upper critical dimension[94]), one finds $\phi = 2$ and $D = \xi_0^2/(r_B - r_A)$. Since $x_c(L_{RR})$ must be positive, (2.4) implies that a rare region needs to be larger than $L_{\min} = (D/x_c^0)^{1/\phi}$ to develop local magnetic order.

As the last ingredient of our optimal fluctuation theory, we now analyze the random distribution of the atoms in the sample. For simplicity, we assume that the lattice sites are occupied *independently* by either A or B atoms with probabilities $1-x$ and x, respectively. Modifications due to deviations from a pure random distribution (i.e., clustering) will be discussed in the concluding section 5.. The probability of finding $N_B = N x_{\rm loc}$ sites occupied by B atoms in a spatial region with a total of $N \sim L_{RR}^d$ sites is given by the binomial distribution

$$P(N, x_{\rm loc}) = \binom{N}{N_B} (1-x)^{N-N_B} x^{N_B} \ . \tag{2.5}$$

We are interested in the regime $x > x_c^0$ where the bulk system will not be magnetically ordered but $x_{\rm loc} = N_B/N < x_c(L_{RR})$ such that local order is possible in the region considered.

To estimate the total zero-temperature order parameter M in the tail of the smeared transition (where the rare regions are very weakly coupled), we can simply sum over all rare regions displaying local order

$$M \sim \int_{L_{\min}}^{\infty} dL_{RR} \int_0^{x_c(L_{RR})} dx_{\rm loc}\, m(N, x_{\rm loc}) P(N, x_{\rm loc}) \ . \tag{2.6}$$

Here, $m(N, x_{\rm loc})$ is the order parameter of a single region of N sites and local composition $x_{\rm loc}$; and we have suppressed a combinatorial prefactor. We now analyze this integral in two parameter regions, (i) the regime where x is somewhat larger than x_c^0 but not by too much, and (ii) the far tail of the transition at $x \to 1$.

If x is not much larger than x_c^0, the rare regions are expected to be large, and we can approximate the binomial distribution (2.5) by a Gaussian,

$$P(N, x_{\rm loc}) = \frac{1}{\sqrt{2\pi N(1-N)}} \exp\left[-N\frac{(x_{\rm loc}-x)^2}{2x(1-x)}\right] \tag{2.7}$$

To exponential accuracy in x, the integral (2.6) can now be easily performed in saddle point approximation. Neglecting $m(N, x_{\rm loc})$, which only modifies power-law prefactors, we find that large rare regions of size $L_{RR}^{\phi} = D(2\phi - d)/[d(x - x_c^0)]$ and maximum possible B-concentration $x_{\rm loc} = x_c^0 - DL_{RR}^{-\phi}$ dominate the integral. Inserting these saddle point values into the integrand yields the composition dependence of the order parameter as[‡]

$$M \sim \exp\left[-C\frac{(x-x_c^0)^{2-d/\phi}}{x(1-x)}\right] \tag{2.8}$$

where $C = 2(D/d)^{d/\phi}(2\phi - d)^{d/\phi - 2}\phi^2$ is a non-universal constant.

Let us now analyze the far tail of the smeared transition, $x \to 1$. In this regime, the binomial distribution cannot be approximated by a Gaussian. Nonetheless, the integral (2.6) can be estimated in saddle-point approximation. We find that for $x \to 1$, the integral is dominated by pure-A regions of the minimum size that permits local magnetic order. This means $L_{RR} = L_{\rm min} = (D/x_c^0)^{1/\phi}$ and $x_{\rm loc} = 0$. Inserting these values into the integrand of (2.6), we find that the leading composition dependence of the order parameter in the limit $x \to 1$ is given by a non-universal power law,

$$M \sim (1-x)^{L_{\rm min}^d} = (1-x)^{(D/x_c^0)^{d/\phi}} \ . \tag{2.9}$$

We thus find that M is nonzero in the entire composition range $0 \le x < 1$, illustrating the notion of a smeared quantum phase transition.

[‡]This result is valid for $d < 2\phi$ which is fulfilled for our transition. In the opposite case, the integral over L_{RR} is dominated by its lower bound, resulting in a purely Gaussian dependence of M on $x - x_c^0$.

So far, we have focused on the zero-temperature order parameter. Other quantities can be found in an analogous manner. Let us, for example, determine the phase boundary, i.e., the composition dependence of the critical temperature T_c. As was discussed in Sec. 2.1, the static magnetism of the rare regions is destroyed at nonzero temperatures. Consequently, magnetic long-range order in the sample can only develop, if the rare regions are coupled by an interaction of the order of the temperature. The typical distance between neighboring locally ordered rare regions can be estimated from their density, ρ, as $r_{\rm typ} \sim \rho^{-1/d} \sim M^{-1/d}$. Within the Landau-Ginzburg-Wilson theory (2.1,2.2), the interaction between two rare regions drops off exponentially with their distance r, $E_{\rm int} \sim \exp(-r/\xi_b)$, where ξ_b is the bulk correlation length. This leads to a double-exponential dependence of T_c on x for compositions somewhat above x_c^0, i.e., $\ln(1/T_c) \sim \exp\{C(x-x_c^0)^{2-d/\phi}/[dx(1-x)]\}$. For $x \to 1$, we find $\ln(1/T_c) \sim (1-x)^{-L_{\rm min}^d/d}$. However, in a real metallic magnet, the locally ordered rare regions are coupled by an RKKY-type interaction that decays as a power law with distance, $E_{\rm int} \sim r^{-d}$, rather than exponentially.[104] (This interaction is not contained in the long-wavelength expansion implied in (2.2).) Therefore, the composition dependence of the critical temperature takes the same form as that of the magnetization,

$$T_c \sim \exp\left[-C\frac{(x-x_c^0)^{2-d/\phi}}{x(1-x)}\right] \tag{2.10}$$

for compositions somewhat above x_c^0 and

$$T_c \sim (1-x)^{L_{\rm min}^d} = (1-x)^{(D/x_c^0)^{d/\phi}} \tag{2.11}$$

in the far tail of the smeared transition, $x \to 1$.

We now turn to the order parameter susceptibility. It consists of two different contributions, one from the paramagnetic bulk system and one from the locally ordered rare regions. The bulk system provides a finite, non-critical background

throughout the tail of the smeared transition. Let us discuss the rare region contribution in more detail. At zero temperature, the total order parameter M is nonzero for all $x < 1$. The rare regions therefore always feel a symmetry-breaking effective field which cuts off any possible divergence of their susceptibilities. We conclude that the zero-temperature susceptibility does not diverge anywhere in the tail of the smeared transition. If the temperature is raised above T_c, the relative alignment of the rare regions is lost, and they behave as independent large (classical) moments, leading to a super-paramagnetic temperature dependence of the susceptibility, $\chi \sim 1/T$ (see Fig. 2.1). At even higher temperatures, when the damping of the quantum dynamics becomes unimportant, we expect the usual non-universal quantum Griffiths power-laws, $\chi \sim T^{\lambda-1}$, where λ is the Griffiths exponent.[97, 98, 105]

3. SMEARED CLASSICAL PHASE TRANSITION

Classical (thermal) phase transitions with uncorrelated disorder cannot be smeared because all rare regions are of finite size and can thus not undergo a true phase transition at any nonzero temperature. However, perfect disorder correlations in one or more dimensions lead to rare regions that are infinitely extended in the thermodynamic limit. If the number of correlated dimensions is high enough, these infinitely large rare regions can undergo the phase transition independently of the bulk system, leading to a smearing of the global phase transition.[92] This happens, for example, in a randomly layered Ising magnet, i.e., an Ising model with disorder correlated in two dimensions. [93]

In this section, we discuss how the theory of Sec. 2. is modified for these smeared classical phase transitions. For definiteness, we consider a classical Landau-Ginzburg-Wilson free energy in d dimensions,

$$S = \int d\mathbf{y}\ \psi(\mathbf{y})[r - \partial_{\mathbf{y}}^2]\psi(\mathbf{y}) + u \int d\mathbf{y}\ \psi^4(\mathbf{y})\,. \tag{2.12}$$

As in the quantum case, we now consider a binary "alloy" $A_{1-x}B_x$ of two materials A and B. The atoms are arranged randomly in $d_\perp$ dimensions, while they are perfectly correlated in $d_\parallel = d - d_\perp$ dimensions. For example, if $d_\perp = 1$ and $d_\parallel = 2$, the system would consist of a random sequence of layers, each made up of only A atoms or only B atoms.

If the correlated dimension $d_\parallel$ is sufficiently large, the "alloy" undergoes a smeared classical phase transition as the composition x is tuned from 0 to 1 at a (fixed) temperature at which material A is magnetically ordered, $r_A < 0$, while material B is in the nonmagnetic phase, $r_B > 0$. The optimal fluctuation theory for the behavior in the tail of the smeared transition can be developed along the same lines as the theory in Sec. 2.. The only important difference stems from the fact that the randomness is restricted to $d_\perp$ dimensions. The dimensionality d in eqs. (2.8) and (2.9) therefore

needs to be replaced by $d_\perp$, leading to

$$M \sim \exp\left[-C\frac{(x-x_c^0)^{2-d_\perp/\phi}}{x(1-x)}\right] \tag{2.13}$$

for compositions somewhat above x_c^0 and

$$M \sim (1-x)^{L_{\min}^{d_\perp}} = (1-x)^{(D/x_c^0)^{d_\perp/\phi}} \tag{2.14}$$

for $x \to 1$. The same substitution of d by $d_\perp$ was also found for smeared classical transitions tuned by temperature rather than composition.[92]

4. COMPUTER SIMULATIONS

To verify the predictions of the optimal fluctuation theory in Sec. 2. and to illustrate our results, we have performed computer simulations of a toy model, viz., a classical Ising model with d space-like dimensions and one time-like dimension. The interactions are between nearest neighbors in the space-like directions but infinite-ranged in the time-like ones. This $(d+1)$-dimensional toy model retains the possibility of static order on the rare regions (which is crucial for the transition being smeared) but permits system sizes large enough to study exponentially rare events. The Hamiltonian reads

$$H = -\frac{1}{L_\tau} \sum_{\langle \mathbf{y},\mathbf{z}\rangle,\tau,\tau'} S_{\mathbf{y},\tau} S_{\mathbf{z},\tau'} - \frac{1}{L_\tau} \sum_{\mathbf{y},\tau,\tau'} J_{\mathbf{y}} S_{\mathbf{y},\tau} S_{\mathbf{y},\tau'} \tag{2.15}$$

Here $\mathbf{y}$ and $\mathbf{z}$ are d-dimensional space-like coordinates and τ is the time-like coordinate. L_τ is the system size in time direction and $\langle \mathbf{y}, \mathbf{z}\rangle$ denotes pairs of nearest neighbors on the hyper-cubic lattice in space. $J_{\mathbf{y}}$ is a quenched random variable having the binary distribution $P(J) = (1-x)\ \delta(J-J_h) + x\ \delta(J-J_l)$ with $J_h > J_l$. In this classical model L_τ plays the role of the inverse temperature in the corresponding quantum system and the classical temperature plays the role of the quantum tuning parameter. Because the interaction is infinite-ranged in time, the time-like dimension can be treated in mean-field theory. For $L_\tau \to \infty$, this leads to a set of coupled mean-field equations for the local magnetizations $m_{\mathbf{y}} = (1/L_\tau) \sum_\tau S_{\mathbf{y},\tau}$. They read

$$m_{\mathbf{y}} = \tanh \beta\ [J_{\mathbf{y}} m_{\mathbf{y}} + \sum_{\mathbf{z}} m_{\mathbf{z}} + h]\ , \tag{2.16}$$

where the sum is over all nearest neighbors of site $\mathbf{y}$ and $h \to 0$ is a very small symmetry-breaking magnetic field which we typically set to 10^{-12}. If all $J_{\mathbf{y}} \equiv J_h$, the system undergoes a (sharp) phase transition at $T_h = J_h + 2d$, and if all $J_{\mathbf{y}} \equiv J_l$, it undergoes the transition at $T_l = J_l + 2d$. In the temperature range $T_h > T > T_l$, the phase transition can therefore be tuned by composition x.

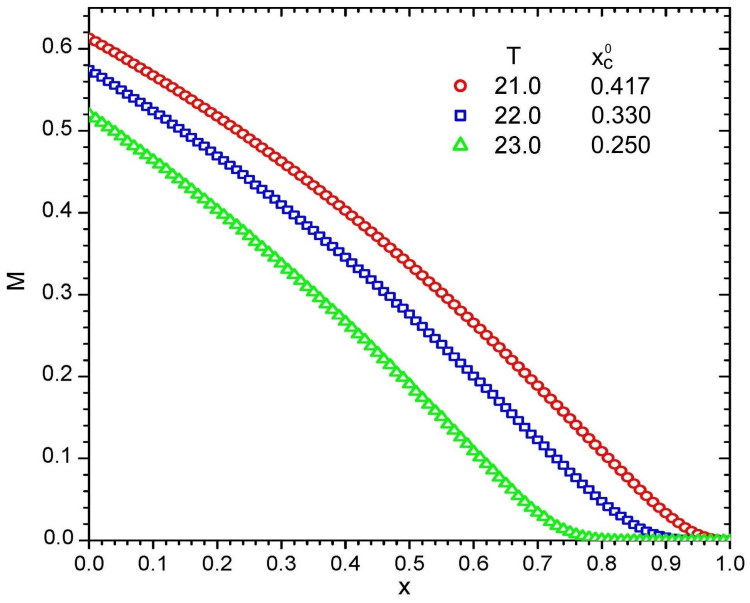

Figure 4.1: (Color online) Magnetization M vs composition x for a $(3+1)$-dimensional system having $J_h = 20$, $J_l = 8$ and several values of the classical temperature T. The data represent averages over 100 samples of size $L = 100$. The values of the critical concentration in "average potential approximation," x_c^0, are shown for comparison.

The mean-field equations (2.16) can be solved efficiently in a self-consistency cycle. Using this approach, we studied systems in one, two, and three space dimensions. The system sizes were up to L=10000 in 1d, and up to $L = 100$ in 2d and 3d. For each parameter set, the data were averaged over a large number of disorder realizations. Details will be given with the individual results below.

Fig. 4.1 shows an overview over the magnetization M as a function of composition x for a $(3+1)$-dimensional system at several values of the classical temperature in the interval $T_h > T > T_l$. The figure clearly demonstrates that the magnetic phase extends significantly beyond the "average potential" value $x_c^0 = (T_h - T)/(T_h - T_l)$. In this sense, the magnetic phase in our binary alloy benefits from the randomness. In agreement with the smeared phase transition scenario, the data also show that $M(x)$ develops a pronounced tail towards $x = 1$. (By comparing different system sizes, we can exclude that the tail is due to simple finite-size rounding.[92]) We performed

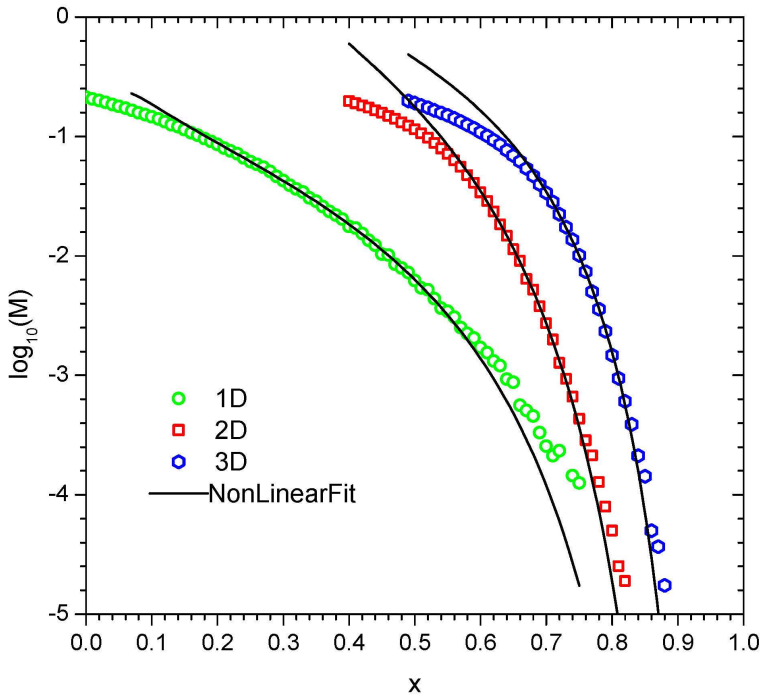

Figure 4.2: (Color online) $\log(M)$ vs x in the tail of the transition for three example systems: (i) $(3+1)$-dimensional system with $L = 100, J_h = 20, J_l = 8$, and $T = 23$, (ii) $(2+1)$-dimensional system with $L = 100, J_h = 15, J_l = 8$, and $T = 18$, and (iii) $(1+1)$-dimensional system with $L = 10000, J_h = 11, J_l = 8$, and $T = 12.8$. All data are averages over 100 disorder configurations. The solid lines are fits to (2.8), with the fit intervals restricted to $x \in (0.25, 0.55)$ in (1+1) dimensions, (0.6,0.72) in (2+1) dimensions and (0.7,0.82) for the (3+1)-dimensional example.

similar simulations for systems in one and two space dimensions, with analogous results.

To verify the theoretical predictions of the optimal fluctuation theory developed in Sec. 2., we now analyze the tail of the smeared phase transition in more detail. Fig. 4.2 shows a semi-logarithmic plot of the magnetization M vs. the composition x for a $(1+1)$-dimensional system, a $(2+1)$-dimensional system, and a $(3+1)$-dimensional one. In all examples, the data follow the theoretical prediction (2.8) over at least 2 orders of magnitude in M in a transient regime of intermediate compositions x.

We also check the behavior of the magnetization for compositions very close to $x = 1$. Since (2.9) predicts a non-universal power law, we plot $\log(M)$ vs. $\log(1-x)$ for a $(3+1)$-dimensional system in Fig. 4.3. The figure shows that the magnetization tail indeed decays as a power of $(1-x)$ with $x \to 1$. The exponent increases with increasing temperature in agreement with the prediction that it measures the minimum size $N_{\min} \sim L_{\min}^d$ a rare regions needs to have to undergo the transition independently. The inset of Fig. 4.3 shows a fit of the exponent to $L_{\min}^d \sim [x_c^0(T)]^{-3/2} = [(T_h - T)/(T_h - T_l)]^{-3/2}$. The equation describes the data reasonably well; the deviations at small exponents can be explained by the fact that our theory assumes the rare-region size to be a continuous variable which is not fulfilled for rare regions consisting of just a few lattice sites.

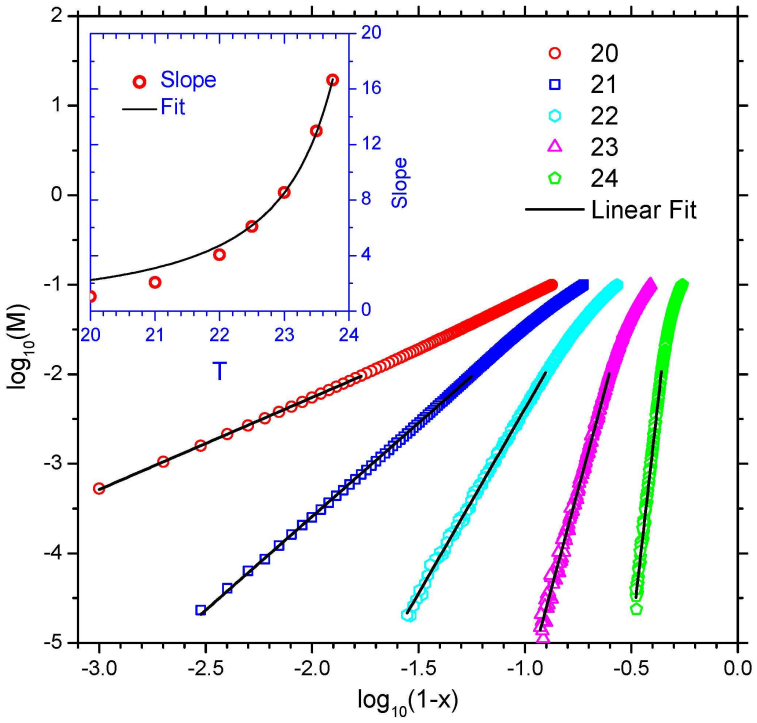

Figure 4.3: (Color online) $\log(M)$ vs $\log(1-x)$ for a $(3+1)$-dimensional system with $L = 100$, $J_h = 20$, $J_l = 8$ and several temperatures. All data are averages over 100 disorder configurations. The solid lines are fits to the power-law (2.9). The inset shows the exponent as a function of temperature, with the solid line being a fit to $[x_c^0(T)]^{-3/2}$.

Our computer simulation thus confirm the theoretical predictions in both composition regions in the tail of the transition. In a transient regime above x_c^0, we observe the exponential dependence (2.8) while the magnetization for $x \to 1$ follows the non-universal power law (2.9).

5. CONCLUSIONS

In summary, we have investigated phase transitions that are tuned by changing the composition x in a random binary alloy $A_{1-x}B_x$ where pure A is in the ordered phase while pure B is in the disordered phase. If individual, rare A-rich spatial regions develop true static order, they can be aligned by an infinitesimal residual interaction. This results in the smearing of the global phase transition, in agreement with the classification put forward in Ref.

As an example, we have studied the quantum phase transition of an itinerant Ising magnet of the type $A_{1-x}B_x$. At zero temperature, the ordered phase in this binary alloy extends over the entire composition range $x < 1$, illustrating the notion of a smeared quantum phase transition. Upon raising the temperature, a sharp phase transition is restored, but the transition temperature $T_c(x)$ is nonzero for all $x < 1$ and reaches zero only right at $x = 1$ (see Fig. 2.1). Using optimal fluctuation theory, we have derived the functional forms of various thermodynamic observables in the tail of the smeared transition. We have also briefly discussed smeared classical phase transitions that can occur in systems with correlated disorder, and we have performed computer simulations of a toy model that confirm and illustrate the theory.

Although our results are qualitatively similar to those obtained for smeared phase transitions occurring at fixed randomness as a function of temperature or an appropriate quantum control parameter, the functional forms of observables are not identical. The most striking difference can be found in the far tail of the transition. In the case of composition-tuning, the order parameter vanishes as a non-universal power of the distance from the end of the tail ($x = 1$), reflecting the fact that the minimum rare region size required for local magnetic order is finite. In contrast, if the transition occurs at fixed composition as a function of temperature or some quantum control parameter, the order parameter vanishes exponentially,[90, 92] because the minimum size of an ordered rare region diverges in the far tail. These differences

illustrate the fact that the behavior of observables at a smeared phase transition is generally *not* universal in the sense of critical phenomena; it depends on details of the disorder distribution and how the transition is tuned. Only the question of whether or not a particular phase transition is smeared is universal, i.e., determined only by symmetries and dimensionalities.

Let us briefly comment on the relation of our theory to percolation ideas. The optimal fluctuation theory of Sec. 2.2 applies for compositions x larger than the percolation threshold of the A-atoms. Because the A-clusters are disconnected in this composition range, percolation of the A atoms does not play a role in forming the tail of the ordered phase at large x. Instead, distant rare regions are coupled via the fluctuations of the paramagnetic bulk phase and, in metallic magnets, via the RKKY interaction. Percolation does play a role, though, in the crossover between the inhomogeneous order in the tail of the transition and the bulk order at lower x.

We note in passing that the behavior of a diluted system (where B represents a vacancy) with *nearest-neighbor* interactions is not described by our theory. In this case, the A-clusters are not coupled at all for compositions x larger than the A percolation threshold. Therefore they cannot align, and long-range order is impossible. As a result, the super-paramagnetic behavior of the locally ordered clusters extends all the way down to zero temperature. This was recently discussed in detail on the example of a diluted dissipative quantum Ising model.[106]

In the present paper, we have assumed that the A and B atoms are distributed independently over the lattice sites, i.e., we have assumed that there are no correlations between the atom positions. It is interesting to ask how the results change if this assumption is not fulfilled, for example because like atoms tend to cluster. As long as the correlations of the atom positions are short-ranged (corresponding to a finite, microscopic length scale for clustering), our results will not change *qualitatively*. All arguments in the optimal fluctuation theory still hold using a typical cluster of like atoms instead of a single atom as the basic unit. However, such clustering will lead

to significant *quantitative* changes (i.e., changes in the non-universal constants in our results), as it greatly increases the probability of finding large locally ordered rare regions. We thus expect that clustering of like atoms will enhance the tail and move the phase boundary $T_c(x)$ towards larger x. A quantitative analysis of this effect requires explicit information about the type of correlations between the atom positions and is thus relegated to future work.

Let us finally turn to experiment. Tails of the ordered phase have been observed at many quantum phase transitions. However, it is often not clear whether these tails are an intrinsic effect or due to experimental difficulties such as macroscopic concentration gradients or other macroscopic sample inhomogeneities. Recent highly sensitive magneto-optical experiments on $Sr_{1-x}Ca_xRuO_3$ have provided strong evidence for a smeared ferromagnetic quantum phase transition.[§] The behavior of the magnetization and critical temperature in the tail of the smeared transition agree well with the theory developed here. Moreover, the effects of clustering discussed above may explain the wide variation of the critical composition between about 0.5 and 1 reported in earlier studies.[107, 108, 109] We expect that our smeared quantum phase transition scenario applies to a broad class of itinerant systems with quenched disorder.

[§]L. Demko et al., unpublished.

6. ACKNOWLEDGEMENTS

We thank I. Kezsmarki for helpful discussions. This work has been supported in part by the NSF under grant no. DMR-0906566.

III. DISORDER CORRELATIONS AT SMEARED PHASE TRANSITIONS

Christopher Svoboda, David Nozadze, Fawaz Hrahsheh, and Thomas Vojta

[1] *Department of Physics, Missouri University of Science & Technology, Rolla, MO 65409*

ABSTRACT*

We investigate the influence of spatial disorder correlations on smeared phase transitions, taking the magnetic quantum phase transition in an itinerant magnet as an example. We find that even short-range correlations can have a dramatic effect and qualitatively change the behavior of observable quantities compared to the uncorrelated case. This is in marked contrast to conventional critical points, at which short-range correlated disorder and uncorrelated disorder lead to the same critical behavior. We develop an optimal fluctuation theory of the quantum phase transition in the presence of correlated disorder, and we illustrate the results by computer simulations. As an experimental application, we discuss the ferromagnetic quantum phase transition in $Sr_{1-x}Ca_xRuO_3$.

*Published in Europhysics Letters **97**, 20007 (2012).

1. INTRODUCTION

Quenched disorder has various important consequences in condensed matter. For example, disorder can change the universality class of a critical point [110, 111] or even change the order of a phase transition [112, 113, 114].

In theoretical studies, the disorder is often assumed to be uncorrelated in space even though many sample preparation techniques will produce some degree of correlations between the impurities and defects. As long as the correlations are short-ranged, i.e., characterized by a finite correlation length $\xi_{\rm dis}$, this assumption is usually justified if one is interested in the universal properties of critical points. (There are exceptions for special, fine-tuned local correlations [115]). The reason why short-range correlated disorder leads to the same behavior as uncorrelated disorder can be easily understood within the renormalization group framework. Under repeated coarse graining, a nonzero disorder correlation length $\xi_{\rm dis}$ decreases without limit. The disorder thus becomes effectively uncorrelated on the large length scales that determine the critical behavior.

A formal version of this argument follows from the Harris criterion [116]. It states that a clean critical point is stable against weak *uncorrelated* disorder if its correlation length critical exponent ν fulfills the inequality $d\nu > 2$ where d is the space dimensionality. If the inequality is violated, the disorder is relevant and changes the critical behavior. According to Weinrib and Halperin [117], *spatially correlated* disorder leads to the same inequality as long as its correlations decay faster than r^{-d} with distance r. Thus, short-range correlated disorder and uncorrelated disorder have the same effect on the stability of a clean critical point.

In this Letter, we demonstrate that spatial disorder correlations are much more important at *smeared* phase transitions, a broad class of classical and quantum phase transitions characterized by a gradual, spatially inhomogeneous onset of the ordered phase [97]. Specifically, we show that short-range correlated disorder and uncorrelated

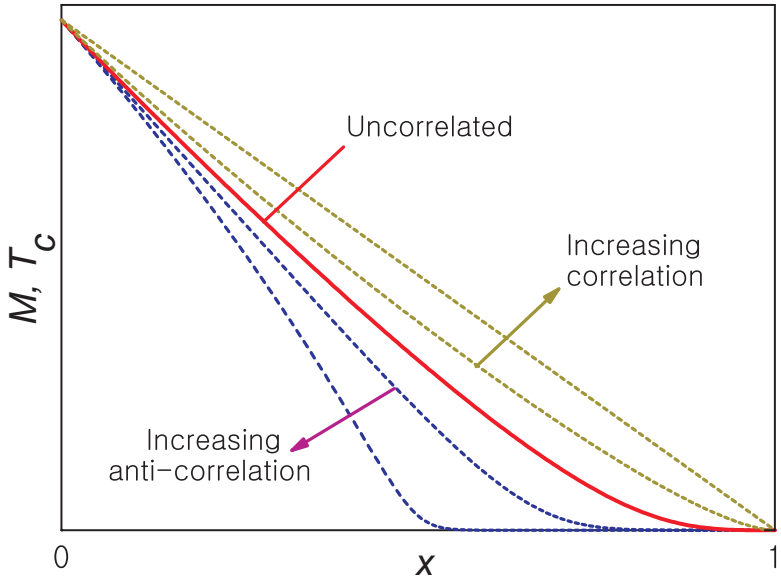

Figure 1.1: (Color online) Schematic of the zero-temperature magnetization-composition curve (M vs x) and the finite-temperature phase boundary (T_c vs x) at a smeared quantum phase transition in a random binary alloy $A_{1-x}B_x$. The cases of uncorrelated, correlated, and anti-correlated disorder are contrasted.

disorder lead to qualitatively different behaviors. The disorder correlations do not only influence quantities usually considered non-universal such as the location of the phase boundary, they also change the functional dependence of the order parameter and other quantities on the tuning parameters of the transition, as indicated in Fig. 1.1. We propose that this mechanism may be responsible for the unusually wide variations reported in the literature on the properties of the ferromagnetic quantum phase transition (QPT) in $Sr_{1-x}Ca_xRuO_3$.

In the following, we sketch the derivation of our theory, compute observables, and illustrate them by simulations. We also discuss the generality of our findings, and we compare them to experiment.

2. SMEARED QUANTUM PHASE TRANSITION

For definiteness, we consider a magnetic QPT in a metallic system with Ising order parameter symmetry. In the absence of quenched disorder, the Landau-Ginzburg-Wilson free energy functional of this transition is given by [94, 95]

$$S = \int dydz\ \psi(y)\Gamma(y,z)\psi(z) + u\int dy\ \psi^4(y)\,, \tag{3.1}$$

where ψ is the order parameter field, $y \equiv (\mathbf{y},\tau)$ comprises d-dimensional spatial position $\mathbf{y}$ and imaginary time τ, the integration means $\int dy \equiv \int d\mathbf{y}\int_0^{1/T} \mathrm{d}\tau$, and u is the standard quartic coefficient. The Fourier transform of the Gaussian vertex $\Gamma(y,z)$ reads

$$\Gamma(\mathbf{q},\omega_n) = r + \xi_0^2\mathbf{q}^2 + \gamma_0(\mathbf{q})\,|\omega_n|\ . \tag{3.2}$$

Here, r is the distance from criticality,[†] ξ_0 is a microscopic length, and ω_n is a Matsubara frequency. The dynamical part of $\Gamma(\mathbf{q},\omega_n)$ is proportional to $|\omega_n|$. This reflects the Landau damping of the order parameter fluctuations by gapless electronic excitations in a metallic system. The coefficient $\gamma_0(\mathbf{q})$ is $\mathbf{q}$-independent for an antiferromagnetic transition but proportional to $1/|\mathbf{q}|$ or $1/|\mathbf{q}|^2$ for ballistic and diffusive ferromagnets, respectively.

We now consider a random binary alloy $\mathrm{A}_{1-x}\mathrm{B}_x$ consisting of two materials A and B. Pure substance B has a non-magnetic ground-state, implying a positive distance from quantum criticality, $r_\mathrm{B} > 0$. Substance A has a magnetically ordered ground state with $r_\mathrm{A} < 0$. By randomly substituting B atoms for A atoms, one can drive the system through a QPT from a magnetic to a nonmagnetic ground state.

Due to statistical fluctuations, the distribution of A and B atoms in the alloy will not be spatially uniform. Some regions may contain significantly more A atoms

[†]Strictly, one needs to distinguish the bare distance from criticality that appears in (3.2) from the renormalized one that measures the distance from the true critical point. We suppress this difference because it is unimportant for our purposes.

than the average. If the local A-concentration is sufficiently high, such regions will be locally in the magnetic phase even if the bulk system is nonmagnetic. Because the magnetic fluctuations are overdamped, the quantum dynamics of sufficiently large such locally magnetic spatial regions completely freezes (for Ising symmetry [96]). At zero temperature, these rare regions thus develop static magnetic order independently of each other. This destroys the sharp QPT by smearing [90, 97, 98] and is manifest in a pronounced tail in the zero-temperature magnetization-composition curve [118].

At any nonzero temperature, the static magnetic order on individual, independent rare regions is destroyed because they can fluctuate via thermal excitations. Therefore, a finite interaction between the rare regions of the order of the thermal energy is necessary to align them. This restores a conventional sharp phase transition at any nonzero temperature. However, the smeared character of the underlying QPT leads an unusual concentration dependence of the critical temperature T_c which displays a tail towards large x [90, 118].

The effects of disorder correlations can be easily understood at a qualitative level. For positive correlations, like atoms tend to cluster. This increases, at fixed composition, the probability of finding large A-rich regions compared to the uncorrelated case. The tail of magnetization-composition curve therefore becomes larger (see Fig. 1.1). In contrast, like atoms repel each other in the case of negative correlations (anti-correlations). This decreases the probability of finding large A-rich regions and thus suppresses the tail.

3. OPTIMAL FLUCTUATION THEORY

To quantify the influence of the disorder correlations, we now develop an optimal fluctuation theory [90, 118]. We focus on the "tail" of the smeared transition (large x) where a few rare regions show magnetic order but their interactions are weak because they are far apart.

We roughly estimate the transition point in the alloy $A_{1-x}B_x$, by setting the average distance from criticality to zero, $r_{\rm av} = (1-x)r_{\rm A} + x r_{\rm B} = 0$. This defines the critical composition in "average-potential" approximation,

$$x_c^0 = -r_{\rm A}/(r_{\rm B} - r_{\rm A})\,. \tag{3.3}$$

For compositions $x > x_c^0$, static magnetic order can only develop on rare, atypical spatial regions with a higher than average A-concentration. Specifically, a single A-rich rare region of linear size $L_{\rm RR}$ can show magnetic order, if the local concentration $x_{\rm loc}$ of B atoms is below some critical value x_c. Because the rare region has a finite size, the critical concentration is shifted from the bulk value x_c^0. According to finite-size scaling [102, 103]

$$x_c(L_{\rm RR}) = x_c^0 - D L_{\rm RR}^{-\phi}\,, \tag{3.4}$$

where ϕ is the finite-size shift exponent and D is a non-universal constant. In a three-dimensional itinerant magnet, ϕ takes the mean-field value of 2 because the clean transition is above its upper critical dimension. As $x_c(L_{\rm RR})$ must be positive, a rare region must be larger than $L_{\rm min} = (D/x_c^0)^{1/\phi}$ to show magnetic order.

In the tail of the smeared transition, the magnetically ordered rare regions are far apart and interact only weakly. To find the total magnetization M one can thus

simply sum over all magnetically ordered rare regions. This gives

$$M \sim \int_{L_{\min}}^{\infty} dL_{RR} \int_{0}^{x_c(L_{\rm RR})} dx_{\rm loc} P(N, x_{\rm loc}) m(N, x_{\rm loc}) \,, \tag{3.5}$$

where $P(N, x_{\rm loc})$ is the probability for finding a region of N sites and local composition $x_{\rm loc}$ (i.e., a region containing $N_B = N x_{\rm loc}$ atoms of type B), and $m(N, x_{\rm loc})$ is its magnetization

Let us analyze the spatial distribution of atoms in the sample to determine the probability $P(N, x_{\rm loc})$. Specifically, let us assume that the random positions of the A and B atoms are positively correlated such that like atoms form clusters of typical correlation volume (number of lattice sites) $V_{\rm dis} \approx 1 + a\xi_{\rm dis}^d$ where $\xi_{\rm dis}$ is the disorder correlation length and a is a geometric prefactor. The probabilities for finding A and B clusters in the sample are $1 - x$ and x, respectively. The number $n_{\rm cl}$ of correlation clusters contained in a large spatial region of N sites ($N \gg V_{\rm dis}$) is approximately

$$n_{\rm cl} \approx N/V_{\rm dis} = N/(1 + a\xi_{\rm dis}^d) \ . \tag{3.6}$$

The probability $P(N, x_{\rm loc})$ for finding a region of N sites and local composition $x_{\rm loc}$ is therefore equal to the probability $P_{\rm clus}(n_{\rm cl}, n_{\rm B})$ for finding $n_{\rm B} = x n_{\rm cl}$ clusters of B atoms among all the $n_{\rm cl}$ clusters contained in the region. It can be modeled by a binomial distribution

$$P_{\rm clus}(n_{\rm cl}, n_{\rm B}) = \binom{n_{\rm cl}}{n_{\rm B}} (1-x)^{n_{\rm cl} - n_{\rm B}} x^{n_{\rm B}} \ . \tag{3.7}$$

We now distinguish two cases, (i) the regime where x is not much larger than x_c^0, and (ii) the far tail of transition at $x \to 1$.

(i) If x is just slightly larger than x_c^0, rare regions are large and the probability (3.7) can be approximated by a Gaussian

$$P_{\rm clus} \approx \frac{1}{\sqrt{2\pi x(1-x)/n_{\rm cl}}} \exp\left[-n_{\rm cl}\frac{(x_{\rm loc}-x)^2}{2x(1-x)}\right] . \tag{3.8}$$

We estimate the integral (3.5) in saddle point approximation. Neglecting subleading contributions from $m(N, x_{\rm loc})$, we find that rare regions of size $L_{\rm RR}^{\phi} = D(2\phi-d)/[d(x-x_c^0)]$ and composition $x_c(L_{\rm RR})$ dominate the integral. The resulting $M(x)$ dependence reads

$$M \sim \exp\left[-\frac{C}{(1+a\xi_{\rm dis}^d)}\frac{(x-x_c^0)^{2-d/\phi}}{x(1-x)}\right] , \tag{3.9}$$

where $C = 2(D/d)^{d/\phi}(2\phi-d)^{d/\phi-2}\phi^2$ is a non-universal constant. In this regime, varying the disorder correlation length thus modifies the non-universal prefactor of the exponential dependence of M on x.

(ii) An even more striking effect occurs in the tail of the transition for $x \to 1$. As rare regions cannot be large in this regime, the binomial distribution (3.7) cannot be approximated by a Gaussian. However, within saddle point approximation, the integral (3.5) is dominated by rare regions containing only A atoms and having the minimum size permitting local order. Inserting $L_{RR} = L_{\rm min} = (D/x_c^0)^{1/\phi}$ and $x_{\rm loc} = 0$ into (3.5), we find that the composition dependence of the magnetization is given by the power law,

$$M \sim (1-x)^{\beta} \qquad (x \to 1) , \tag{3.10}$$

with $\beta = aL_{\rm min}^d/(1+a\xi_{\rm dis}^d)$. In this regime, the disorder correlations thus modify the seeming critical exponent of the order parameter. The exponent value is given by the minimum number of correlation clusters necessary to form a magnetically ordered rare region. The results for uncorrelated disorder [118] are recovered by substituting $\xi_{\rm dis} = 0$ into (3.9) and (3.10).

So far we have assumed that a typical disorder correlation cluster of A atoms is smaller than the minimum rare region size required for magnetic order. For larger disorder correlation length $\xi_{\rm dis} \geq L_{\rm min}$, a single correlation cluster is already large enough to order magnetically. As a result, (almost) all A atoms contribute to the total magnetization. Correspondingly, the composition dependence of the order parameter is given by

$$M \sim (1-x)\,. \tag{3.11}$$

To combine the power laws (3.10) and (3.11) for different ranges of $\xi_{\rm dis}$, we construct the heuristic formula

$$\beta = (aL_{\rm min}^d + a\xi_{\rm dis}^d)/(1 + a\xi_{\rm dis}^d) \tag{3.12}$$

which can be used to fit experimental data or simulation results.

Other observables such as the finite-temperature phase boundary can be found in similar fashion. As discussed above, at $T \neq 0$, individual rare regions do not develop a static magnetization. Instead, global magnetic order arises via a conventional (sharp) phase transition at some transition temperature T_c which can be estimated from the condition that the interaction energy between the rare regions is of the order of the thermal energy. To determine the interaction energy, we note that in a metallic magnet, the rare-regions are coupled by an RKKY interaction which falls off as r^{-d} with distance r. As the typical distance between neighboring rare regions behaves as $r \sim M^{-1/d}$ [90], the composition dependence of the critical temperature is analogous to that of the magnetization. In particular,

$$T_c(x) \sim (1-x)^\beta \tag{3.13}$$

in the tail of the smeared transition, $x \to 1$.

4. SIMULATIONS

We now verify and illustrate the theoretical predictions by performing computer simulations of a toy model [90, 92]. Its Hamiltonian is motivated by the so-called quantum-to-classical mapping [119] which relates a quantum phase transitions in d space dimensions to a classical transition in $d+1$ dimensions. The extra space dimension corresponds to imaginary time in the quantum problem. Consequently, we consider a (3+1)-dimensional classical Ising model on a hypercubic lattice with three space dimensions and a single imaginary time-like dimension. The interaction in the time-like direction is long-ranged as the $|\omega_n|$ frequency dependence in (3.2) corresponds to a $1/\tau^2$ in imaginary time. In the toy model, we replace this interaction by an infinite-range interaction in time direction, both on the same site and between spatial neighbors.[‡] This correctly reproduces the smeared character of the phase transition due to static magnetic order on the rare regions. The Hamiltonian of the toy model takes the form

$$H = -\frac{1}{L_\tau} \sum_{\langle \mathbf{y},\mathbf{z}\rangle,\tau,\tau'} J_0 S_{\mathbf{y},\tau} S_{\mathbf{z},\tau'} - \frac{1}{L_\tau} \sum_{\mathbf{y},\tau,\tau'} J_{\mathbf{y}} S_{\mathbf{y},\tau} S_{\mathbf{y},\tau'} \ , \tag{3.14}$$

where $\mathbf{y}$ and $\mathbf{z}$ are space coordinates, τ is the time-like coordinate, and $S_{\mathbf{y},\tau} = \pm 1$. L_τ is the system size in time and $\langle \mathbf{y}, \mathbf{z}\rangle$ denotes pairs of nearest neighbors in space. $J_{\mathbf{y}}$ is a binary random variable whose value, J_h or J_l, is determined by the type of atom on lattice site $\mathbf{y}$. The values at different sites $\mathbf{y}$ and $\mathbf{z}$ are *not* independent, they are correlated according to some correlation function $\mathcal{C}(\mathbf{y}-\mathbf{z})$. The average concentrations of J_h-sites and J_l-sites are $1-x$ and x, respectively.

Treating the time-like dimension within mean-field theory, which is exact because of the infinite range of the interactions, a set of coupled nonlinear equations

[‡]Even though the bare action (3.1, 3.2) does not have an interaction between spatial neighbors at different imaginary times τ, such a coupling will be generated in perturbation theory (or under RG) from the short-range spatial interaction and the long-range interaction in time.

emerge for the local magnetizations $m_{\mathbf{y}} = (1/L_\tau) \sum_\tau S_{\mathbf{y},\tau}$,

$$m_{\mathbf{y}} = \tanh \frac{1}{T_{cl}} \left(J_{\mathbf{y}} m_{\mathbf{y}} + \sum_{\mathbf{z}} J_0 m_{\mathbf{z}} + h \right) . \tag{3.15}$$

Here, the $\mathbf{z}$-sum is over the nearest neighbors of site $\mathbf{y}$, and h is a tiny symmetry-breaking magnetic field. According to the quantum-to-classical mapping, the classical temperature T_{cl} is not related to the physical temperature of the underlying quantum system (which is encoded in L_τ) but rather some quantum control parameter that tunes the distance from the quantum phase transition.

The local mean-field equations (3.15) can be solved efficiently in a self-consistency cycle. In the two clean limits with either $J_{\mathbf{y}} = J_h$ or $J_{\mathbf{y}} = J_l$ for all $\mathbf{y}$, the phase transition occurs at $T_h = J_h + 6J_0$ and $T_l = J_l + 6J_0$, respectively. We choose a classical temperature between T_h and T_l and control the transition by changing the composition x.

To generate the correlated binary random variables representing the site occupations, a version of the Fourier-filtering method [120] is implemented. This method starts from uncorrelated Gaussian random numbers $u_{\mathbf{y}}$ and turns them into correlated Gaussian random numbers $v_{\mathbf{y}}$ characterized by some correlation function $\mathcal{C}(\mathbf{r})$. This is achieved by transforming the Fourier components $\tilde{u}_{\mathbf{q}}$ of the uncorrelated random numbers according to

$$\tilde{v}_{\mathbf{q}} = \left[\tilde{\mathcal{C}}(\mathbf{q}) \right]^{\frac{1}{2}} \tilde{u}_{\mathbf{q}}, \tag{3.16}$$

where $\tilde{\mathcal{C}}(\mathbf{q})$ is the Fourier transform of $\mathcal{C}(\mathbf{r})$. The $v_{\mathbf{y}}$ then undergo binary projection to determine the occupation of site $\mathbf{y}$; the site is occupied by atom A if $v_{\mathbf{y}}$ is greater than a composition-dependent threshold and by atom B if $v_{\mathbf{y}}$ is less than the threshold.

In the majority of our calculations, we focus on attractive short-range disorder correlations of the form $\mathcal{C}(\mathbf{r}) = \exp\left(-r^2/2\xi_{\text{dis}}^2\right)$. Figure 4.1 shows examples of the resulting atom distributions for several values of the disorder correlation length ξ_{dis}. The formation of clusters of like atoms is clearly visible.

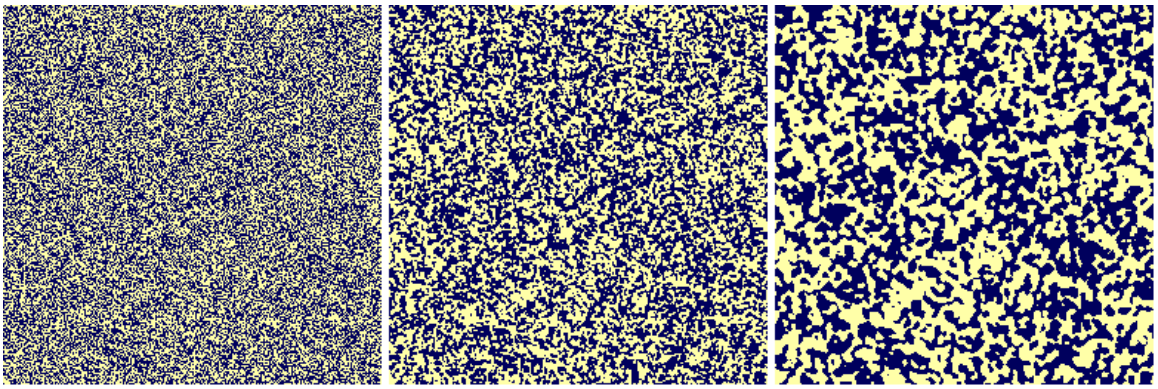

Figure 4.1: (Color online) Examples of the atom distribution in a plane of 256^2 sites for several values of the disorder correlation length $\xi_{\rm dis} = 0, 1.0, 2.0$ from left to right ($x = 0.5$).

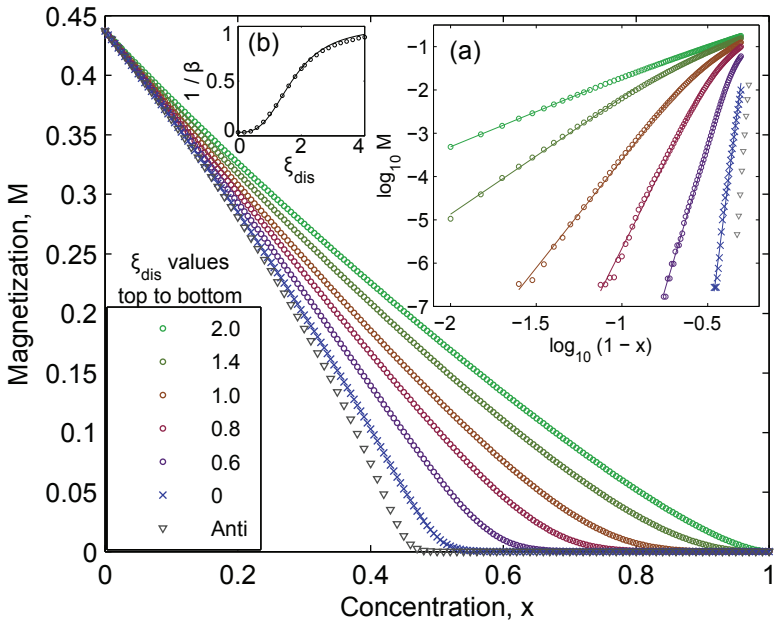

Figure 4.2: (Color online) Magnetization M vs. composition x for several values of the disorder correlation length $\xi_{\rm dis}$ using one disorder realization of 256^3 sites, $J_h = 20$, $J_l = 8$, $J_0 = 1$, $T_{cl} = 24.25$, and $h = 10^{-10}$. Also shown is one curve for the case of anti-correlations (128^3 sites), for details see text. Inset (a): log-log plot of M vs. $(1 - x)$ confirming the power-law behavior in the tail of the smeared transition. The tail exponent β shown in inset (b) agrees very well with (3.12) as shown by the solid fit line.

We now discuss the results of the mean-field equations (3.15). Figure 4.2 presents the total magnetization M as function of composition x for several values of $\xi_{\rm dis}$ with all other parameters held constant. At a given composition x, the magneti-

zation M increases significantly even for small ξ_{dis} of the order of the lattice constant. Moreover, the seeming transition point (at which M appears to reach 0) rapidly moves towards larger compositions, almost reaching $x = 1$ for a correlation length $\xi_{\text{dis}} = 2$. Inset (a) of Fig. 4.2 shows a plot of $\log M$ versus $\log(1 - x)$ confirming the power-law behavior (3.10) in the tail of the transition. The dependence on ξ_{dis} of the exponents β extracted from these power laws is analyzed in inset (b) of Fig. 4.2. It can be fitted well with the heuristic formula (3.12).

In addition to the attractive (positive) correlations, we now briefly consider the case of anti-correlations (like atoms repel each other). We model the anti-correlations by a correlation function having values $\mathcal{C}(0) = 1$, $\mathcal{C}(\mathbf{r}) = -c$ for nearest neighbors, and $\mathcal{C}(\mathbf{r}) = 0$ otherwise. The positive constant c controls the strength of the anti-correlations. A characteristic magnetization-composition curve for such anti-correlated disorder (with $c = 1/6$) is included in Fig. 4.2. The data show that the magnetization is reduced compared to the uncorrelated case, and the tail becomes less pronounced. Analogous simulations using different values of c show that this effect increases with increasing strength of the anti-correlations, as indicated in Fig. 1.1.

5. CONCLUSIONS

In summary, we have studied the effects of spatially correlated disorder on smeared phase transitions. We have found that even short-range disorder correlations (extending over just a few lattice constants) lead to qualitative modifications of the behavior at smeared transitions compared to the uncorrelated case, including changes in the exponents that characterize the order parameter and the critical temperature. In other words, systems with uncorrelated disorder and with short-range correlated disorder behave differently

This is in marked contrast to critical points, at which uncorrelated disorder and short-range correlated disorder lead to the same critical behavior. (Long-range correlations do change the critical behavior [117, 121].) What causes this difference between critical points and smeared transitions? The reason is that critical behavior emerges in the limit of infinitely large length scales while smeared transitions are governed by a finite length scale, viz., the minimum size of ordered rare regions. This renders the renormalization group arguments underlying the generalized Harris criterion [116, 117] inapplicable.

The majority of our calculations are for the case of like atoms attracting each other. For these positive correlations, large locally ordered rare regions can form more easily than in the uncorrelated case. Thus, the tail of the smeared transition is enhanced; and the phase boundary as well as the magnetization curve move toward larger x as indicated in Fig. 1.1. We have also briefly considered the case of like atoms repulsing each other. These anti-correlations suppress the formation of large locally ordered rare regions compared to the uncorrelated case. As a result, the phase boundary and the magnetization curve will move toward smaller x. In addition to short-range correlations, we have also studied long-range power-law correlations which are interesting because they lead to a broad spectrum of cluster sizes. Detailed results will be published elsewhere [122].

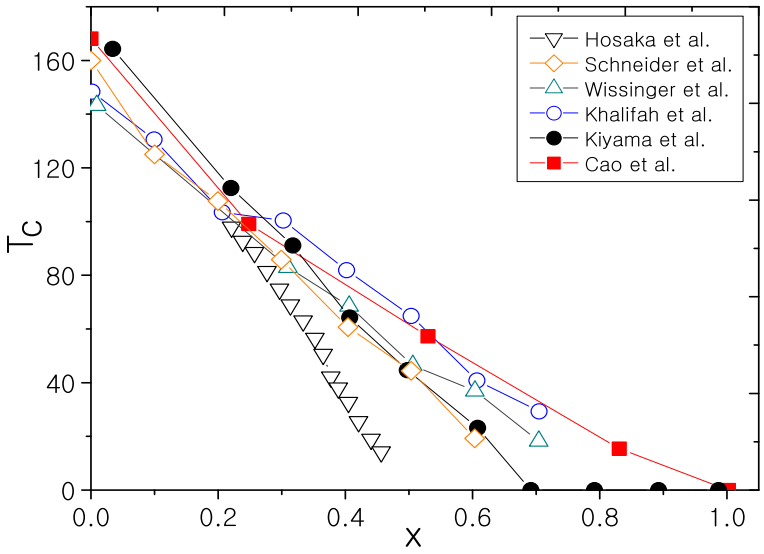

Figure 5.1: (Color online) Experimental temperature-composition phase diagrams of $Sr_{1-x}Ca_xRuO_3$. Data from Hosaka et al. [123], Schneider et al. [124], Wissinger et al. [125], and Khalifah et al. [126] are for thin films while those of Kiyama et al. [109], and Cao et al. [107] are for bulk samples. Published magnetization curves show similar variations.

Turning to experiment, our results imply that smeared phase transitions are very sensitive to slight short-range correlations in the spatial positions of impurities or defects. In particular, an analysis of the data in terms of critical exponents will give values that depend on these correlations. We believe that a possible realization of the effects discussed in this paper can be found in $Sr_{1-x}Ca_xRuO_3$. This well-studied material undergoes a ferromagnetic QPT as a function of Ca concentration. Because $Sr_{1-x}Ca_xRuO_3$ is a metallic system with Ising spin symmetry, the transition is expected to be smeared [90]. Interestingly, the reported experimental phase diagrams (see Fig. 5.1) and magnetization curves show unusually large variations. Not only does the apparent critical composition change between $x \approx 0.5$ and 1; the functional form of the magnetization curves also varies. Although part of these discrepancies may be due to the difference between film and bulk samples [125], large variations within each sample type remain. We propose that disorder correlations, i.e., clustering or anti-clustering of like atoms may be responsible for at least part of these variations.

Finally, we emphasize that even though we have considered the QPT in itinerant magnets as an example, our theory is very general and should be applicable to all phase transitions smeared by disorder including QPTs [91, 127, 128], classical transitions in layered systems [92, 93] and non-equilibrium transitions [129]

We thank I. Kezsmarki for helpful discussions. This work has been supported in part by the NSF under grant No. DMR- 0906566.

IV. DISORDER PROMOTES FERROMAGNETISM: ROUNDING OF THE QUANTUM PHASE TRANSITION IN $SR_{1-X}CA_XRUO_3$

L. Demkó[1,2], S. Bordács[3,4], T. Vojta[5,6], D. Nozadze[6], F. Hrahsheh[6], C. Svoboda[6], B. Dóra[7,8], H. Yamada[9], M. Kawasaki[10,11,12], Y. Tokura[1], and I. Kézsmárki[1]

[1]*Department of Physics, Budapest University of Technology and Economics and Condensed Matter Research Group of the Hungarian Academy of Sciences, 1111 Budapest, Hungary*

[2]*Multiferroics Project, ERATO, Japan Science and Technology Agency (JST), c/o Department of Applied Physics, University of Tokyo, Tokyo 113-8656, Japan*

[3]*Department of Physics, Budapest University of Technology and Economics and Condensed Matter Research Group of the Hungarian Academy of Sciences, 1111 Budapest, Hungary*

[4]*Multiferroics Project, ERATO, Japan Science and Technology Agency (JST), c/o Department of Applied Physics, University of Tokyo, Tokyo 113-8656, Japan*

[5]*Max-Planck-Institut für Physik Komplexer Systeme, Nöthnitzer Str. 38, 01187 Dresden, Germany*

[6]*Department of Physics, Missouri University of Science and Technology, Rolla, MO 65409, USA*

[7]*Department of Physics, Budapest University of Technology and Economics and Condensed Matter Research Group of the Hungarian Academy of Sciences, 1111 Budapest, Hungary*

[8]*Max-Planck-Institut für Physik Komplexer Systeme, Nöthnitzer Str. 38, 01187 Dresden, Germany*

[9]*National Institute of Advanced Industrial Science and Technology (AIST), Tsukuba, Ibaraki 305-8562, Japan*

[10] *Cross-Correlated Materials Research Group (CMRG), RIKEN Advanced Science Institute (ASI), Wako 351-0198, Japan*

[11] *WPI-AIMR, Tohoku University, Sendai 980-8577, Japan*

[12] *Department of Applied Physics, University of Tokyo, Tokyo, 110-8656, Japan*

[13] *Department of Physics, Budapest University of Technology and Economics and Condensed Matter Research Group of the Hungarian Academy of Sciences, 1111 Budapest, Hungary*

ABSTRACT*

The subtle interplay of randomness and quantum fluctuations at low temperatures gives rise to a plethora of unconventional phenomena in systems ranging from quantum magnets and correlated electron materials to ultracold atomic gases. Particularly strong disorder effects have been predicted to occur at zero-temperature quantum phase transitions. Here, we demonstrate that the composition-driven ferromagnetic-to-paramagnetic quantum phase transition in $Sr_{1-x}Ca_xRuO_3$ is completely destroyed by the disorder introduced via the different ionic radii of the randomly distributed Sr and Ca ions. Using a magneto-optical technique, we map the magnetic phase diagram in the composition-temperature space. We find that the ferromagnetic phase is significantly extended by the disorder and develops a pronounced tail over a broad range of the composition x. These findings are explained by a microscopic model of smeared quantum phase transitions in itinerant magnets. Moreover, our theoretical study implies that correlated disorder is even more powerful in promoting ferromagnetism than random disorder.

Classical or thermal phase transitions generally remain sharp in the presence of disorder, though their critical behavior might be affected by the randomness. On the other hand, zero-temperature quantum phase transitions [119, 130, 131] – which

*Published in Physical Review Letters **108**, 185701 (2012).

are induced by a control parameter such as the pressure, chemical composition or magnetic field – are more susceptible to the disorder. Nevertheless, most disordered quantum phase transitions have been found sharp as the correlation length characterizing the spatial fluctuation of the neighboring phases diverges at the transition point.

In recent years, it has become clear that the large spatial regions free of randomness, which are rare in a strongly disordered material and hereafter referred to as *rare regions*, can essentially change the physics of phase transitions [97]. Close to a magnetic transition, such rare regions can be locally in the magnetically ordered phase – with slow fluctuations leading to the famous Griffiths singularities [132] – even if the bulk system is still nonmagnetic. These rare regions are extremely influential close to quantum phase transitions. and expected to dominate the thermodynamics. They give rise to the the so-called quantum Griffiths phases [97, 98, 132] as recently observed in magnetic semiconductors [133], heavy-fermion systems [134], and transition metal alloys [135].

When the rare regions are embedded in a dissipative environment the disorder effects are further enhanced. For example, in metallic magnets, the magnetization fluctuations are coupled to electronic excitations having arbitrarily low energies. This leads to an over-damped fluctuation dynamics. Sufficiently strong damping completely freezes the dynamics of the locally ordered rare regions [96], allowing them to develop a static magnetic order. It has been predicted [90] that this mechanism destroys the sharp magnetic quantum phase transition in a disordered metal by rounding and a spatially inhomogeneous ferromagnetic phase appears over a broad range of the control parameter.

The family of perovskite-type $ARuO_3$ ruthanates (with A an alkaline earth ion) offers an ideal setting to test these predictions. $SrRuO_3$ is a ferromagnetic metal with a Curie temperature of $T_C = 165\,\mathrm{K}$. On the other hand, no long-range magnetic order develops in $CaRuO_3$ and recent studies indicate paramagnetic behavior or

the presence of short-range antiferromagnetic correlations in the ground state [136]. It is demonstrated that tiny Co doping can drive the system to a low-temperature spin-glass state [137], however, the ground state of $CaRuO_3$ is still under debate. Earlier studies of the transport, thermal and magnetic properties of $Sr_{1-x}Ca_xRuO_3$ solid solutions revealed that the composition x is an efficient control parameter and the substitution of the Sr ions by the smaller Ca ions gradually suppresses the ferromagnetic character and with it the Curie temperature [107, 108, 109, 138]. However, estimates of the critical Ca concentration at which T_C vanishes show large variations depending on the way of the assignment, experimental methodology and sample synthesis (e.g. bulk crystals versus thin films with strain due to lattice mismatch with the substrate). In addition, the random distribution of Sr and Ca ions introduces strong disorder in the exchange interactions controlling the magnetic state.

To investigate the magnetic properties of $Sr_{1-x}Ca_xRuO_3$ with high accuracy, we have grown a composition-spread epitaxial film of size 10 mm×4 mm and thickness 200 nm ($\sim$ 500 unit cells) on a $SrTiO_3$ (001) substrate [139, 140] which sets the easy magnetization direction normal to the film plane [141]. The Ca concentration changes linearly from x=0.13 to 0.53 along the long side of the sample, as shown in Fig. 1.a. The large atomically-flat area observed in the atomic force microscope image (Fig. 1.a) demonstrates the high quality of this film.

The composition and temperature dependence of the magnetic properties of the $Sr_{1-x}Ca_xRuO_3$ film were probed by a home-built magneto-optical Kerr microscope equipped with a He-flow optical cryostat. Its magneto-optical Kerr rotation for visible light is dominated by the charge transfer excitations between the O 2p and Ru 4d t_{2g} states [123]. The large magnitude of the magneto-optical Kerr effect, being the consequence of strong spin-orbit coupling in ruthenates [142], was found to be proportional to the magnetization measured by a SQUID magnetometer on uniform thin films. We have performed all these experiments using a red laser diode. The resulting precisions of the magnetization (M) and susceptibility (χ) measurements

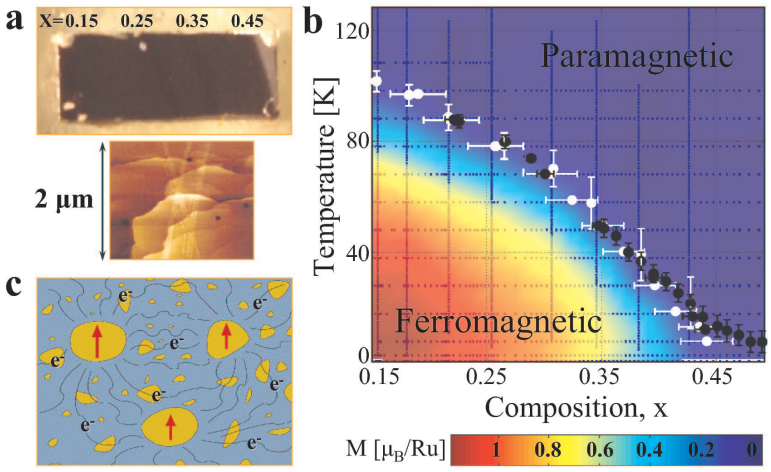

Figure 1.: (Color online) Morphology and magnetic characterization of the composition-spread $Sr_{1-x}Ca_xRuO_3$ epitaxial film. **(a)** Photographic image of the $10\times4\,\mathrm{mm}^2$ film with the local concentration, x, indicated along the composition-spread direction. The large terraces of mono-atomic layers in the atomic force microscope image demonstrates the high quality of the film. **(b)** The contour plot of the remanent magnetization (M) over the composition-temperature phase diagram. The dotted mesh is the measured data set used for the interpolation of the surface. The ferromagnetic-paramagnetic phase boundary, $T_C(x)$, derived from the susceptibility and magnetization data (see text for details) is also indicated by the black and grey symbols, respectively. **(c)** Schematic of the magnetism in the tail of the smeared transition. The spins on Sr-rich rare regions (bright islands) form locally ordered "superspins". Their dynamics freezes due to the coupling to electronic excitations which also tends to align them giving rise to an inhomogeneous long-range ferromagnetic order.

were $6\cdot10^{-3}\,\mu_B$ per Ru atom and $8\cdot10^{-3}\,\mu_B\mathrm{T}^{-1}$ per Ru atom, respectively. Since the composition gradient of the sample is about $0.04\,\mathrm{mm}^{-1}$, the spatial resolution, $\delta\lesssim20\,\mu$m, of our microscope corresponds to a resolution of $\delta x\approx0.001$ in the composition, allowing us to achieve an exceptionally fine mapping of the magnetization versus the control parameter of the quantum phase transition. See Supplemental Material at [143] for more details on the sample preparation, characterization, and on the experimental methodology.

An overview of the results is given in Fig. 1.b which shows a color contour map of the remanent magnetization M as a function of the temperature T and the

composition x. It was obtained by interpolating a large collection of $M(x)$ and $M(T)$ curves measured at constant temperatures and concentrations, respectively. The data clearly show that the area of the ferromagnetic phase and the magnitude of the low-temperature magnetization are gradually suppressed with increasing x. Figure 2. displays the temperature dependence of the magnetization and susceptibility for selected compositions. With increasing x, the upturn region in the magnetization curves significantly broadens and the width of the ac susceptibility peaks increases. This already hints at an unconventional smearing of the paramagnetic-to-ferromagnetic phase transition at higher values of the composition x. The critical temperature, $T_C(x)$ in Fig. 1.b, separating the ferromagnetic and paramagnetic states in the composition-temperature phase diagram was identified with the peak positions in the susceptibility and in the first derivative of magnetization using both the temperature and the concentration sweeps.

The $T_C(x)$ line in Fig. 1.b does not show a singular drop at any concentration, instead it grows a tail extending beyond $x = 0.52$ where the zero-temperature magnetization is about three orders of magnitude smaller than the saturation value for $SrRuO_3$. Similar behavior is also observed in the low-temperature magnetization M as a function of the composition, x, as shown in Fig. 3.a. (We found that all $M(x)$ curves measured below T=6 K collapse onto each other without any detectable temperature variation.) $M(x)$ has an inflection point at $x \approx 0.44$ followed by a pronounced tail region in which the magnetization decays slowly towards larger x. The existence of an ordered ferromagnetic moment is further confirmed by the hysteresis in the $M(B)$ loops even at $x = 0.52$ (see the inset of Fig. 3.a). Thus, the evolution of both the magnetization and the critical temperature with x provide strong evidence for the ferromagnetic-to-paramagnetic quantum phase transition being smeared.

How can the unconventional smearing of the quantum phase transition and the associated tail in the magnetization be understood quantitatively? As the magnetization fluctuations in a metallic ferromagnet are over-damped, sufficiently large

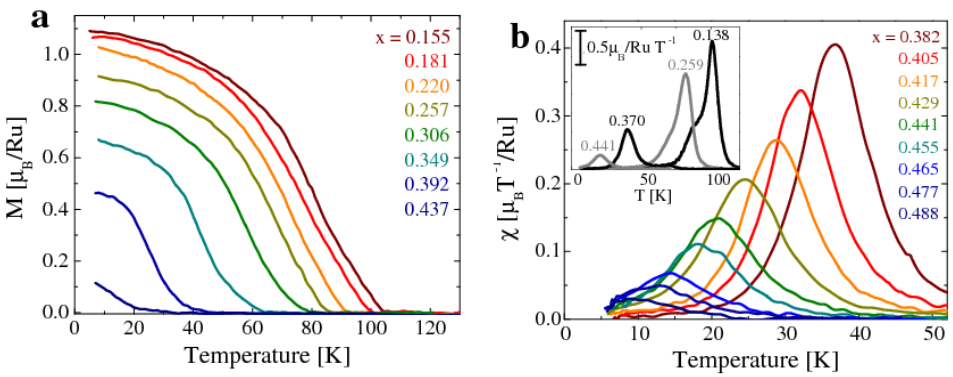

Figure 2.: (Color online) Temperature dependence of **(a)** the remanent magnetization M and **(b)** ac susceptibility χ for selected compositions, x. The main panel of **(b)** focuses on the region $x \gtrsim 0.4$, and the inset displays representative susceptibility curves over the full range of x. Both the magnetization and susceptibility curves show the continuous suppression of the ferromagnetic phase with increasing x and the broadening of the transition.

Sr-rich rare regions can develop true magnetic order (see Fig. 1.c) even if the bulk system is paramagnetic [90, 96]. Macroscopic ferromagnetism arises because these rare regions are weakly coupled by an effective long-range interaction [144, 145]. To model this situation, we observe that the probability for finding N_{Sr} strontium and N_{Ca} calcium atoms in a region of $N = N_{\mathrm{Sr}} + N_{\mathrm{Ca}}$ unit cells (at average composition x) is given by the binomial distribution $P(N_{\mathrm{Sr}}, N_{\mathrm{Ca}}) = \binom{N}{N_{\mathrm{Sr}}}(1-x)^{N_{\mathrm{Sr}}} x^{N_{\mathrm{Ca}}}$. Such a region orders magnetically if the local calcium concentration $x_{\mathrm{loc}} = N_{\mathrm{Ca}}/N$ is below some threshold x_c. Actually, taking finite-size effects into account [118], the condition reads $x_{\mathrm{loc}} < x_c - A/L_{RR}^2$ where L_{RR} is the size of the rare region, and A is a non-universal constant. To estimate the total magnetization in the tail of the transition ($x > x_c$), one can simply integrate the binomial distribution over all rare regions fulfilling this condition. This yields [118], up to power-law prefactors,

$$M \propto \exp\left[-C\frac{(x-x_c)^{2-d/2}}{x(1-x)}\right] \tag{4.1}$$

where C is a non-universal constant. This equation clearly illustrates the notion of "smeared" quantum phase transition: the order parameter vanishes only at $x = 1$ and

develops a long, exponential tail upon approaching this point. As x_c represents the composition where the hypothetical homogeneous (clean) system having the average ion size would undergo the quantum phase transition, the extension of the ferromagnetic phase beyond x_c is an effect of the disorder. Starting from atomic-scale disorder our theory is applicable as long as a large number of clusters are probed within the experimental resolution, so that the measured quantities represent an average over the random cluster distribution. The smooth dependence of the magnetization on x together with the small spot size of the beam ($<300\,\mu\mathrm{m}^2$) verifies that this is indeed the case. Based on the given spot size the upper bound for the typical cluster size is estimated to be 1-2 $\mu\mathrm{m}^2$ (see Supplemental Material).

As a direct test of our theory we fit the lowest-temperature $M(x)$ data with Eq. (4.1). We take the spatial dimensionality $d = 3$ due to the large thickness of the sample far beyond the spin correlation length in the system. As can be discerned in Fig. 3.b, the magnetization data in the tail ($x \gtrsim 0.44$) follow the theoretical curve over about 1.5 orders of magnitude down to the resolution limit of the instrument. For the critical composition of the hypothetical clean system, we obtain $x_c = 0.38$, though the quality of the fit is not very sensitive to its precise value because the drop in M occurs over a rather narrow x interval. The composition dependence of the critical temperature T_C can be estimated along the same lines by comparing the typical interaction energies between the rare regions with the temperature and the same functional dependence on x was found [118]. The experimental data in the tail region follow this prediction with the same $x_c = 0.38$ value, as can be seen from the corresponding fit in Fig. 3.b.

To summarize, we have studied the paramagnetic-to-ferromagnetic quantum phase transition of $Sr_{1-x}Ca_xRuO_3$ by means of a composition-spread epitaxial film. We found that the disorder significantly extends the ferromagnetic phase. Moreover, the phase transition in this itinerant system does not exhibit any of the singularities associated with a quantum critical point. Instead, both the magnetization and

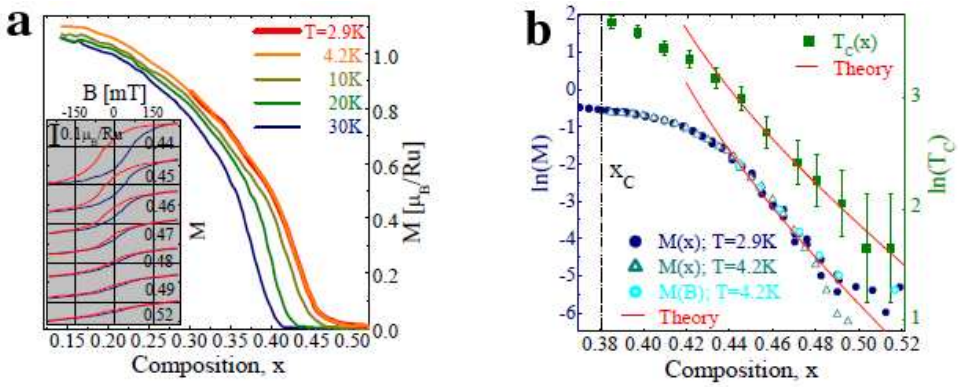

Figure 3.: (Color online) The smearing of the quantum phase transition in $Sr_{1-x}Ca_xRuO_3$. **(a)** The composition dependence of the remanent magnetization M at selected temperatures. The inset shows that the hysteresis in the field loops at T=4.2 K gradually vanishes towards larger x but still present even at $x \approx 0.52$. **(b)** Semilogarithmic plots of the magnetization and the transition temperature T_C as functions of the control parameter in the tail region. The symbols represent the experimental data while solid lines correspond to the theory which predicts $x_c = 0.38$ as the location of the quantum phase transition in the (hypothetical) clean system.

critical temperature display pronounced tails towards the paramagnetic phase. The functional forms of these tails agree well with the predictions of our theoretical model. Our calculations also show that disorder, if correlated over a few unit cells, is even more powerful in promoting an inhomogeneous ferromagnetic phase. We thus conclude that our results provide, to the best of our knowledge, the first quantitative confirmation of a smeared quantum phase transition in a disordered metal. We expect that this scenario applies to a broad class of itinerant systems with quenched disorder.

We thank A. Halbritter and G. Mihály for fruitful discussions. This work was supported by KAKENHI, MEXT of Japan, by the Japan Society for the Promotion of Science (JSPS) through its "Funding Program for World-Leading Innovative R&D on Science and Technology (FIRST Program)", by Hungarian Research Funds OTKA PD75615, CNK80991, K73361, Bolyai program, TÁMOP-4.2.1/B-09/1/KMR-2010-0002, as well as by the NSF under grant No. DMR-0906566.

V. ROUNDING OF A FIRST-ORDER QUANTUM PHASE TRANSITION TO A STRONG-COUPLING CRITICAL POINT

Fawaz Hrahsheh[1], José A Hoyos[2], and Thomas Vojta[1]

[1]Department of Physics, Missouri University of Science and Technology, Rolla, MO 65409, USA

[2]Instituto de Física de São Carlos, Universidade de São Paulo, C.P. 369, São Carlos, São Paulo 13560-970, Brazil

ABSTRACT*

We investigate the effects of quenched disorder on first-order quantum phase transitions on the example of the N-color quantum Ashkin-Teller model. By means of a strong-disorder renormalization group, we demonstrate that quenched disorder rounds the first-order quantum phase transition to a continuous one for both weak and strong coupling between the colors. In the strong coupling case, we find a distinct type of infinite-randomness critical point characterized by additional internal degrees of freedom. We investigate its critical properties in detail and find stronger thermodynamic singularities than in the random transverse field Ising chain. We also discuss the implications for higher spatial dimensions as well as unusual aspects of our renormalization-group scheme.

*Published in Physical Review B **86**, 214204 (2012).

1. INTRODUCTION

The effects of disorder on quantum phase transitions have gained increasing attention recently, in particular since experiments have discovered several of the exotic phenomena predicted by theory (see, e.g., Refs. [146, 147]). Most of the existing work has focused on continuous transitions while first-order quantum phase transitions have received less attention.

In contrast, the influence of randomness on pure systems undergoing a *classical* first-order transition has been comprehensively studied. Using a beautiful heuristic argument, Imry and Wortis [148] reasoned that quenched disorder should round classical first-order phase transitions in sufficiently low dimension and thus produce new continuous phase transitions. This analysis was extended by Hui and Berker.[149] Aizenman and Wehr [67] rigorously proved that first-order phase transitions cannot exist in disordered systems in dimensions $d \leq 2$. If the randomness breaks a continuous symmetry, the marginal dimension is $d = 4$.

The question of whether or not disorder can round a first-order *quantum* phase transition (QPT) to a continuous one was asked by Senthil and Majumdar,[150] and, more recently, by Goswami *et al.*[151] Using a strong-disorder renormalization group (SDRG) technique, they found that the transitions in the random quantum Potts and clock chains [150] were governed by the well-known infinite-randomness critical point (IRCP) of the random transverse-field Ising chain.[27, 28] The same holds for the N-color quantum Ashkin-Teller (AT) model in the weak-coupling (weak interaction between the colors) regime.[151] This implies that disorder can indeed round first-order quantum phase transitions.

In the strong-coupling regime of the AT model, on the other hand, the renormalization-group (RG) analysis of the authors of Ref. [151] breaks down. Goswami *et al.* speculated that this implies persistence of the first-order QPT in the presence of disorder, requiring important modifications of the Aizenman-Wehr theorem. However,

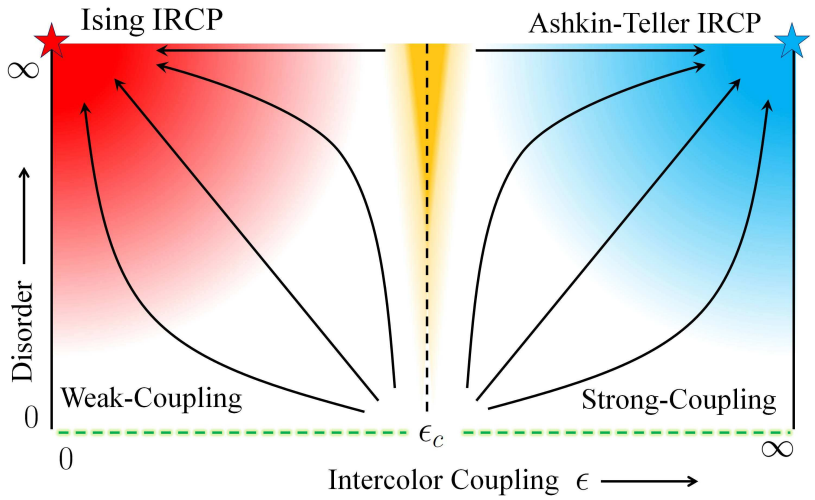

Figure 1.1: (Color online) Schematic of the renormalization-group flow diagram in the disorder-coupling strength parameter space. For $\epsilon < \epsilon_c$ (left arrows), the critical flow approaches the usual Ising infinite-randomness critical point of Ref. [28]. For $\epsilon > \epsilon_c$ (right arrows), we find a distinct infinite-randomness critical point with even stronger thermodynamic singularities.

shortly after, Greenblatt *et al.* [68, 152] proved rigorously that the Aizenman-Wehr theorem also holds for quantum systems at zero temperature. In this paper, we resolve the apparent contradiction between these results. We show that quenched disorder rounds the first-order QPT of the AT model in the strong-coupling regime as well as in the weak-coupling regime. Moreover, we unveil a distinct type of infinite-randomness critical point governing the transition in the strong-coupling regime. It is characterized by additional internal degrees of freedom which appear because a higher symmetry is dynamically generated at criticality. As a consequence, the critical point displays even stronger thermodynamic singularities than the transverse-field Ising IRCP. To obtain these results, we have developed an implementation of the SDRG method that works for both weak and strong coupling. In particular, this method can deal with the diverging intercolor interactions as well as the associated additional degeneracies. A schematic of the resulting RG flow in the critical plane is shown in Fig. 1.1.

Our paper is organized as follows: In Sec. 2., we define the model and discuss a few of its basic properties. Section 3. is devoted to our strong-disorder renormalization group scheme. The resulting phase diagram and observables are discussed in Sec. 4.. We conclude in Sec. 5..

2. QUANTUM ASHKIN-TELLER MODEL

The Hamiltonian of the one-dimensional N-color quantum AT model [153, 154, 155] is given by

$$H = -\sum_{\alpha=1}^{N}\sum_{i=1}^{L}\left(J_i\sigma^z_{\alpha,i}\sigma^z_{\alpha,i+1} + h_i\sigma^x_{\alpha,i}\right) \\ -\sum_{\alpha<\beta}^{N}\sum_{i=1}^{L}\left(\epsilon_{J,i}J_i\sigma^z_{\alpha,i}\sigma^z_{\alpha,i+1}\sigma^z_{\beta,i}\sigma^z_{\beta,i+1} + \epsilon_{h,i}h_i\sigma^x_{\alpha,i}\sigma^x_{\beta,i}\right). \tag{5.1}$$

Here, i indexes the lattice sites, α and β index colors, and σ^x and σ^z are the usual Pauli matrices. The interactions J_i and transverse fields h_i are independent random variables taken from distributions restricted to positive values, while $\epsilon_{h,i}$ and $\epsilon_{J,i}$ (also restricted to be positive) parametrize the strength of the coupling between the colors.[†] Various versions of the AT model have been used to describe the layers of atoms absorbed on surfaces, organic magnets, current loops in high-T_c superconductors as well as the elastic response of DNA molecules. Note the invariance of the Hamiltonian under the following duality transformation: $\sigma^z_{\alpha,i}\sigma^z_{\alpha,i+1} \to \tau^x_{\alpha,i}$, $\sigma^x_{\alpha,i} \to \tau^z_{\alpha,i}\tau^z_{\alpha,i+1}$, $J_i \rightleftarrows h_i$, and $\epsilon_{J,i} \rightleftarrows \epsilon_{h,i}$, where τ^x and τ^z are the dual Pauli operators. The bulk phases of the AT model (5.1) are easily understood. If the typical interaction J_{typ} is larger than the typical field h_{typ}, the system is in the ordered (Baxter) phase in which each color orders ferromagnetically. When $h_{typ} \gg J_{typ}$, the model is in the paramagnetic phase. If there is a direct transition between these two phases, duality requires that it occurs at $J_{typ} = h_{typ}$. In the clean version of our system with $N \geq 3$, the QPT between the paramagnetic and ordered (Baxter) phases is of first-order type.[153, 154, 155, 156]

[†]Even if we assume uniform nonrandom values of ϵ_J and ϵ_h, they will acquire randomness under renormalization.

3. STRONG-DISORDER RENORMALIZATION GROUP

To tackle the Hamiltonian (5.1), we now develop a SDRG method. In the weak-coupling regime ($\epsilon_h, \epsilon_J \ll \epsilon_c$, where ϵ_c is some N-dependent threshold), our method agrees with that of Goswami *et al.*[151] Here, we focus on the strong coupling regime $\epsilon_h, \epsilon_J \gg \epsilon_c$ where the method of the authors of Ref. [151] breaks down.

The basic idea of the SDRG method consists in identifying the largest local energy scale and perturbatively integrating out the corresponding high-energy degree of freedom. As we are in the strong-coupling regime, this largest local energy is either a four-spin interaction ("AT interaction") $k_i = \epsilon_{J,i} J_i$ or a two-color field-like term ("AT field") $g_i = \epsilon_{h,i} h_i$. We thus define our high-energy cutoff $\Omega = \max\{k_i, g_i\}$.

We now derive the decimation procedure. If the largest local energy is an AT field located, say, at site 2, the unperturbed Hamiltonian for the decimation of this

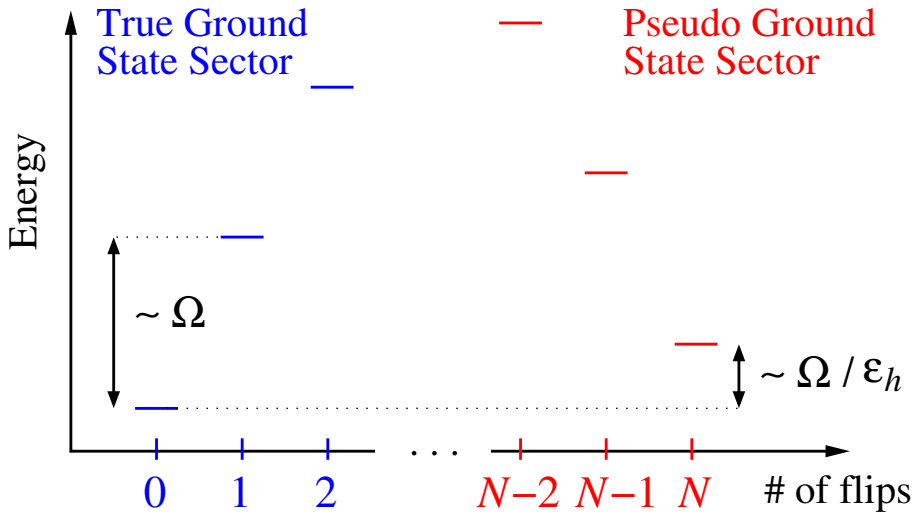

Figure 3.1: (Color online) Spectrum of the unperturbed Hamiltonian (5.2) as function of the number of colors flipped with respect to the ground state $|\rightarrow, \rightarrow, \cdots, \rightarrow\rangle$. As long as $T \lesssim \Omega/\epsilon_h$, the pseudo ground state $|\phi_0'\rangle = |\leftarrow, \leftarrow, \cdots, \leftarrow\rangle$ can be neglected when computing observables (stage 1 of the RG). When $T \gtrsim \Omega/\epsilon_h$, $|\phi_0\rangle$ and $|\phi_0'\rangle$ become effectively degenerate implying that both states need to be taken into account (stage 2 of the RG).

site reads

$$H_0 = -\frac{g_2}{\epsilon_{h,2}} \sum_{\alpha=1}^{N} \sigma^x_{\alpha,2} - g_2 \sum_{\alpha<\beta} \sigma^x_{\alpha,2}\sigma^x_{\beta,2}. \tag{5.2}$$

The ground state (GS) of H_0 is $|\phi_0\rangle = |\rightarrow, \rightarrow, \cdots, \rightarrow\rangle$, with energy $E_0 = -Ng_2/\epsilon_{h,2} - N(N-1)g_2/2$, where each arrow represents a different color. Flipping n colors leads to $\binom{N}{n}$ degenerate excited states with energy $E_n = E_0 + 2ng_2/\epsilon_{h,2} + 2n(N-n)g_2$. In the strong-coupling regime, $\epsilon_h \gg 1$, the state $|\phi_0'\rangle = |\leftarrow, \leftarrow, \cdots, \leftarrow\rangle$ plays a special role. Its energy $E_0' = Ng_2/\epsilon_{h,2} - N(N-1)g_2/2$ differs from that of the true ground state only by the subleading Ising term $E_0' - E_0 = 2Ng_2/\epsilon_{h,2}$ (see Fig. 3.1). It can thus be considered a "pseudo ground state" which may be important for a correct description of the low-energy physics. The true and pseudo ground states each have their own sets of low-energy excitations which we call the ground-state and pseudo-ground-state sectors of low energy states.

The couplings of site 2 to its neighbors,

$$\begin{aligned} V = &-\frac{k_1}{\epsilon_{J,1}} \sum_{\alpha=1}^{N} \sigma^z_{\alpha,1}\sigma^z_{\alpha,2} - k_1 \sum_{\alpha<\beta} \sigma^z_{\alpha,1}\sigma^z_{\alpha,2}\sigma^z_{\beta,1}\sigma^z_{\beta,2} \\ &-\frac{k_2}{\epsilon_{J,2}} \sum_{\alpha=1}^{N} \sigma^z_{\alpha,2}\sigma^z_{\alpha,3} - k_2 \sum_{\alpha<\beta} \sigma^z_{\alpha,2}\sigma^z_{\alpha,3}\sigma^z_{\beta,2}\sigma^z_{\beta,3}, \end{aligned} \tag{5.3}$$

is the perturbation part of the Hamiltonian. We now decimate site 2 in the second-order perturbation theory, keeping both the true ground state and the pseudo ground state. It is important to note that second-order perturbation theory does not mix states from the two sectors as long as $N > 4$. (The sectors are coupled in a higher order of perturbation theory, but these terms are irrelevant at our IRCP). After decimating site 2, the effective interaction Hamiltonian of the neighboring sites reads (in the large-ϵ_J limit)

$$\tilde{H}_{eff} = -\frac{\tilde{k}}{\tilde{\epsilon}_J} \sum_{\alpha=1}^{N} \sigma^z_{\alpha,1}\sigma^z_{\alpha,3} - \tilde{k} \sum_{\alpha<\beta} \sigma^z_{\alpha,1}\sigma^z_{\alpha,3}\sigma^z_{\beta,1}\sigma^z_{\beta,3} - \tilde{\omega}\tilde{\zeta}, \tag{5.4}$$

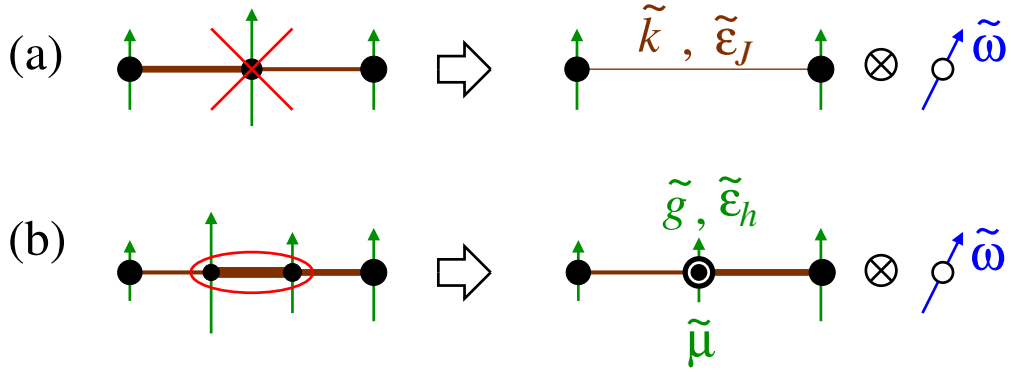

Figure 3.2: (Color online) a) Decimating a site results in a renormalized bond (characterized by $\tilde{k}$ and $\tilde{\epsilon}_J$) between its neighbors, and it introduces an extra binary "sector" degree of freedom represented as an Ising spin $\tilde{\zeta} = \pm 1$ in an external field $\tilde{\omega}$ [see Eq. (5.7)]. b) Decimating a bond results in a renormalized site characterized by $\tilde{g}$, $\tilde{\epsilon}_h$ and another sector degree of freedom.

with

$$\tilde{k} = \frac{k_1 k_2}{2(N-2)g_2}, \quad \tilde{\epsilon}_J = \frac{\epsilon_{J,1}\epsilon_{J,2}}{2}\frac{N-1}{N-2}, \quad \tilde{\omega} = N g_2/\epsilon_{h,2}. \tag{5.5}$$

Here, $\tilde{\zeta} = \pm 1$ is a new Ising degree of freedom which represents the energy splitting between the true and the pseudo ground states. In the large-ϵ_J regime, it is only very weakly coupled to the rest of the chain and can be considered free. In Fig. 3.2(a), we sketch this decimation procedure.

The decimation of a bond can be treated in the same way. If an AT four-spin interaction, say k_2, is the largest local energy, the unperturbed Hamiltonian reads

$$H_0 = -\frac{k_2}{\epsilon_J}\sum_{\alpha=1}^{N}\sigma^z_{\alpha,2}\sigma^z_{\alpha,3} - k_2\sum_{\alpha<\beta}^{N}\sigma^z_{\alpha,2}\sigma^z_{\alpha,3}\sigma^z_{\beta,2}\sigma^z_{\beta,3}. \tag{5.6}$$

Its GS is obtained by any sequence of parallel nearest-neighbors pairs (e.g. $|\phi_0\rangle = |\uparrow\uparrow,\uparrow\uparrow,\downarrow\downarrow,\downarrow\downarrow,\uparrow\uparrow,\downarrow\downarrow,\cdots,\uparrow\uparrow\rangle$) with energy $E_0 = -Nk_2/\epsilon_{J,2} - N(N-1)k_2/2$. As above, in the strong-coupling limit $\epsilon_{J,2} \gg 1$, H_0 has a pseudo-GS consisting of a sequence of anti-parallel nearest-neighbors pairs (e.g. $|\phi_0'\rangle = |\uparrow\downarrow,\uparrow\downarrow,\downarrow\uparrow,\downarrow\uparrow,\uparrow\downarrow,\downarrow\uparrow,\cdots,\uparrow\downarrow\rangle$) with energy $E_0' = Nk_2/\epsilon_J - N(N-1)k_2/2$.

When integrating out the bond, the two-site cluster gets replaced by a single site which contains one additional internal binary degree of freedom, namely, whether the cluster is in the GS sector or in the pseudo-GS sector. Its effective Hamiltonian reads

$$\tilde{H}_{eff} = -\frac{\tilde{g}}{\tilde{\epsilon}_h} \sum_{\alpha=1}^{N} \sigma^x_{\alpha,2} - \tilde{g} \sum_{\alpha<\beta} \tilde{\sigma}^x_{\alpha,2} \tilde{\sigma}^x_{\beta,2} - \tilde{\omega}\tilde{\zeta} \tag{5.7}$$

with

$$\tilde{g} = \frac{g_2 g_3}{2k_2[N-2]}, \quad \tilde{\epsilon}_h = \frac{\epsilon_{h,2}\epsilon_{h,3}}{2} \frac{N-1}{N-2}, \quad \tilde{\omega} = N k_2/\epsilon_{J,2}. \tag{5.8}$$

Here, $\tilde{\zeta}$ distinguishes the two sectors as before. The duality of the Hamiltonian can be seen by comparing Eqs. (5.5) and (5.8) after exchanging the roles of k and g as well as ϵ_h and ϵ_J.

Note that the magnetic moment $\tilde{\mu}$ of the new effective site depends on the internal degree of freedom $\tilde{\zeta}$ [see Fig. 3.2(b)] because neighboring spins are parallel in the GS sector but antiparallel in the pseudo-GS sector. We will come back to this point when discussing observables.

The SDRG proceeds by iterating these decimations. In this process, the coupling strengths ϵ_J, ϵ_h flow to infinity if their initial values are greater than some $\epsilon_c(N)$. This means that the Ising terms J_i, h_i become less and less important with decreasing energy scale Ω. The large-ϵ approximation thus becomes asymptotically exact. The remaining energies are the AT four-spin interactions k_i and the AT fields g_i. Their recursions relations have the same multiplicative structure as the recursions of Fisher's solution [28] of the random transverse-field Ising model. The flow of the distributions $P(k_i)$, $R(g_i)$ and their fixed points are thus identical to those of Fisher's solution, see Fig. 1.1. We conclude that the distributions of k, g have an infinite-randomness critical fixed point featuring exponential instead of power-law scaling. [27, 28, 77] As the Ising coupling J_i, h_i have vanished, this critical fixed point has the symmetry of the AT interaction and field terms which is higher than that of the full Hamiltonian.

4. PHASE DIAGRAM AND OBSERVABLES

The zero-temperature phase diagram of our system is determined by the low-energy limit of the SDRG flow. There are three classes of fixed points parameterized by the distance from criticality $r = \ln(g_{typ}/k_{typ}) = \langle \ln g \rangle - \langle \ln k \rangle$ (where $\langle \cdots \rangle$ denotes the disorder average): The critical fixed point at $r = 0$, and two lines of fixed points for the ordered ($r < 0$) and for the disordered ($r > 0$) Griffiths phases. This implies that there is a direct continuous phase transition between the ordered (Baxter) and disordered phases. We found no evidence for additional phases or phase transitions. In agreement with the Aizenman-Wehr theorem,[152] we thus conclude that disorder turns the clean first-order QPT into a continuous QPT in both strong-coupling and weak-coupling regimes. We now turn to the behavior of observables at low temperatures. Let us fix the intercolor coupling parameter at some $\epsilon > \epsilon_c$ and

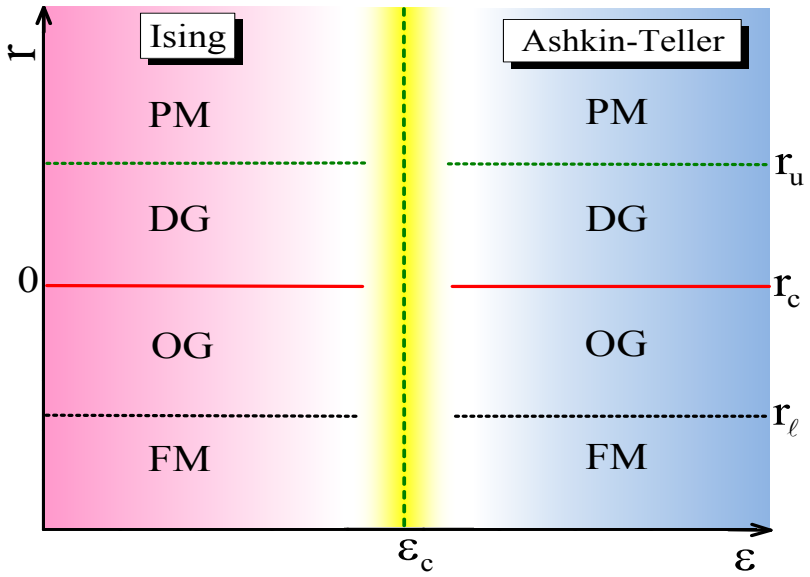

Figure 4.1: (Color online) Phase diagram of the N-color quantum Ashkin-Teller model as function of $r = \ln(h_{typ}/J_{typ})$ and the intercolor coupling ϵ at fixed disorder strength. The critical line is located at $r = r_c = 0$ ($J_{typ} = h_{typ}$) as expected from the duality transformation. PM and FM denote the conventional paramagnetic and ferromagnetic (Baxter) phases. OG and DG denote the ordered and disordered Griffiths phases.

tune the transition by the ratio $h_{typ}/J_{typ} = g_{typ}/k_{typ}$ (see Fig. 4.1). The basic idea is as follows.[157] We decimate the system until the cutoff energy scale Ω reaches the temperature T. For low enough T, the distributions of all energy scales in the renormalized system become very broad, and thus, the remaining degrees of freedom can be considered as free. Applying this procedure, we have to distinguish two stages depending on the importance of the pseudo ground state. (1) Both AT and Ising couplings are above the temperature. (In this stage, we decimate sites and bonds whose internal sector degrees of freedom are frozen in the true ground state, $\tilde{\zeta} = 1$.) (2) The temperature is below the AT couplings but above the Ising couplings. (Here we still decimate sites and bonds, but their internal degrees of freedom are free, i.e., they can be in either of the two sectors, $\tilde{\zeta} = \pm 1$.)

Let us illuminate this RG scheme on the example of the entropy. [‡] When the RG flow stops at $\Omega = T$, all spins are completely free. A surviving cluster has 2^N available states (two per independent color) giving an entropy contribution of $N \ln 2$, i.e., $S_{\text{chain}} = n_T N \ln 2$, where n_Ω is the density of surviving clusters at energy scale Ω (Ref. [28]). Moreover, during stage 2 of the flow, residual entropy was accumulated in the internal degrees of freedom, each of them contributing $\ln 2$ to the entropy. Noticing that each stage-2 RG decimation generates one extra degree of freedom, and that stage 2 starts when $\Omega/\epsilon_{J,h} = T$, ($\epsilon_x$ is the *typical* value of $\epsilon_{x,i}$ at energy scale Ω), the extra contribution to the entropy is $S_{\text{extra}} = [w_J(n_{\epsilon_J T} - n_T) + w_h(n_{\epsilon_h T} - n_T)] \ln 2$, with $w_J = 1 - w_h$ being the fraction of coupling decimations in the entire stage 2 of the RG flow. To compute S_{extra} we need to know how ϵ_J and ϵ_h depend on Ω. From the recursions (5.8) and (5.5), it is clear that $\ln \epsilon_h$ (and $\ln \epsilon_J$) scale like the number of sites (bonds) in a renormalized cluster (larger bond).

At criticality, $w_J = w_h = 1/2$, $n_\Omega \sim [\ln(\Omega_I/\Omega)]^{-1/\psi}$, with $\psi = 1/2$ being the tunneling exponent, and $\ln \epsilon_h = \ln \epsilon_J \sim [\ln(\Omega_I/\Omega)]^{\phi}$, with $\phi = \frac{1}{2}(1 + \sqrt{5})$ (Refs. [28]

[‡] We will focus at low enough temperatures such that the RG flow reaches the nontrivial second stage A detailed discussion for the high-temperature behavior including crossovers will be given elsewhere[158]

and [159]). Thus, summing the two contributions we find that

$$S = C_1 \left[\ln\left(\frac{\Omega_I}{T}\right)\right]^{-\frac{1}{\psi\phi}} \ln 2 + C_2 \left[\ln\left(\frac{\Omega_I}{T}\right)\right]^{-\frac{1}{\psi}} N \ln 2, \tag{5.9}$$

where C_1 and C_2 are nonuniversal constants, and Ω_I is the bare energy cutoff. As $\phi > 1$, the low-T entropy becomes dominated by the extra degrees of freedom $S \to S_{\text{extra}} \sim [\ln(\Omega_I/T)]^{-1/(\phi\psi)}$.

In the ordered Griffiths phase ($r < 0$), $w_J \to 1$ and $\ln \epsilon_J = A z^{\nu\psi(\phi-1)} \ln(\Omega_I/\Omega)$, with A being a nonuniversal constant of order unity, $\nu = 2$ the correlation length exponent, and $z = 1/(2|r|)$ the dynamical exponent. As $n_\Omega \sim |r|^\nu (\Omega/\Omega_I)^{1/z}$, we find that

$$S_{\text{extra}} \sim |r|^\nu (T/\Omega_I)^{1/(z+Az^\phi)} \ln 2, \tag{5.10}$$

which dominates over the chain contribution proportional to $T^{1/z} N \ln 2$. As expected from duality, the same result holds for the disordered phase ($r > 0$).

To discuss the magnetic susceptibility, we need to find the effective magnetic moment μ_{eff} of a cluster surviving at the RG energy scale $\Omega = T$. If all internal degrees of freedom were in their ground state, μ_{eff} would be given by the number of sites in the cluster. However, analogously to the entropy, μ_{eff} is modified because of the stage 2 of the RG flow. In this stage, the internal degrees of freedom are free, meaning not all spins in a surviving cluster are parallel, reducing the effective moment. A detailed analysis based on the central limit theorem [158] gives $\mu_{\text{eff}} \sim [\ln(\Omega_I/T)]^{\phi/2+1/2}$ at criticality and $\mu_{\text{eff}} \sim r^{\nu\psi(1-\phi)}[\ln(\Omega_I/T)]^{1/2}$ in the disordered Griffiths phase, as well as $\mu_{\text{eff}} \sim r^{-\phi/2} T^{-1/(2z)}$ in the ordered Griffiths phase.

The magnetic susceptibility $\chi(T)$ can now be computed. All eliminated clusters had AT fields greater than the temperature, and thus do not contribute to χ since they are fully polarized in the x-direction, whereas the surviving clusters are

effectively free and contribute with a Curie term: $\chi \sim \mu_{\rm eff}^2 n_T/T$. We find that

$$\chi \sim [\ln(\Omega_I/T)]^{\phi+1-1/\psi}/T \tag{5.11}$$

in the critical region, while it becomes

$$\chi \sim r^{\nu+2\nu\psi(1-\phi)} T^{1/z-1} \ln(\Omega_I/T) \tag{5.12}$$

in the disordered Griffiths phase, and take a Curie form $\chi \sim |r|^{\nu-\phi} T^{-1}$ in the ordered Griffiths phase.

5. CONCLUSION

In summary, we have solved the random quantum Ashkin-Teller model by means of a strong-disorder renormalization-group method that works not just for weak-coupling but also in the strong-coupling regime and yields asymptotically exact results. In the concluding paragraphs, we put our results into broader perspective.

First, we have demonstrated that random disorder turns the first-order QPT between the paramagnetic and Baxter phases into a continuous one not just in the weak-coupling regime but also in the strong-coupling regime. This resolves the seeming contradiction between the quantum Aizenman-Wehr theorem [68, 152] and the conclusion that the first-order transition may persist for sufficiently large coupling strength.[151]

The resulting continuous transition is controlled by two different IRCPs in the weak and strong coupling regimes. For weak coupling, the critical point is in the universality class of the random transverse-field Ising chain. [28] For strong coupling, we find a distinct type of IRCP which features a higher symmetry than the underlying Hamiltonian. The associated internal degrees of freedom lead to even stronger thermodynamic singularities both at criticality and in the Griffiths phases.

Our results apply to $N > 4$ colors where the true and pseudo ground-state sectors are not coupled. As a result, the Ising terms in the Hamiltonian are irrelevant perturbations (in the renormalization group sense) at our IRCP. The case $N \leq 4$ is special because the two sectors get coupled and thus requires a separate investigation. Interestingly, novel behavior has been recently verified for the *classical* transition in the two-dimensional AT model [160] for $N = 3$.

Our explicit calculations were for one space dimension. However, we believe that many aspects of our results carry over to higher dimensions. In particular, the SDRG recursion relations take the same form in all dimensions (as they are purely local). This implies that the RG flow for large inter-color coupling ϵ will be toward

$\epsilon \to \infty$ as in one dimension. Moreover, the flows of the AT energies g and k (although not exactly solvable in $d > 1$) are identical to the flows of the random transverse-field Ising model in the same dimension. In two and three dimensions, these flows have been studied numerically,[19, 161, 162] yielding IRCPs as in one dimension. We thus conclude that the strong-coupling regime of the random quantum AT model will be controlled by an Ashkin-Teller IRCP not just in one dimension but also in two and three dimensions.

We note that our method is also interesting from a general renormalization-group point of view. After a decimation, the resulting system cannot be represented solely in terms of a renormalized quantum AT Hamiltonian because the internal degree of freedom needs to be taken into account. Normally, the appearance of new variables dooms an RG scheme. [§] Here, however, the new variables, despite their influence on observables, are inert in the sense that they do not influence the RG flow of the other terms in the Hamiltonian, which makes the problem tractable. We expect that this insight may be applicable to renormalization-group schemes in other fields.

The strong-disorder RG approach to the random quantum AT model gives asymptotically exact results for both sufficiently weak and sufficiently strong coupling ($\epsilon \ll 1$, $\epsilon \gg 1$), see Fig. 1.1. The behavior for moderate ϵ is not exactly solved. In the simplest scenario, the weak-coupling and strong-coupling IRCPs are separated by a unique multicritical point at some intermediate coupling, however, more complicated scenarios cannot be excluded. The resolution of this question will likely come from numerical implementations of the SDRG and /or (quantum) Monte Carlo simulations.

This work has been supported in part by the NSF under Grants No. DMR-0906566 and DMR-1205803, by FAPESP under Grant No. 2010/ 03749-4, and by CNPq under Grants No. 590093/2011-8 and No. 302301/2009-7.

[§] Or it requires a generalization that includes all new terms in the starting Hamiltonian

VI. DISORDERED BOSONS IN ONE DIMENSION: FROM WEAK TO STRONG RANDOMNESS CRITICALITY

Fawaz Hrahsheh, and Thomas Vojta

[1]*Department of Physics, Missouri University of Science & Technology, Rolla, MO 65409*

ABSTRACT*

We investigate the superfluid-insulator quantum phase transition of one-dimensional bosons with off-diagonal disorder by means of large-scale Monte-Carlo simulations. For weak disorder, we find the transition to be in the same universality class as the superfluid-Mott insulator transition of the clean system. The nature of the transition changes for stronger disorder. Beyond a critical disorder strength, we find nonuniversal, disorder-dependent critical behavior. We compare our results to recent perturbative and strong-disorder renormalization group predictions. We also discuss experimental implications as well as extensions of our results to other systems.

Bosonic many-particle systems can undergo quantum phase transitions between superfluid and localized ground states due to interactions and lattice effects. These superfluid-insulator transitions occur in a wide variety of experimental systems ranging from helium in porous media, Josephson junction arrays, and granular superconductors to ultracold atomic gases [163, 164, 165, 166, 167, 168, 169, 170]. In many

*Published in Physical Review Letter **109** 265303 (2012).

of these applications, the bosons are subject to quenched disorder or randomness. Understanding the effects of disorder on the superfluid-insulator transition and on the resulting insulating phases is thus a prime question.

The case of one space dimension is especially interesting because the superfluid phase is rather subtle and displays quasi-long-range order instead of true long-range order. Moreover, the Anderson localization scenario for non-interacting bosons suggests that disorder becomes more important with decreasing dimensionality.

Giarmarchi and Schulz [171, 172] studied the influence of weak disorder on the interacting superfluid by means of a perturbative renormalization group analysis. They found the superfluid-insulator transition to be of Kosterlitz-Thouless (KT) type [72], with universal critical exponents and a universal value of the Luttinger parameter $g = \pi\sqrt{\rho_s \kappa}$ at criticality (ρ_s denotes the superfluid stiffness and κ the compressibility). This analysis was recently extended to second order in the disorder strength, with unchanged conclusion [173].

A different scenario emerges, however, from the real-space strong-disorder renormalization group approach. In a series of papers [174, 175, 176], Altman et al. studied one-dimensional interacting lattice bosons in various types of disorder. In all cases, they found that the superfluid-insulator transition is characterized by KT-like scaling of lengths and times, but it occurs at a nonuniversal, disorder-dependent value of the Luttinger parameter. The transition is thus in a different universality class than the weak-disorder transition [171, 172]. However, Monte-Carlo simulations [177] did not find any evidence in favor of the strong-disorder critical point.

In view of these seemingly incompatible results, it is important to determine whether or not both types of superfluid-insulator critical points indeed exist in systems of interacting disordered bosons in one dimension. Moreover, it is important to study whether they can be reached for realistic disorder strengths.

In this Letter, we employ large-scale Monte-Carlo simulations to address these questions. We focus on the case of off-diagonal disorder at large commensurate filling;

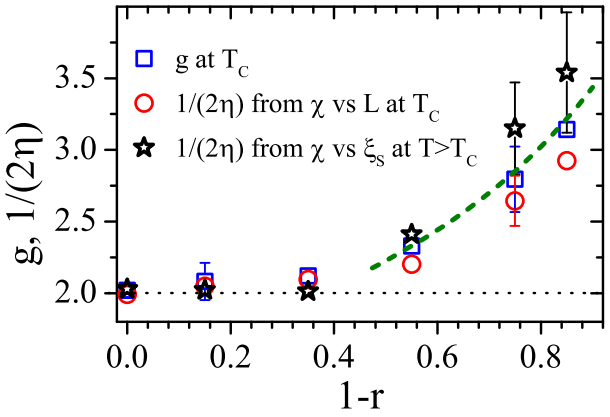

Figure 1.: (Color online) Critical Luttinger parameter g and exponent η [plotted as $1/(2\eta)$] of the superfluid-insulator transition as functions of the disorder strength $1-r$. The critical behavior appears universal for weak disorder while it becomes disorder-dependent for strong disorder. The lines are guides to the eye only.

other types of disorder will be discussed in the conclusions. Our results can be summarized as follows (see Fig. 1.). For weak disorder, we find a KT critical point in the universality class of the clean (1+1) dimensional XY model, with universal exponents and a universal value of the Luttinger parameter at the transition. This agrees with the predictions of the perturbative renormalization group. If the disorder strength is increased beyond a threshold value, the nature of the transition changes. While the scaling of length and time scales remains KT-like, the critical exponents and the Luttinger parameter become non-universal, in agreement with the strong-disorder scenario [174, 175, 176]. In the remainder of this Letter, we explain how these results were obtained, we discuss their generality as well as implications for experiment.

The starting point is the disordered one-dimensional quantum rotor Hamiltonian

$$H = -\sum_j J_j \cos(\hat{\phi}_{j+1} - \hat{\phi}_j) + \frac{1}{2}\sum_j U_j(\hat{n}_j - \bar{n}_j)^2 \tag{6.1}$$

which represents, e.g., a chain of superfluid grains with Josephson couplings J_j, charging energies U_j and offset charges $\bar{n}_j$. $\hat{n}_j$ is the charge on grain j and $\hat{\phi}_j$ is the phase of the superfluid order parameter. This model has a superfluid ground state if the Josephson couplings dominate. With increasing charging energies it undergoes a quantum phase transition to an insulating ground state. In addition to Josephson junction arrays, the Hamiltonian (6.1) describes a wide variety of other systems that undergo superfluid-insulator transitions.

Within the strong-disorder approach [174, 175, 176], the type of insulator depends on the symmetry properties of the offset charge distribution. In contrast, these details were found unimportant at the critical point. In the following, we therefore focus on purely off-diagonal disorder, $\bar{n}_j = 0$. In this case, the Hamiltonian (6.1) can be mapped onto a classical $(1+1)$-dimensional XY model [74]

$$H_{\rm cl} = -\sum_{j,\tau} \left[J_j^s \cos(\phi_{j+1,\tau} - \phi_{j,\tau}) + J_j^t \cos(\phi_{j,\tau+1} - \phi_{j,\tau}) \right] \tag{6.2}$$

where j and τ index the lattice sites in the space and time-like directions, respectively. The coupling constants J_j^s/T and J_j^t/T are determined by the parameters of the original Hamiltonian (6.1) with T being an effective "classical" temperature, not equal to the real physical temperature which is zero. In the following, we fix J_j^s and J_j^t and drive the XY model (6.2) through the transition by tuning T. The interactions J_j^s and/or J_j^t are independent random variables drawn from probability distributions $P^s(J^s)$ and $P^t(J^t)$. They depend on the space coordinate j only; this means the disorder is columnar (perfectly correlated in time direction).

To determine the critical behavior of the classical XY model (6.2), we performed large-scale Monte-Carlo simulations using the efficient Wolff cluster algorithm [83]. We studied square lattices with linear sizes up to $L = 3200$ and averaged the results over large numbers (200 to 3000, depending on L) of disorder realizations. Each sample was equilibrated using 200 to 400 Monte-Carlo sweeps, i.e., total spin flips per

site. (The actual equilibration times both above and at the critical temperature T_c did not exceed about 20 sweeps.) During the measurement period of 5000 to 30000 sweeps, we calculated observables such as specific heat, magnetization, susceptibility, spin-wave stiffness as well as correlation functions. In most simulations, we employed a uniform $J_j^s = 1$ and drew the J_j^t from a binary probability distribution

$$P^t(J^t) = c\delta(J^t - r) + (1 - c)\delta(J^t - 1) \ . \tag{6.3}$$

Here, c is the concentration of weak bonds which we fixed at $c = 0.8$. The disorder strength was tuned by changing the value r of the weak bonds. In addition to the clean case $r = 1$ (which corresponds to the pure superfluid-Mott insulator transition), we used $r = 0.85, 0.65, 0.45, 0.25$, and 0.15. We also carried out test calculations with random J^s. All simulations were performed on the Pegasus Cluster at Missouri S&T, using about 400,000 CPU hours

We now turn to the results. To find T_c for each disorder strength r, we analyzed the behavior of the correlation length ξ_s (in the space-like direction indexed by j). It is calculated, as usual, from the second moment of the disorder-averaged correlation function. In the high-temperature phase but close to the transition, ξ_s is expected to follow the form

$$\xi_s = A \exp\left[B(T - T_c)^{-1/2}\right] \tag{6.4}$$

both in the clean KT universality class [72] and in the strong-disorder scenario [174, 175, 176]. A and B are non-universal constants. For all disorder strength, our data follow this prediction with high accuracy, see Fig. 2. for an example. We extract T_c from fits of the data to (6.4) restricted to $\xi_s > 10$ to be in the critical region but $\xi_s < L/10$ to avoid finite-size effects. In the clean case ($r = 1$), we obtain $T_c = 0.8924$ in excellent agreement with high-precision values in the literature [178] [†].

[†]The remaining small difference can be attributed to logarithmic corrections to (6.4) which we did not account for.

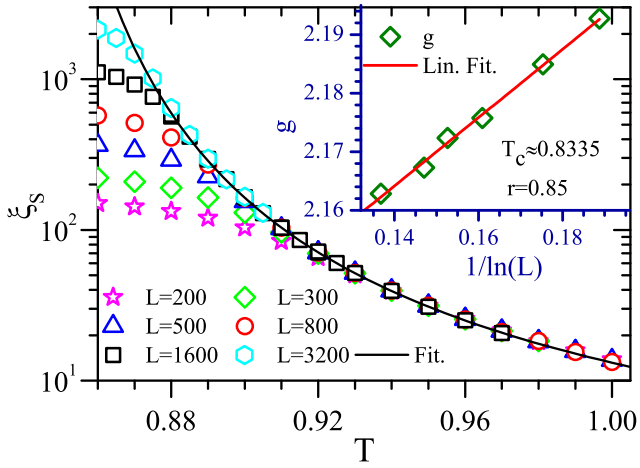

Figure 2.: (Color online) Spatial correlation length ξ_s vs. temperature T for disorder strength $r = 0.85$ and system sizes $L = 200$ to 3200. The solid line is a fit to the KT form (6.4). Inset: Luttinger parameter g at T_c vs. system size L.

In addition to the correlation length ξ_s in the space-like direction, we also studied the correlation length ξ_t in the time-like direction. We found $\xi_t \propto \xi_s$ for all disorder strengths which implies a dynamical exponent of $z = 1$.

The order parameter susceptibility χ can be analyzed analogously. In the high-temperature phase close to the transition, it is predicted to behave as

$$\chi \propto \xi_s^{2-\eta} \propto \exp\left[D(T - T_c)^{-1/2}\right] \ . \tag{6.5}$$

Here, η is the correlation function critical exponent and $D = (2 - \eta)B$. Figure 3. shows that the data for all disorder strengths r follow this prediction with high accuracy. The critical temperatures extracted from the corresponding fits are listed in the legend of the figure. Their values have small statistical errors ranging from about 3×10^{-4} for the weak disorder cases to 2×10^{-3} for strong disorder. The systematic errors due to corrections to the leading scaling form (6.5) are somewhat larger. We estimate them from the robustness of the fit against changing the fit interval. This yields systematic errors ranging from about 5×10^{-3} for weak disorder to 2×10^{-2}

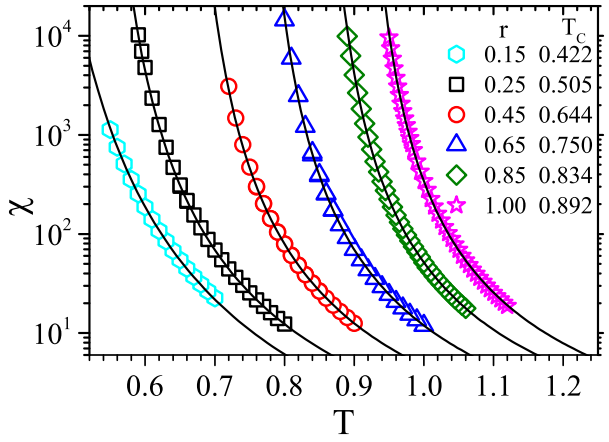

Figure 3.: (Color online) Susceptibility χ vs. temperature T for several disorder strengths. The maximum system sizes are at least $L = 1500$. The solid lines are fits to the KT form (6.5). The resulting estimates of T_c are listed in the legend.

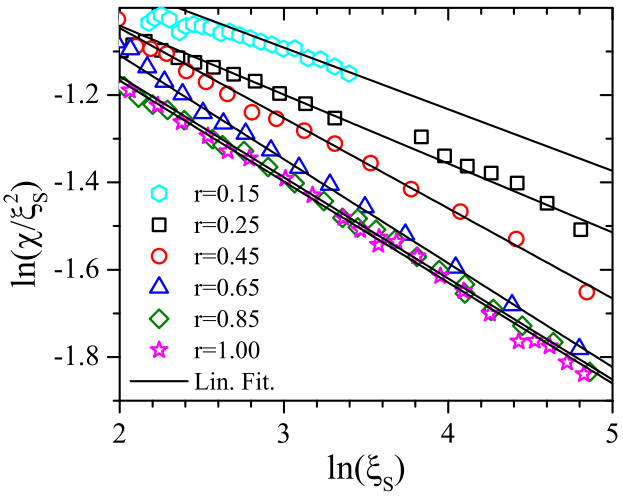

Figure 4.: (Color online) $\ln(\chi/\xi_s^2)$ vs. $\ln(\xi_s)$ for several disorder strengths and maximum system size $L \geq 1500$ ($L = 500$ for $r = 0.15$). The solid lines are linear fits; their slopes give $-\eta$.

for strong disorder. Within these errors the critical temperatures extracted from χ agree well with those from the correlation lengths.

Equation (6.5) suggests a direct way to measure the exponent η: if one plots $\ln(\chi/\xi_s^2)$ vs. $\ln(\xi_s)$, the data should be on a straight line with slope $-\eta$. Figure 4. presents this analysis for different disorder strengths. In the clean case, $r = 1$, we find $\eta = 0.243$ in good agreement with the exact value $1/4$ [72]. The weak-disorder

curves ($r = 0.85$ and 0.65) are parallel to the clean one within their statistical errors. Fits in the range $20 < \xi_s < L/10$ give exponents η close to 1/4. In contrast, the strong-disorder curves ($r = 0.45,\ 0.25,\ 0.15$) are less steep, resulting in smaller η. They are also noisier which leads to larger error bars. All η values are shown in Fig. 1.. They provide evidence for universal critical behavior (in the clean 2D XY universality class) for weak disorder but nonuniversal behavior for strong disorder.

In addition to simulations in the high-temperature phase, we also studied the finite-size scaling properties of observables right at the critical temperature T_c. Let us first consider the Luttinger parameter $g = \pi\sqrt{\rho_s \kappa}$. Under the quantum-to-classical mapping [74], the compressibility κ of the quantum rotor Hamiltonian (6.1) maps onto the spin-wave stiffness ρ_t in the time-like direction of the classical XY model (6.2). In our simulations, the Luttinger parameter is thus given by

$$g = (\pi/T)\sqrt{\rho_s \rho_t}\ . \tag{6.6}$$

The stiffnesses ρ_s and ρ_t are not calculated by actually applying twisted boundary conditions during the simulation but by using the relation given by Teitel and Jayaprakash [179] (for a derivation see, e.g., Ref. [51]).

Within KT theory, the Luttinger parameter close to the transition behaves as $g(T) = g(T_c) + a(T_c - T)^{1/2}$ where a is a constant and $T \le T_c$. Together with (6.4), this suggests the leading finite-size corrections to g at T_c to take the form

$$g(T_c, L) = g(T_c, \infty) + b/\ln(L) \tag{6.7}$$

where b is another constant. Calculating the Luttinger parameter at T_c for different system sizes and extrapolating using (6.7) yields the infinite-system value $g(T_c, \infty)$ [‡]. We performed this analysis for all disorder strengths r and found that the g vs.

[‡]The extrapolation of g to $L = \infty$ is nontrivial as g shows a singular temperature dependence and a jump to 0 for $T > T_c$. The data must be in the critical region, $|T - T_c| \lesssim [\ln(L/A)]^{-2}$, which appears to be fulfilled in our case.

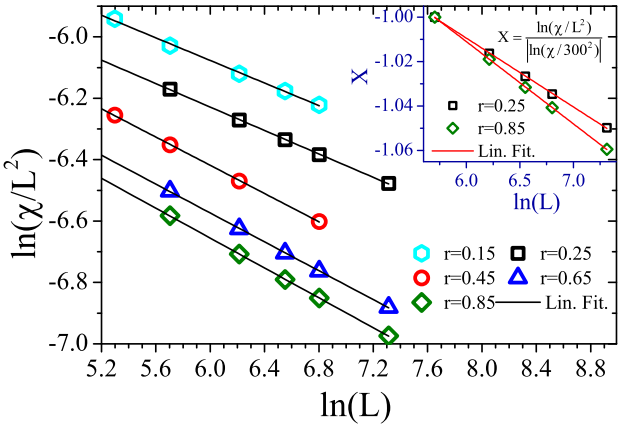

Figure 5.: (Color online) Susceptibility at T_c plotted as $\ln(\chi/L_s^2)$ vs. $\ln(L)$ for several disorder strengths. The solid lines are linear fits; their slopes give $-\eta$ (values are shown in Fig. 1.) . The inset demonstrates the change of slope with increasing r.

$1/\ln(L)$ data indeed fall onto straight lines (the inset of Fig. 2. shows an example). The resulting extrapolated values are displayed in Fig. 1.. For weak disorder ($r = 0.85$ and 0.65), the Luttinger parameters at T_c agree with the clean value, $g = 2$, within their error bars (which are combinations of the statistical Monte-Carlo error and the uncertainty in T_c). For stronger disorder ($r = 0.45$, 0.25, 0.15), $g(T_c, \infty)$ takes larger, disorder-dependent values.

Finally, we turn to the finite-size behavior of the susceptibility at T_c. According to finite-size scaling, the leading size-dependence should be of the form

$$\chi(T_c, L) \sim L^{2-\eta} \tag{6.8}$$

which provides another way to measure η. Figure 5. shows plots of $\ln(\chi/L^2)$ vs. $\ln(L)$ for all disorder strengths r. For weak disorder ($r = 0.85$ and 0.65), the resulting values of the exponent η are again close to the clean value 1/4. For larger disorder ($r = 0.45$, 0.25, and 0.15), we find disorder-dependent values that roughly agree with those extracted in the high-temperature phase (Fig. 4.).

In summary, we used large-scale Monte-Carlo simulations to investigate the superfluid-insulator quantum phase transition of one-dimensional bosons with off-diagonal disorder. For weak disorder, our data provide evidence for a KT critical point in the universality class of the clean (1+1) dimensional classical XY model, with universal critical exponents $\eta = 1/4$ and $z = 1$ as well as a universal value $g = 2$ of the critical Luttinger parameter. These results agree with the Harris criterion [18] which predicts weak disorder to be an irrelevant perturbation at the clean KT transition. For stronger disorder, the universality class of the transition changes. It is still of KT-type [ξ_s and χ follow (6.4) and (6.5)] but the critical exponent η and the critical Luttinger parameter become disorder-dependent (non-universal) [§]. This agrees with the strong-disorder scenario [174, 175, 176].

The important question of whether the boundary between the weak and strong disorder regimes is sharp or just a crossover cannot be finally decided by means of our current numerical capabilities. The data in Fig. 1. would be compatible with both scenarios within their error bars.

Earlier Monte-Carlo simulations [177] did not observe the strong-disorder regime. We believe that the binary disorder used in [177] (equivalent to disorder in J^s with $c = 0.5$ and $r = 0.33$ in our model) may not have been sufficiently strong. In particular, $c = 0.5$ is much less favorable for the formation of rare regions than our $c = 0.8$. To test this hypothesis, we performed a few simulation using $c = 0.5$ and $r = 0.33$. They resulted in critical behavior compatible with the clean 2D XY universality class, in agreement with Ref. [177] [¶].

It is interesting to ask whether the different critical behaviors in the weak and strong-disorder regimes are accompanied by qualitative differences in the bulk phases. In particular, are there two different insulating phases or are the weak and

[§]Fig. 1. suggests that $g = 1/(2\eta)$ not just at the clean KT critical point but also at the strong disorder critical point. To the best of our knowledge, the latter has not yet been established theoretically.

[¶]Ref. [177] also studied power-law distributed interactions, but the results showed significant finite-size effects.

strong-disorder regimes continuously connected? A detailed analysis of the insulating phase(s) will also shed light on the mechanism that destroys the superfluid stiffness above T_c. Is it due to the proliferation of single quantum phase slips as at a clean KT transition or due to the formation of phase slip "dipoles" as suggested in Ref. [174, 175, 176]? Simulations to address these questions are under way.

All our explicit results are for off-diagonal disorder and large commensurate filling. They do not directly apply to the generic dirty-boson problem with diagonal disorder considered in [171, 172] [‖]. Note, however, that the critical behavior does not depend on the disorder type within the strong-disorder scenario [174, 175, 176]. Simulating the generic case would require a different approach (such as the link-current formulation [74]) because the mapping onto a classical XY model is not valid for diagonal disorder.

Finally, we turn to the experimental accessibility of the weak and strong-disorder regimes. Our results show that the transition between them occurs at a moderate disorder strengths. We therefore expect both regimes to be accessible in principle in experiments on systems such as ultracold atoms or Josephson junction chains (see also Ref. [180]).

We acknowledge discussions with Ehud Altman, David Pekker, Nikolay Prokof'ev, Gil Refael, and Zoran Ristivojevic. This work has been supported by the NSF under Grant Nos. DMR-0906566 and DMR-1205803.

[‖] The critical value of g in the perturbative theory [171] with diagonal disorder is 3/2 rather than 2.

SECTION

2. SUMMARY AND OUTLOOK

The main motivation of this work is to make a step forward toward a deeper understanding of the impurity effects in quantum magnets, superconductors and superfluids. In particular, we try to answer the following question: How are phase transitions and critical behaviors in these systems influenced by disorder.

In Section 1 we started by introducing basic concepts of phase transitions and critical behavior in Subsection 1.1. In addition we explained the Landau theory which introduces the idea of order parameters. Then, we discussed the scaling theory and its applications before we finished with an introduction to quantum phase transitions.

In Subsection 1.2, we gave a overview over quenched disorder effects. First, we explained the Harris criterion which governs how weak disorder can affect a clean phase transition. Then, we discussed how disorder effects are significantly increased by forming rare regions which can behave independently from the bulk systems. These rare regions lead to Griffiths singularities close to the phase transition. Sometimes they even destroy the phase transition by smearing, for example in metallic systems at zero temperature. Finally, we described the effects of disorder on first-order phase transitions, and when they are rounded to second-order phase transitions.

In Subsection 1.3, we turned to the renormalization group theory which is a powerful technique to study phase transitions. Specifically, we introduced the strong-disorder renormalization group theory (SDRG) which we will use extensively in this thesis.

In the last Subsection 1.4, we introduced a special type of phase transitions, the Kosterlitz-Thouless (KT) transitions. This type of transitions occurs in planar magnets as well as superconducting and superfluid thin films, Coulomb gas systems, and one-dimensional interacting bosonic systems. An example of a KT transition can be found in the 2D classical XY model where the order-parameter has a continuous $O(2)$ symmetry. This transition is caused by the so-called vortex unbinding process.

The remainder of this thesis consists of reprints of six published refereed papers. In Paper I, we investigate Griffith's rare regions effects in a layered Heisenberg model by Monte Carlo simulations. The results of this work confirm the predictions of an earlier SDRG study. We found that the critical point is of infinite-randomness type and accompanied by power-law Griffiths singularities.

In Papers II, III, and IV, we investigate the smearing of phase transitions tuned by changing the chemical composition. Section 4 focuses on the smearing effects of uncorrelated disorder. Section 5 studies how the disorder correlations enhance the smearing effects. Finally, we introduce an experimental realization of the smeared quantum phase transition in section 6.

Paper V studies how the rare regions round the first-order quantum phase transition in the N-color Ashkin-Teller model by means of a strong-disorder renormalization group theory. In this project, we developed a new implementation of the SDRG theory that works not only for weak coupling but also for strong intercolor interactions.

Paper VI deals with the disorder effects on the superfluid-insulator transition in a one-dimensional quantum bosonic system. It focuses on the change of the critical behavior of the Kosterlitz-Thouless transition with increasing disorder.

In summary, we have described how quenched disorder influences classical and quantum phase transitions in magnetic systems, superconductors, and superfluids.

Our investigations so far focused on weak disorder that affects the transition but leaves the bulk phases unchanged. If the disorder changes the bulk phases, even

richer disorder effects are expected, and new theories might be needed to study these phenomena. Moreover, in this work, we have investigated quantum phase transitions for which the quantum-to-classical mapping at zero temperature can be employed. The effects of disorder on other quantum phase transitions such as transitions in Kondo lattice systems received less attention which means that exotic phases and critical behaviors might be waiting to be discovered.

BIBLIOGRAPHY

[1] S. L. Sondhi, S. M. Girvin, J. P. Carini, and D. Shahar. Continuous quantum phase transitions. *Rev. Mod. Phys.*, 69:315, 1997.

[2] S. Sachdev. Quantum phase transitions. *Physics World*, 12(4):33, 1999.

[3] S. Sachdev. *Quantum phase transitions*. Cambridge University Press, Cambridge, 1999.

[4] T. Vojta. Quantum phase transitions in electronic systems. *Ann. Phys. (Leipzig)*, 9:403, 2000.

[5] M. Vojta. Quantum phase transitions. *Rep. Progr. Phys.*, 66:2069, 2003.

[6] L. D. Landau. *Phys. Z. Sowjetunion*, 11:26, 1937.

[7] L. D. Landau. *Zh. Eksp. Teor. Fiz.*, 7:19, 1937.

[8] L. D. Landau. *Phys. Z. Sowjetunion*, 11:545, 1937.

[9] L. D. Landau. *Zh. Eksp. Teor. Fiz.*, 7:627, 1937.

[10] B. Widom. Surface tension and molecular correlations near the critical point. *J. Chem. Phys.*, 43:3892, 1965.

[11] M. N. Barber. Finite-size scaling. In C. Domb and J. L. Lebowitz, editors, *Phase Transitions and Critical Phenomena*, volume 8, pages 145–266. Academic, New York, 1983.

[12] J. Cardy, editor. *Finite-size scaling*. North Holland, Amsterdam, 1988.

[13] G. Grinstein. Phases and phase transitions of quneched disordered systems. In E. G. D. Cohen, editor, *Fundamental Problems in Statistical Mechanics VI*, page 147. Elsevier, New York, 1985.

[14] J. Hertz. Quantum critical phenomena. *Phys. Rev. B*, 14:1165, 1976.

[15] S. Chakravarty, B. I. Halperin, and D. R. Nelson. Two-dimensional quantum Heisenberg antiferromagnet at low temperatures. *Phys. Rev. B*, 39:2344, 1989.

[16] M. Suzuki. *Progr. Theor. Phys.*, 56:1454, 1976.

[17] M. Suzuki. Generalized trotter's formula and systematic approximants of exponential operators and inner derivations with applications to many-body problems. *Commun. Math. Phys.*, 51:183, 1976.

[18] A. B. Harris. Effect of random defects on the critical behaviour of Ising models. *J. Phys. C*, 7:1671, 1974.

[19] O. Motrunich, S. C. Mau, D. A. Huse, and D. S. Fisher. Infinite-randomness quantum Ising critical fixed points. *Phys. Rev. B*, 61:1160, 2000.

[20] T. Vojta. Quantum griffiths effects and smeared phase transitions in metals: theory and experiment. *J. Low Temp. Phys.*, 161:299, 2010.

[21] T. Vojta. Rare region effects at classical, quantum, and non-equilibrium phase transitions. *J. Phys. A*, 39:R143, 2006.

[22] C. Holm and W. Janke. Critical exponents of the classical three-dimensional Heisenberg model: A single-cluster Monte-Carlo study. *Phys. Rev. B*, 48:936, 1993.

[23] A. M. Ferrenberg and D. P. Landau. *Phys. Rev. B*, 44:5081, 1991.

[24] H. G. Ballesteros, L. A. Fernandez, V. Martin-Mayor, A. Munoz Sudupe, G. Parisi, and J. J. Ruiz-Lorenzo. *Phys. Rev. B*, 58:2740, 1998.

[25] B. M. McCoy and T. T. Wu. Random impurities as the cause of smooth specific heats near the critical temperature. *Phys. Rev. Lett.*, 21:549, 1968.

[26] B. M. McCoy and T. T. Wu. Theory of a two-dimensional Ising model with random impurities. i. thermodynamics. *Phys. Rev.*, 176:631, 1968.

[27] D. S. Fisher. Random transverse field Ising spin chains. *Phys. Rev. Lett.*, 69:534, 1992.

[28] D. S. Fisher. Critical behavior of random transverse-field Ising spin chains. *Phys. Rev. B*, 51:6411, 1995.

[29] S. K. Ma, C. Dasgupta, and C. K. Hu. Random antiferomagnetic chain. *Phys. Rev. Lett.*, 43:1434, 1979.

[30] C. Dasgupta and S.-K. Ma. Low-temperature properties of the random Heisenberg antiferromagnetic chain. *Phys. Rev. B*, 22:1305, 1980.

[31] R. B. Griffiths. Nonanalytic behavior above the critical point in a random Ising ferromagnet. *Phys. Rev. Lett.*, 23:17, 1969.

[32] M. Randeria, J. P. Sethna, and R. G. Palmer. Low-frequency relaxation in Ising spin-glasses. *Phys. Rev. Lett.*, 54:1321, 1985.

[33] M. Wortis. Griffiths singularities in the randomly dilute one-dimensional Ising model. *Phys. Rev. B*, 10:4665, 1974.

[34] A. B. Harris. Nature of the Griffiths singularity in dilute magnets. *Phys. Rev. B*, 12:203, 1975.

[35] Y. Imry. Griffiths singularity in finite macroscopically large dilute Ising models. *Phys. Rev. B*, 15:4448, 1977.

[36] A. J. Bray and D. Huifang. *Phys. Rev. B*, 40:6980, 1989.

[37] T. Vojta and J. Schmalian. Quantum Griffiths effects in itinerant Heisenberg magnets. *Phys. Rev. B*, 72:045438, 2005.

[38] S. Huether, R. Kinney, and T. Vojta. *Phys. Rev. B*, 74:094425, 2006.

[39] R. Sknepnek and T. Vojta. *Phys. Rev. B*, 69:174410, 2004.

[40] T. Vojta. Smearing of the phase transition in Ising systems with planar defects. *J. Phys. A*, 36:10921, 2003.

[41] S. Guo, D. P. Young, R. T. Macaluso, D. A. Browne, N. L. Henderson, J. Y. Chan, L. Henry, and J. F. DiTusa. Discovery of griffiths phase in itinerant magnetic semiconductor $Fe_{1-x}Co_xS_2$. *Phys. Rev. Lett.*, 100:017209, 2007.

[42] S. Guo, D. P. Young, R. T. Macaluso, D. A. Browne, N. L. Henderson, J. Y. Chan, L. L. Henry, and J. F. DiTusa. Magnetic and thermodynamic properties of cobalt-doped iron pyrite: Griffiths phase in a magnetic semiconductor. *Phys. Rev. B*, 81:144423, 2010.

[43] S. Guo, D. P. Young, R. T. Macaluso, D. A. Browne, N. L. Henderson, J. Y. Chan, L. L. Henry, and J. F. DiTusa. Charge transport in cobalt-doped iron pyrite. *Phys. Rev. B*, 81:144424, 2010.

[44] J. G. Sereni, T. Westerkamp, R. Küchler, N. Caroca-Canales, P. Gegenwart, and C. Geibel. Ferromagnetic quantum criticality in the alloy $CePd_{1-x}Rh_x$. *Phys. Rev. B*, 75:024432, 2007.

[45] T. Westerkamp, M. Deppe, R. Küchler, M. Brando, C. Geibel, P. Gegenwart, A. P. Pikul, and F. Steglich. Kondo-cluster-glass state near a ferromagnetic quantum phase transition. *Phys. Rev. Lett.*, 102:206404, 2009.

[46] S. Ubaid-Kassis, T. Vojta, and A. Schroeder. Quantum griffiths phase in the weak itinerant ferromagnetic alloy $Ni_{1-x}V_x$. *Phys. Rev. Lett.*, 104:066402, 2010.

[47] F. Bölling. *Phys. Kondens. Mater.*, 7:162, 1968.

[48] T. Vojta. Disorder-induced rounding of certain quantum phase transitions. *Phys. Rev. Lett.*, 90:107202, 2003.

[49] J. A. Hoyos and T. Vojta. Theory of smeared quantum phase transitions. *Phys. Rev. Lett.*, 100:240601, 2008.

[50] J. A. Hoyos and T. Vojta. Smeared quantum phase transition in the dissipative random quantum ising model. *Physica E*, 42:383–387, 2010.

[51] F. Hrahsheh, H. Barghathi, and T. Vojta. Infinite- randomness criticality in a randomly layered heisenberg magnet. *J. Phys. B*, 84:184202, 2011.

[52] A. J. Millis. Effect of a nonzero temperature on quantum critical points in itinerant fermion systems. *Phys. Rev. B*, 48:7183, 1993.

[53] D. Belitz, T. R. Kirkpatrick, and T. Vojta. How generic scale invariance influences quantum and classical phase transitions. *Rev. Mod. Phys.*, 77:579, 2005.

[54] T. Vojta, D. Belitz, R. Narayanan, and T. R. Kirkpatrick. *Europhys. Lett.*, 36:191, 1996.

[55] T. Vojta, D. Belitz, R. Narayanan, and T. R. Kirkpatrick. Quantum critical behavior of clean itinerant ferromagnets. *Z. Phys. B*, 103:451, 1997.

[56] D. Belitz, T. R. Kirkpatrick, and T. Vojta. Nonanalytic behavior of the spin susceptibility in clean fermi systems. *Phys. Rev. B*, 55:9452, 1997.

[57] T. R. Kirkpatrick and D. Belitz. Long-range order versus random-singlet phases in quantum antiferromagnetic systems with quenched disorder. *Phys. Rev. Lett.*, 76:2571, 1996.

[58] A. J. Millis, D. K. Morr, and J. Schmalian. Local defect in metallic quantum critical systems. *Phys. Rev. Lett.*, 87:167202, 2001.

[59] A. J. Millis, D. K. Morr, and J. Schmalian. Quantum Griffiths effects in metallic systems. *Phys. Rev. B*, 66:174433, 2002.

[60] A. J. Legget, S. Chakravarty, A. T. Dorsey, M. P. A. Fisher, A. Garg, and W. Zwerger. *Rev. Mod. Phys.*, 59:1, 1987.

[61] D. J. Thouless. *Phys. Rev.*, 187:732, 1969.

[62] J. Cardy. *J. Phys. A*, 14:1407, 1981.

[63] C. Svoboda, D. Nozadze, F. Hrahsheh, and T. Vojta. *Europhysics Letters*, 97:20007, 2012.

[64] Y. Imry and S. K. Ma. *Phys. Rev. Lett.*, 35:1399, 1975.

[65] R. Peierls. *Proc. Camb. Phil. Soc.*, 32:477–481, 1936.

[66] R. B. Griffiths. Peierls proof of spontaneous magnetization in a two-dimensional ising ferromagnet. *Phys. Rev.*, 136:A437–A439, 1964.

[67] M. Aizenman and J. Wehr. Rounding of first-order phase transitions in systems with quenched disorder. *Phys. Rev. Lett.*, 62:2503, 1989.

[68] R. Greenblatt, M. Aizenman, and J. Lebowitz. Rounding of first order transitions in low-dimensional quantum systems with quenched disorder. *J. Math. Phys.*, 53:023301, 2012.

[69] L. P. Kadanoff. Scaling laws for ising models near tc. *Physics*, 2:263, 1966.

[70] K. G. Wilson. *Phys. Rev. B*, 4:3174, 1971.

[71] N. D. Mermin and H. Wagner. Absence of ferromagnetism or antiferromagnetism in one- or two-dimensional isotropic Heisenberg models. *Phys. Rev. Lett.*, 17:1133, 1966.

[72] J. M. Kosterlitz and D. J. Thouless. *J. Phys. C*, 6:1181, 1973.

[73] B. Kaufman and L. Onsager. *Phys. Rev.*, 76:1244, 1949.

[74] M. Wallin, E. S. Sorensen, S. M. Girvin, and A. P. Young. Superconductor-insulator transition in two-dimensional dirty boson systems. *Phys. Rev. B*, 49:12115, 1994.

[75] M. Thill and D. A. Huse. Equilibrium behaviour of quantum Ising spin glass. *Physica A*, 214:321, 1995.

[76] M. Guo, R. N. Bhatt, and D. A. Huse. *Phys. Rev. B*, 54:3336, 1996.

[77] H. Rieger and A. P. Young. Griffiths singularities in the disordered phase of a quantum ising spin glass. *Phys. Rev. B*, 54:3328, 1996.

[78] B. M. McCoy and T. T. Wu. Theory of a two-dimensional Ising model with random impurities. ii. spin correlation functions. *Phys. Rev.*, 188:982, 1969.

[79] B. M. McCoy. Incompleteness of the critical exponent description for ferromagnetic systems containing random impurities. *Phys. Rev. Lett.*, 23:383, 1969.

[80] R. Sknepnek and T. Vojta. Smeared phase transition in a three-dimensional Ising model with planar defects: Monte-Carlo simulations. *Phys. Rev. B*, 69:174410, 2004.

[81] P. Mohan, R. Narayanan, and T. Vojta. Infinite randomness and quantum griffiths effects in a classical system: the randomly layered heisenberg magnet. *Phys. Rev. B*, 81:144407, 2010.

[82] P. C. Hohenberg and B. I. Halperin. *Rev. Mod. Phys.*, 49:435, 1977.

[83] U. Wolff. Collective Monte-Carlo updating for spin systems. *Phys. Rev. Lett.*, 62:361, 1989.

[84] N. Metropolis, A. Rosenbluth, M. Rosenbluth, and A. Teller. Equation of state calculations by fast computing machines. *J. Chem. Phys.*, 21:1087, 1953.

[85] A. J. Bray. *Phys. Rev. Lett.*, 60:720, 1988.

[86] M. Caffarel, P. Azaria, B. Delamotte, and D. Mouhanna. Monte carlo calculation of the spin stiffness of the two-dimensional heisenberg model. *Europhys Lett.*, 26:493, 1994.

[87] C. Pich, A. P. Young, H. Rieger, and N. Kawashima. Critical behavior and Griffiths-mccoy singularities in the two-dimensional random quantum Ising ferromagnet. *Phys. Rev. Lett.*, 81:5916, 1998.

[88] R. Sknepnek, T. Vojta, and M. Vojta. Exotic vs. conventional scaling and universality in a disordered bilayer quantum Heisenberg antiferromagnet. *Phys. Rev. Lett.*, 93:097201, 2004.

[89] Moreno Marcellini, Martin Pärnaste, Björgvin Hjörvarsson, and Maximilian Wolff. Influence of the distribution of the inherent ordering temperature on the ordering in layered magnets. *Phys. Rev. B*, 79(14):144426, Apr 2009.

[90] T. Vojta. *Phys. Rev. Lett.*, 90:107202, 2003.

[91] J. A.. Hoyos and T. Vojta. *Phys. Rev. Lett.*, 100:240601, 2008.

[92] T. Vojta. *J. Phys. A*, 36:10921, 2003.

[93] R. Sknepnek and T. Vojta. *Phys. Rev. B*, 69:174410, 2004.

[94] J. Hertz. *Phys. Rev. B*, 14:1165, 1976.

[95] A. J. Millis. *Phys. Rev. B*, 48:7183, 1993.

[96] A. J. Millis, D. K. Morr, and J. Schmalian. *Phys. Rev. Lett.*, 87:167202, 2001.

[97] T. Vojta. *J. Phys. A*, 39:R143, 2006.

[98] T. Vojta. *J. Low Temp. Phys.*, 161:299, 2010.

[99] I. M. Lifshitz. *Usp. Fiz. Nauk*, 83:617, 1964.

[100] I. M. Lifshitz. *Sov. Phys. Usp*, 7:549, 1965.

[101] B. I. Halperin and M. Lax. *Phys. Rev.*, 148:722, 1966.

[102] M. N. Barber. Finite-size scaling. In C. Domb and J. L. Lebowitz, editors, *Phase Transitions and Critical Phenomena*, volume 8, pages 145–266. Academic, New York, 1983.

[103] J. Cardy, editor. *Finite-size scaling*. North Holland, Amsterdam, 1988.

[104] V. Dobrosavljević and E. Miranda. *Phys. Rev. Lett.*, 94:187203, 2005.

[105] A. H. Castro Neto and B. A. Jones. *Phys. Rev. B*, 62:14975, 2000.

[106] J. A.. Hoyos and T. Vojta. *Phys. Rev. B*, 74:140401(R), 2006.

[107] G. Cao, S. McCall, M. Shepard, J. E. Crow, and R. P. Guertin. *Phys. Rev. B*, 56:321, 1997.

[108] K. Yoshimura, T. Imai, T. Kiyama, K. R. Thurber, A. W. Hunt, and K. Kosuge. *Phys. Rev. Lett.*, 83:4397, 1999.

[109] Takashi Kiyama, Kazuyoshi Yoshimura, Koji Kosuge, Hiroyuki Mitamura, and Tsuneaki Goto. *J. Phys. Soc. Jpn.*, 68:3372, 1999.

[110] A. B. Harris and T. C. Lubensky. *Phys. Rev. Lett.*, 33:1540, 1974.

[111] G. Grinstein and A. Luther. *Phys. Rev. B*, 19:3580, 1976.

[112] Y. Imry and M. Wortis. *Phys. Rev. B*, 19:3580, 1979.

[113] M. Aizenman and J. Wehr. *Phys. Rev. Lett*, 62:2503, 1989.

[114] K. Hui and A. N. Berker. *Phys. Rev. Lett.*, 62:2507, 1989.

[115] J. A. Hoyos, N. Laflorencie, A. P Vieira, and T. Vojta. *Europhys. Lett.*, 93:30004, 2011.

[116] A. B. Harris. *J. Phys. C: Solid State Phys.*, 7:1671, 1974.

[117] A. Weinrib and B. I. Halperin. *Phys. Rev. B*, 27:413, 1983.

[118] F. Hrahsheh, D. Nozadze, and T. Vojta. *Phys. Rev. B*, 83:224402, 2011.

[119] S. Sachdev. *Quantum Phase Transitions*. Cambridge University Press, Cambridge, England, 1999.

[120] H. A. Makse, S. Havlin, M. Schwartz, and H. E. Stanley. *Phys. Rev. E*, 53:5445, 1996.

[121] H. Rieger and F. Igloi. *Phys. Rev. Lett.*, 83:3741, 1999.

[122] C. Svoboda and et al. unpublished.

[123] Noriko Hosaka, Hiroyuki Yamada, Yoshiaki Shimada, Jun Fujioka, Sándor Bordács, István Kézsmárki, Masashi Kawasaki, and Yoshinori Tokura. *Appl. Phys. Express*, 1:113001, 2008.

[124] M. Schneider, V. Moshnyaga, and P. Gegenwart. *Phys. Status Solidi B*, 247:577, 2010.

[125] M. Wissinger, D. Fuchs, L. Dieterle, H. Leiste, R. Schneider, D. Gerthsen, and H. V. Löhneysen. *Phys. Rev. B*, 83:144430, 2011.

[126] P. Khalifah, I. Ohkubo, H. M. Christen, and D. G. Mandrus. *Phys. Rev. B*, 70:134426, 2004.

[127] G. Schehr and H. Rieger. *Phys. Rev. Lett.*, 96:227201, 2006.

[128] G. Schehr and H. Rieger. *J. Stat. Mech.*, page P04012, 2008.

[129] T. Vojta. *Phys. Rev. E*, 70:026108, 2004.

[130] S. L. Sondhi, S. M. Girvin, J. P. Carini, and D. Shahar. *Rev. Mod. Phys.*, 69:315, 1997.

[131] H. V. Löhneysen, A. Rosch, M. Vojta, and P. Wölfle. *Rev. Mod. Phys.*, 79, 2007.

[132] R. B. Griffiths. *Phys. Rev. Lett.*, 23:17–19, 1969.

[133] S. Guo, D. P. Young, R. T. Macaluso, D. A. Browne, N. L. Henderson, J. Y. Chan, L. L. Henry, and J. F. DiTusa. *Phys. Rev. Lett.*, 100:017209, 2008.

[134] T. Westerkamp, M. Deppe, R. Küchler, M. Brando, C. Geibel, P. Gegenwart, A. P. Pikul, and F. Steglich. *Phys. Rev. Lett.*, 102:206404, 2009.

[135] Sara Ubaid-Kassis, T. Vojta, and Almut Schroeder. *Phys. Rev. Lett.*, 104:066402, 2010.

[136] N. Kolev, C. L. Chen, M. Gospodinov, R. P. Bontchev, V. N. Popov, A. P. Litvinchuk, M. V. Abrashev, V. G. Hadjiev, and M. N. Iliev. *Phys. Rev. B*, 66:014101, 2002.

[137] Y. Bréad, V. Hardy, B. Raveau, A. Maignan, H-J. Lin, L-Y. Jang, H. H. Hsieh, and C. T. Chen. *J. Phys. Condens. Matter*, 19:216212, 2007.

[138] J. Okamoto, T. Okane, Y. Saitoh, K. Terai, S. I. Fujimori, Y. Muramatsu, K. Yoshii, K. Mamiya, T. Koide, A. Fujimori, Z. Fang, Y. Takeda, and M. Takano. *Phys. Rev. B*, 76:184441, 2007.

[139] I. Ohkubo, H. M. Christen, P. Khalifah, S. Sathyamurthy, H. Y. Zhai, C. M. Rouleau aand D. G. Mandrus, and D. H. Lowndes. *Appl. Surf. Sci.*, 223:35, 2004.

[140] M. Ohtani, M. Lippmaa, T. Ohnishi, and M. kawasaki. *Rev. Sci. Instrum.*, 76:062218, 2005.

[141] C. U. Jung, H. Yamada, M. Kawasaki, and Y. Tokura. *Appl. Phys. Lett.*, 84:2590, 2004.

[142] G. Herranz, N. Dix, F. Sánchez, B. Martínez, J. Fontcuberta, M. V. García-Cuenca, C. Ferrater, M. Varela, D. Hrabovsky, and A. R. Fert. *J. Appl. Phys.*, 97:10M321, 2005.

[143] See supplemental material at http://link.aps.org/supplemental/10.1103/physrevlett.108. 185701 for details on the sample preparation, characterization, and on the experimental methodology.

[144] T. R. Kirkpatrick and D. Belitz. *Phys. Rev. B*, 53:14364, 1996.

[145] D. Belitz, T. R. Kirkpatrick, and T. Vojta. *Rev. Mod. Phys.*, 77:579, 2005.

[146] T. Vojta. Rare region effects at classical, quantum and nonequilibrium phase transitions. *J. Phys. A*, 39:R143–R205, 2006.

[147] T. Vojta. Quantum griffiths effects and smeared phase transitions in metals: Theory and experiment. *J. Low Temp. Phys*, 161:299–323, 2010.

[148] Y. Imry and M. Wortis. Influence of quenched impurities on first-order phase transitions. *Phys. Rev. B*, 19:3580, 1979.

[149] Kenneth Hui and A. Nihat Berker. Random-field mechanism in random-bond multicritical systems. *Phys. Rev. Lett.*, 62:2507, 1989.

[150] T. Senthil and S. N. Majumdar. Critical properties of random quantum Potts and clock models. *Phys. Rev. Lett.*, 76:3001, 1996.

[151] P. Goswami, D. Schwab, and S. Chakravarty. Rounding by disorder of first-order quantum phase transitions: Emergence of quantum critical points. *Phys. Rev. Lett.*, 100:015703, 2008.

[152] R. Greenblatt, M. Aizenman, and J. Lebowitz. Rounding of first order transitions in low-dimensional quantum systems with quenched disorder. *Phys. Rev. Lett.*, 103:197201, 2009.

[153] Gary S. Grest and Michael Widom. N-color Ashkin-Teller model. *Phys. Rev. B*, 24(11):6508–6515, Dec 1981.

[154] Eduardo Fradkin. N-color Ashkin-Teller model in two dimensions: Solution in the large-N limit. *Phys. Rev. Lett.*, 53(21):1967–1970, Nov 1984.

[155] R. Shankar. Ashkin-Teller and Gross-Neveu models: New relations and results. *Phys. Rev. Lett.*, 55(5):453–456, Jul 1985.

[156] H.A. Ceccatto. Quantum n-colour ashkin-teller model: exact solution in the large-n limit. *J. Phys. A*, 24:2829, 1991.

[157] R. N. Bhatt and P. A. Lee. *Phys. Rev. Lett.*, 48:344, 1982.

[158] F. Hrahsheh, J. Hoyos, and T. Vojta. Rounding of first-order quantum phase transition to a strong-coupling critical point. *Unpublished*.

[159] T. Vojta, C. Kotabage, and J. A. Hoyos. Infinite-randomness quantum critical points induced by dissipation. *Phys. Rev. B*, 79:024401, 2009.

[160] A Bellafard, H. G. Katzgraber, M. Troyer, and S. Chakravarty. Bond disorder induced criticality of the three-color ashkin-teller model. 2012.

[161] F. Iglói and C. Monthus. Strong disorder renormalization group approach of random systems. *Phys. Rep.*, 412:277, 2005.

[162] István A. Kovács and Ferenc Iglói. Infinite-disorder scaling of random quantum magnets in three and higher dimensions. *Phys. Rev. B*, 83:174207, 2011.

[163] B. C. Crooker, B. Hebral, E. N. Smith, Y. Takano, and J. D. Reppy. *Phys. Rev. Lett.*, 51:666, 1983.

[164] M. H. W. Chan, K. I. Blum, S. Q. Murphy, G. K. S. Wong, and J. D. Reppy. *Phys. Rev. Lett.*, 61:1950, 1988.

[165] D. B. Haviland, Y. Liu, , and A. M. Goldman. *Phys. Rev. Lett.*, 62:2180, 1989.

[166] A. F. Hebard and M. A. Paalanen. *Phys. Rev. Lett.*, 65:927, 1990.

[167] A. Bezryadin, C. N. Lau, and M. Tinkham. Quantum suppression of superconductivity in ultrathin nanowires. *Nature*, 404:971, 2000.

[168] M. Greiner, O. Mandel, T. Esslinger, T. W. Hänsch, and I. Bloch. Quantum phase transition from a superfluid to a Mott insulator in a gas of ultracold atoms. *Nature*, 415:39, 2002.

[169] B. Damski, J. Zakrzewski, L. Santos, P. Zoller, and M. Lewenstein. *Phys. Rev. Lett.*, 91:080403, 2003.

[170] L. Fallani, J. E. Lye, V. Guarrera, C. Fort, and M. Inguscio. *Phys. Rev. Lett.*, 98:130404, 2007.

[171] T. Giamarchi and H. J. Schulz. *EPL (Europhysics Letters)*, 3:1287, 1987.

[172] T. Giamarchi and H. J. Schulz. *Phys. Rev. B*, 37:325, 1988.

[173] Z. Ristivojevic, A. Petković, P. Le Doussal, and T. Giamarchi. *Phys. Rev. Lett.*, 109:026402, 2012.

[174] Y. Kafri E. Altman and, A. Polkovnikov, and G. Refael. *Phys. Rev. Lett.*, 93:150402, 2004.

[175] Y. Kafri E. Altman and, A. Polkovnikov, and G. Refael. *Phys. Rev. Lett.*, 100:170402, 2008.

[176] Y. Kafri E. Altman and, A. Polkovnikov, and G. Refael. *Phys. Rev. B*, 81:174528, 2010.

[177] N. Prokofev K. G. Balabanyan and B. Svistunov. *Phys. Rev. Lett.*, 95:055701, 2005.

[178] M. Hasenbusch. *J. Phys. A*, 38:5869, 2005.

[179] S. Teitel and C. Jayaprakash. *Phys. Rev. B*, 27:598, 1983.

[180] R. Vosk and E. Altman. *J. Phys. B*, 85:024531, 2012.

VITA

Fawaz Hrahsheh was born on November 24, 1980 in Almafraq, Jordan. He finished his elementary school in Almusheirfah, Jerash and his secondary school from Irhab bani Hasan in Almafraq in 1998. He received his bachelor degree from Jordan University of Science and Technology (JUST) in 2002. After two years of working as a teacher in Jordan ministry of education, he joined the group of Dr. A. Obeidat as a graduate student at the department of physics at JUST. In August 2006, he received his MS in theoretical physics from JUST. In August 2007, he moved to Missouri University of Science and Technology (Missouri S&T) in Rolla-USA to begin his PhD study under supervision of Dr. G. Wilemski. In parallel to his work with Dr. Wilemksi, he joined the research group of Dr. Thomas Vojta in 2010 until he earned his PhD degree in physics in May 2013.